

DTIC FILE COPY

2

Report No. CG-D-12-88

AD-A198 628

# DEVELOPMENT OF A CHROMATIC/LUMINANCE CONTRAST SCALE

Lynn A. Olzak  
James P. Thomas  
Harold Stanislaw

Visual Psychophysics Laboratory  
Department of Psychology  
University of California  
Los Angeles, CA 90024-1563

DTIC  
ELECTE  
JUL 12 1988  
S D



INTERIM REPORT  
DECEMBER 1987

**DISTRIBUTION STATEMENT A**

Approved for public release  
Distribution Unlimited

This document is available to the U.S. public through the  
National Technical Information Service, Springfield, Virginia 22161

Prepared for:

U.S. Department Of Transportation  
United States Coast Guard  
Office of Engineering and Development  
Washington, DC 20593

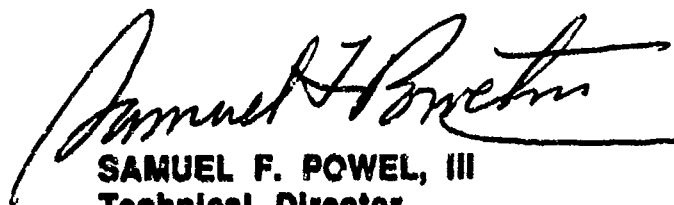
88 7 11 099

## NOTICE

This document is disseminated under the sponsorship of the Department of Transportation in the interest of information exchange. The United States Government assumes no liability for its contents or use thereof.

The United States Government does not endorse products or manufacturers. Trade or manufacturers' names appear herein solely because they are considered essential to the object of this report.

The contents of this report reflect the views of the Coast Guard Research and Development Center, which is responsible for the facts and accuracy of data presented. This report does not constitute a standard, specification, or regulation.



**SAMUEL F. POWEL, III**  
Technical Director

**U.S. Coast Guard Research and Development Center**  
Avery Point, Groton, Connecticut 06340-6096



AD-A198 628

Technical Report Documentation Page

1. Report No. DSCG-D-12-88		2. Government Accession No.		3. Recipient's Catalog No.	
4. Title and Subtitle Development of a Chromatic/Luminance Contrast Scale				5. Report Date December 1987	
				6. Performing Organization Code	
7. Author(s) Olzak, L. A., Thomas, J. P., and Stanislaw, H.				8. Performing Organization Report No. CGR/DC 19/87	
9. Performing Organization Name and Address Visual Psychophysics Laboratory, Department of Psychology, University of California Los Angeles, CA 90024				10. Work Unit No. (TRAIS)	
				11. Contract or Grant No. DTICG-39-C-80205	
12. Sponsoring Agency Name and Address Department of Transportation U. S. Coast Guard Office of Engineering and Development Washington, D. C. 20593 DTCG39-86-C-80205				13. Type of Report and Period Covered INTERIM REPORT	
				14. Sponsoring Agency Code G-NSR	
15. Supplementary Notes Contracting Office Technical Representative: Dr. Marc B. Mandler, U. S. Coast Guard Research and Development Center 267-1018 Rus. Doughty					
16. Abstract  A model was developed to predict the detectability of small low-contrast targets viewed against a uniform background in daylight conditions. The model quantitatively describes the interrelationships among detectability, target size, target luminance, target chromaticity, background chromaticity, and background luminance. A theoretical approach was used to develop a general form of the predictive model. Two empirical studies were performed to estimate parameters of the model, and a final study was performed to validate the model. The final model is presented in two forms, both easily used in field situations. The first predicts detectability of a specified target (size, luminance and chromaticity) when viewed against a specified background (luminance and chromaticity). The second predicts the distance at which such a target will be detected. A guide to the use of the model is included. — keywords include					
17. Key Words aids to navigation, luminance contrast, daymarks, detection model, color vision, chromatic contrast			18. Distribution Statement Document is available to the U.S. public through the National Technical Information Service, Springfield, VA 22161		
19. Security Classif. (of this report) UNCLASSIFIED		20. SECURITY CLASSIF. (of this page) UNCLASSIFIED		21. No. of Pages 22. Price	

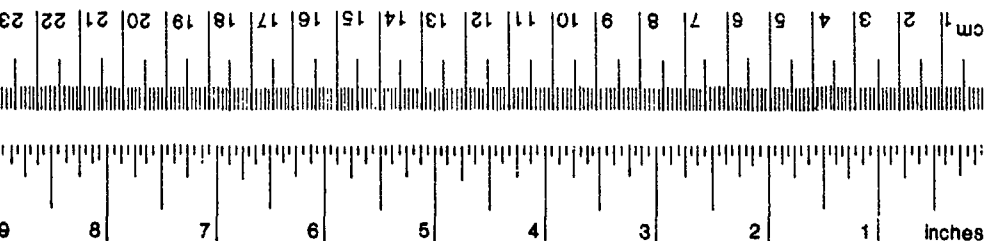
Form DOT F 1700.7 (8/72) Reproduction of form and completed page is authorized.

# METRIC CONVERSION FACTORS

## Approximate Conversions to Metric Measures

Symbol	When You Know	Multiply By	To Find	Symbol
<b>LENGTH</b>				
in	inches	* 2.5	centimeters	cm
ft	feet	30	centimeters	cm
yd	yards	0.9	meters	m
mi	miles	1.6	kilometers	km
<b>AREA</b>				
in <sup>2</sup>	square inches	6.5	square centimeters	cm <sup>2</sup>
ft <sup>2</sup>	square feet	0.09	square meters	m <sup>2</sup>
yd <sup>2</sup>	square yards	0.8	square meters	m <sup>2</sup>
mi <sup>2</sup>	square miles	2.6	square kilometers	km <sup>2</sup>
	acres	0.4	hectares	ha
<b>MASS (WEIGHT)</b>				
oz	ounces	28	grams	g
lb	pounds	0.45	kilograms	kg
	short tons (2000 lb)	0.9	tonnes	t
<b>VOLUME</b>				
tsp	teaspoons	5	milliliters	ml
tbsp	tablespoons	15	milliliters	ml
fl oz	fluid ounces	30	milliliters	ml
c	cups	0.24	liters	l
pt	pints	0.47	liters	l
qt	quarts	0.95	liters	l
gal	gallons	3.8	liters	l
ft <sup>3</sup>	cubic feet	0.03	cubic meters	m <sup>3</sup>
yd <sup>3</sup>	cubic yards	0.76	cubic meters	m <sup>3</sup>
<b>TEMPERATURE (EXACT)</b>				
°F	Fahrenheit temperature	5/9 (after subtracting 32)	Celsius temperature	°C

\*1 in = 2.54 (exactly). For other exact conversions and more detailed tables, see NBS Misc. Publ. 286, Units of Weights and Measures. Price \$2.25. SD Catalog No. C13.10.286.



## Approximate Conversions from Metric Measures

Symbol	When You Know	Multiply By	To Find	Symbol
<b>LENGTH</b>				
mm	millimeters	0.04	inches	in
cm	centimeters	0.4	inches	in
m	meters	3.3	feet	ft
m	meters	1.1	yards	yd
km	kilometers	0.6	miles	mi
<b>AREA</b>				
cm <sup>2</sup>	square centimeters	0.16	square inches	in <sup>2</sup>
m <sup>2</sup>	square meters	1.2	square yards	yd <sup>2</sup>
km <sup>2</sup>	square kilometers	0.4	square miles	mi <sup>2</sup>
ha	hectares (10,000 m <sup>2</sup> )	2.5	acres	
<b>MASS (WEIGHT)</b>				
g	grams	0.035	ounces	oz
kg	kilograms	2.2	pounds	lb
t	tonnes (1000 kg)	1.1	short tons	
<b>VOLUME</b>				
ml	milliliters	0.03	fluid ounces	fl oz
l	liters	0.125	cups	c
l	liters	2.1	pints	pt
l	liters	1.06	quarts	qt
l	liters	0.26	gallons	gal
m <sup>3</sup>	cubic meters	35	cubic feet	ft <sup>3</sup>
m <sup>3</sup>	cubic meters	1.3	cubic yards	yd <sup>3</sup>
<b>TEMPERATURE (EXACT)</b>				
°C	Celsius temperature	9/5 (then add 32)	Fahrenheit temperature	°F

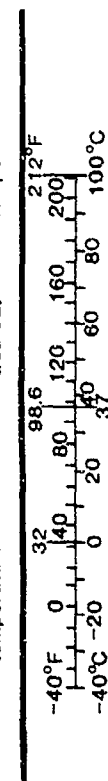


## TABLE OF CONTENTS

I. EXECUTIVE SUMMARY.....	1
II. INTRODUCTION.....	4
A. Scope of the Problem.....	4
B. Approach to the Problem.....	4
III. THEORETICAL DEVELOPMENT.....	6
A. Background and Literature Review.....	6
Trichromacy of Human Vision and the XYZ	
Color Space.....	6
Combining Information from Different	
Dimensions.....	9
Adaptation: The Effect of Background.....	10
Spatial Summation.....	11
The Psychometric Function.....	11
B. Development of Predictive Equations.....	12
Overview.....	12
Theoretical Development.....	12
Summary.....	15
IV. EMPIRICAL STUDIES.....	17
A. Overview.....	17
Experiments.....	17
Apparatus.....	18
Calibration.....	18
B. Experiment I.....	19
Methods.....	19
Observers.....	19
Stimuli.....	19
Procedures.....	21
Results.....	22
Overview.....	22
Step 1: Determination of the Primary	
Response Axes in the Chromatic	
Plane.....	24
Step 2: Determination of Scaling	
Parameters.....	28
Main Analysis: Equiluminous	
Backgrounds.....	28
Interpretation of Results from	
Main Analysis.....	32
Secondary Analysis: Luminance	
Variations in Backgrounds.....	32
Step 3: Combining Rule for Chromatic	
and Luminance Information.....	36
C. Experiment II.....	38
Methods.....	38
Observers.....	38
Stimuli.....	38
Procedures.....	40
Results.....	40

V.	FINAL MODEL AND GUIDE TO ITS USE.....	43
A.	The Model.....	43
	Overview.....	43
	Parameter Estimates.....	43
	Response Axes $c_1$ , $c_2$ , $c_3$ and the	
	Angle $\theta$ .....	44
	Scaling Parameters $a_{ijk}$ .....	44
	Value of the Combining Exponent $p$ .....	46
	Value of the Slope of the Psychometric	
	Function $q$ .....	46
	Predicting Detectability of a Target.....	46
	Predicting Detection Distance.....	53
B.	Using the Model.....	53
	Predicting Detectability of a Target.....	53
	Predicting Detection Distance.....	54
VI.	VALIDATION OF THE MODEL.....	56
	Methods.....	56
	Observers.....	56
	Stimuli.....	56
	Procedures.....	57
	Results.....	58
VII.	SUMMARY AND RECOMMENDATIONS.....	62
	REFERENCES.....	63
	APPENDIX A: Monitor Calibration.....	A-1
	APPENDIX B: Ellipse Fitting Procedures.....	B-1
	APPENDIX C: Additional Figure Sets.....	C-1

#### LIST OF ILLUSTRATIONS

Figure 1.	Background locations in chromaticity space..	20
Figure 2.	Raw threshold data points for a single observer, single background.....	25
Figure 3.	Ellipse fit to data for a single observer, single background.....	27
Figure 4.	Average threshold contour for standard gray background, XZ plane.....	33
Figure 5.	Average threshold contour for standard gray background, XY plane.....	34
Figure 6.	Average threshold contour for standard gray background, YZ plane.....	35

Figure 7. Mean-squared errors for combining parameter $p$ .....	39
Figure 8. Color Plate: Average threshold contour for targets viewed against a pink background....	47
Figure 9. Color Plate: Average threshold contour for targets viewed against an orange background.	48
Figure 10. Color Plate: Average threshold contour for targets viewed against a green background...	49
Figure 11. Color Plate: Average threshold contour for targets viewed against a turquoise background.....	50
Figure 12. Color Plate: Average threshold contour for targets viewed against a blue background....	51
Figure 13. Color Plate: Average threshold contour for targets viewed against a gray background....	52
Figure 14. "Equal Performance" results from validation study: Gray background.....	59
Figure 15. "Equal Increment" results from validation study: Pink and Gray backgrounds.....	61
Figures C-1 through C-11. Individual threshold deviation contours.....	C-2 through C-12
Figures C-12 through C-22. Individual data points with fit ellipses.....	C-13 through C-23
Figures C-23 through C-27. Average threshold deviation contours, XZ plane.....	C-24 through C-28
Figures C-28 through C-32. Average threshold deviation contours, XY plane.....	C-29 through C-33
Figures C-33 through C-37. Average threshold deviation contours, YZ plane.....	C-34 through C-38

#### LIST OF TABLES

Table 1. ANOVA Results: Experiment I.....	30
Table 2. ANOVA Results: Experiment II.....	42
Table 3. Summary of Model Parameters.....	45



Accession No.	
NTIS	DTIC
DTIC	DTIC
DTIC	DTIC
By	
Date	
A-1	

[BLANK]



## DEVELOPMENT OF A CHROMATIC/LUMINANCE CONTRAST SCALE

### I. EXECUTIVE SUMMARY

This report describes the development of a quantitative model for predicting the distance at which a target (e.g., a day-marker or other warning sign) will be detected under daylight viewing conditions. Known spatial, luminance, and chromatic processing capabilities of the human visual system were used to develop a general form of the model. Specific parameters of the model were estimated on the basis of data collected in two empirical studies. The predictive validity of the final model was then assessed in a third study.

The first study provided the basic detection data from which many of the model parameters were estimated. A computer generated stimuli and displayed them on a color monitor, so that thresholds could be measured in the laboratory using a modified method of adjustment. A total of 624 different combinations of target size and target and background luminance and chromaticity were evaluated. Each threshold was measured 5 times in 5 different observers (16,500 thresholds in all). These data were used (as described below) to evaluate parameters relating to four of the five theoretical issues underlying model development.

The second study provided the information necessary to relate the threshold-level data gathered in the first study to higher levels of detectability. A signal detection rating experiment was used to obtain precise estimates of the relative detectability of stimuli that varied in chromatic and luminance contrast. Stimuli were generated as in the first study, with two of the observers from that study participating in the second study.

On the basis of previous vision research, five issues were considered in the construction of the prediction model. The first issue concerns the three dimensional nature of human color vision: the luminance and chromatic characteristics of any stimulus can be completely described by coordinates in a three-dimensional measurement space. Similarly, any response to such stimuli can be described in terms of three response coordinates that represent a transformation of the measurement coordinates. There are many possible measurement spaces. However, tristimulus space -- also known as XYZ space -- is convenient for both theoretical and practical reasons. The Y dimension of tristimulus space is a luminance dimension. The X and Z dimensions are chromatic: X is identified with an approximately red-green axis of chromatic modulation, whereas Z is identified with an approximately blue-yellow axis. The contrast of a target when viewed against a particular background can be described completely by the difference between the target and the background in the X, Y, and Z dimensions. These three difference measures provide the primary input variables for the prediction model.

The response to a target when viewed against a particular background can be plotted as a vector in tristimulus space. For a given background, the response vectors from targets of equal detectability describe ellipsoids. These ellipsoids have centroids that vary with the background's tristimulus coordinates, and primary axes that represent the detectability of targets that vary only in the X, Y, or Z dimension. In the first study, these primary axes were identified as isomorphic to the X, Y, and Z axes of the tristimulus measurement space. Differences in the length of these axes (i.e., differences in the sensitivity to changes along the X, Y and Z axes) were incorporated in the model as scaling constants. Sensitivity was highest to targets that varied along the X (red-green) axis, with a scaling parameter value of 9.2. Sensitivity was slightly lower to targets that varied only in luminance, with a scaling parameter value of 8.8. Sensitivity was lowest to targets that varied along the Z (blue-yellow) axis, with a scaling parameter value of 2.1.

The second issue that was considered in the development of the prediction model was how information is combined across the three primary response dimensions. Such combination may take place whenever targets vary simultaneously along two or more dimensions. The prediction model therefore incorporated two information combination parameters. One described how information is combined between the two chromatic dimensions, X and Z, while the second described how information is combined between the chromatic and luminance axes. Values for these parameters were estimated in the first study. Information was combined across the two chromatic axes with a combining parameter of 2, which corresponds to Euclidean summation. Information was combined across the chromatic and luminance axes with a combining parameter of 3, which corresponds to independent processing with probability summation.

The third issue of importance concerns chromatic adaptation. Mechanisms in the visual system can adapt to the background against which a target is viewed, by changing in sensitivity. The effect of such chromatic adaptation was assessed in the first study. Despite previous evidence to the contrary, the current results indicated that background chromaticity was not a significant factor in predicting detectability. The luminance of the background also had little effect on detectability. Indeed, at the photopic levels of illumination that are typical of daylight viewing, the effect of background luminance was so small that it was ignored for modelling purposes. Instead, detectability was primarily a function of the chromatic and luminance contrast between the background and the target (i.e., the linear difference between the background and the target along the X, Y and Z dimensions). These effects were entered into the model as three input variables:  $\Delta X$ ,  $\Delta Y$ , and  $\Delta Z$ .

The fourth issue of concern is spatial summation. The question here is how detection performance changes with the size

of a target at a fixed distance, or (equivalently) how performance changes with viewing distance for a target of fixed size. This information was gathered in the first study and incorporated into the model by means of a simple linear equation that relates one model parameter to retinal angle subtense.

The final issue of interest concerns the psychometric function. The slope of the psychometric function defines how detection performance is related to the luminance or chromatic contrast of a target. This parameter of the model was estimated to have a value of 1.34, based on data collected during the second study.

Two forms of the final prediction model are presented as simple equations in this report. The first form of the model predicts the relative probability of detecting a given target, when viewed from a specified distance against a given background. The second form of the model predicts the relative distance at which a target will be detected with some specified probability. Both forms of the model require that the user supply three parameter values characterizing the luminance and chromaticity relationship between target and background, and a fourth parameter value that specifies either the distance of interest (for predicting the probability of detection) or the detection probability level of interest (for predicting the distance to detection). Relative predicted values can be transformed into absolute predicted values by specifying a scaling parameter that depends upon the particular task.

A final study assessed the predictive accuracy of the model. Nine computer-generated targets of fixed contrast, but variable size, were successively viewed against one of two different backgrounds. Twenty-six naive observers participated in the study. Half of these viewed targets against a pink background, while the other half viewed targets against a gray background. A method of limits procedure was used to empirically determine the threshold size of each target. The data were compared to values predicted from the model for each target/background combination. In virtually all cases, the predicted values were within the range of empirically determined points. It should be noted that this success was achieved without incorporating the additional task-dependent scaling parameter.

In summary, we have developed a relatively simple model that accurately predicts detection performance for a wide variety of targets and backgrounds. It is easily used in field situations, and requires only that the tristimulus coordinates of the target and background be known. The computational simplicity, wide generality, and easy-to-use nature of the model represent significant advances over previous models of this type.

## II. INTRODUCTION

### A. SCOPE OF THE PROBLEM

The purpose of this program was to provide certain information needed to predict the distance at which a target, such as a day-marker or other warning sign, will be detected under photopic (daylight or early twilight) adaptation conditions. For targets that have high luminance contrast (i.e., are much brighter or much darker than the background) or high chromaticity contrast (i.e., are of a very different hue than the background), detection will be determined primarily by resolution limits of the eye, or acuity. For targets that are of lesser luminance or chromaticity contrast, the problem becomes more complex.

The ability to detect a low-contrast target in a real-world scene potentially depends upon myriad variables that characterize the target itself, the immediate background, and other objects in the scene. Additional considerations that may influence performance include the observer's uncertainty as to shape, size, hue, brightness, and location of the target, and the experience the observer has had at similar detection tasks.

In the work reported here, we focus on a limited subset of these potential variables in order to explicitly model and predict their influence upon detection performance. These variables are the size of a small square target, the luminance and chromaticity of the target, and the chromaticity of a uniform background field. Luminance of the background field is considered briefly. Factors such as uncertainty and experience were minimized, and other potential influences on detection were excluded or held constant.

### B. APPROACH TO THE PROBLEM

Despite the restrictions stated in the previous section, the set of possible luminance and chromatic variations in target/background combinations that might be investigated remains nearly infinite. A logical reduction in this set is accomplished by approaching the problem theoretically, making use of known spatial and chromatic properties of the human visual system. The theoretical concepts are linked to the ultimate goal of a predictive scale by several simple equations, whose parameters can be estimated from experimental data. This approach obviates the necessity to perform full parametric studies; instead, it rationally drives the choice of stimulus set as well as directing the focus of empirical work.

The theoretical approach is divided into five different conceptual areas that are considered in developing the predictive model: (1) Trichromacy of Human Color Vision; (2) Information Combination across Chromatic and Luminance Detecting Mechanisms; (3) Chromatic and Luminance Adaptation; (4) Spatial Summation;

and (5) Slope of the Psychometric Function. The existing theory and research within each of these areas provide the principles and structure for our research program, and motivate the predictive equations. Section III presents existing theory and data within each of these areas, and develops the logical structure underlying the predictive equations.

In more concrete terms, the approach relies on detection threshold measurements of a selected set of target/background combinations to provide basic sensitivity data for targets. These data are used to assess how detectability varies along different dimensions in color space (chromatic and luminance); how information is combined across these dimensions in detecting targets that vary in two or more dimensions; and to assess how detection changes as a function of the background field. These measurements are taken for targets of several sizes in order to estimate how performance changes with size. Finally, slopes of psychometric functions that relate contrast to performance are estimated, so that extrapolations can be made to the detectability of stimuli with other contrast levels.

The data necessary to describe these interrelationships are generated from two main experiments, described in Section IV of this report. The first study provided basic detection data for targets viewed against various equiluminous adapting fields spanning a range of six hues. For one neutral background hue, measures were taken at higher and lower luminance levels to provide supplemental information and confirm the validity and sensitivity of our measures. Targets differed from the background in luminance and/or chromaticity, and detection performance was measured for targets of several sizes. The second study provided information necessary to extrapolate the basic detection data from Experiment I to stimuli with other levels of contrast.

Section V of this report summarizes the results of the empirical information and provides the final predictive equation together with estimated parameters. Two forms of the equation are provided; the first predicts to probability of detection, whereas the second predicts distance to detection. A guide to the use of these predictive forms is included. The results of a final study, intended to assess and validate the predictive power of the model, are presented in Section VI.

### III. THEORETICAL DEVELOPMENT

This section discusses the basic research findings relevant to predicting target detectability against different backgrounds. The detectability of a target against a background is sometimes referred to as discrimination, because it involves the ability to discriminate between two stimulus entities: target and background.

The relevant findings fall into five conceptual areas, each of which is incorporated into the final predictive equations. Section A presents each of the five concepts, including a brief review of pertinent literature. The predictive equations are developed in Section B.

#### A. BACKGROUND AND LITERATURE REVIEW

1) Trichromacy of Human Color Vision and the XYZ Color Space. The first concept pertinent to predicting the detectability of targets against uniform backgrounds is that of the trichromacy of color vision (for general reviews, see DeValois and DeValois, 1975; Boynton, 1975; Pokorny and Smith, 1986). This is the fundamental property that normal human color vision is three dimensional. The trichromacy assertion stems from widespread evidence that it is possible to match any color by a mixture of only three primaries. This result has been long interpreted as suggesting that the visual system requires only three independent mechanisms to process color information.

This property of color vision suggests that data for color matching (or the complementary ability of interest here, color discrimination) can be represented in terms of vectors in a three-dimensional space (Schrodinger, 1920). However, the property of trichromacy itself does not dictate the choice of a particular coordinate system or measurement space. Here, we consider several criteria in the choice of the representation space. The first is that it be closely related to the units in which photometric measurement of the stimuli are made. The second is that the space should be based on a system that is widely used and well-understood. Finally, it should have a direct and meaningful interpretation in terms of perceptual dimensions and physiological mechanisms of human color vision.

Initially, the three dimensions of human color vision are activities in three different classes of cone receptors. Thus, cone excitation space represents one possible representation scheme, and has been used to represent color matching data with varying degrees of success (Boynton and Kambe, 1980; LeGrand, 1949; Nagy, Eskew and Boynton, 1987; Rodieck, 1973). Although closely identified with physiological mechanisms subserving color vision, cone excitation space is not easily interpreted in terms of the perceptually distinct dimensions of luminance and chromaticity. Furthermore, such a space requires rather complex

transformations of measured stimulus values.

At an early stage of visual processing, information from the cones is recombined in an opponent process system having three independent mechanisms that are identified with the perceptual dimensions of luminance and chromaticity. The first is an achromatic, or luminance mechanism. The other two are chromatically opponent, often called the red-green and the blue-yellow mechanisms. A number of models have been developed that closely relate physiological mechanisms of color vision at the opponent process stage to a color measurement space: The CIE XYZ system of units.

The XYZ system of units was defined in 1931 by the Commission Internationale de l'Eclairage (CIE) as a statement of color-matching behavior for a standard observer. Each of the dimensions is defined as follows:

$$X = \int \sum_a \phi_a(\lambda) \bar{x} d\lambda \quad [1]$$

$$Y = \int \sum_a \phi_a(\lambda) \bar{y} d\lambda \quad [2]$$

$$Z = \int \sum_a \phi_a(\lambda) \bar{z} d\lambda \quad [3]$$

where  $\phi(\lambda)$  denotes the spectral composition of light from three primaries ( $a = 1, 2, \text{ and } 3$ ), and  $\bar{x}$ ,  $\bar{y}$ , and  $\bar{z}$  are standard color matching functions. An important property of the XYZ system is that luminance information is wholly contained in the Y dimension. The achromatic or luminance mechanism at the opponent stage of processing is almost universally identified with this Y variable (Guth, Massof, and Benzsawel, 1980; Jameson and Hurvich, 1955; Vos and Walraven, 1971). Activity in each of the two chromatic mechanisms is taken to be determined by a linear combination of X, Y, and Z.

An increasingly useful concept is that of the isoluminant plane, described by variations in the XZ plane of the space. Every point in the the plane has the same luminance, but the points differ in the relative activity represented in the cone classes and in the two opponent chromatic mechanisms. Thus, in the XZ plane of tristimulus space, activity in each of the chromatic mechanisms can be represented by a combination of X and Z. Variation along the X axis roughly corresponds to variation along a red-green dimension whereas variation along the Z axis roughly corresponds to a blue-yellow dimension.

The XYZ system links colorimetric and photometric behavior such that any stimulus can be described by its three tristimulus values: X, Y and Z. Any two stimuli having equal XYZ coordinates appear identical to the standard observer. The color-matching function upon which Y is based ( $y(\lambda)$ ) is equivalent to  $V(\lambda)$ , the CIE photopic luminous efficiency function for the standard observer, so that photometric quantities can be directly computed using  $y(\lambda)$ . In the most concrete terms, the practical result of

this property is that stimuli with equal Y values (measured in footlamberts (ftL) or candelas per square meter ( $\text{cd/m}^2$ )) appear equally luminous to the standard observer, regardless of hue.

It should be noted that results of many previous studies on color discrimination have been plotted in a transformation of XYZ space referred to as chromaticity space with axes x, y, and z. The transformation normalizes the coordinates so that  $x+y+z=1.0$ , as follows:

$$x = \frac{X}{X + Y + Z} \quad [4]$$

$$y = \frac{Y}{X + Y + Z} \quad [5]$$

$$z = \frac{Z}{X + Y + Z} \quad [6]$$

This transformation has the advantage that from any two dimensions, the third is easily derived. Thus, the three-dimensional XYZ space can be easily represented in two dimensions, usually x and y. We have found that this transformation unnecessarily complicates both the interpretability and the predictive simplicity of discrimination data. Therefore, for most purposes, we present our data in the untransformed XYZ space.

The trichromacy of color vision and the choice of the CIE XYZ color space is important for the present research because it defines a space in which background fields, target stimuli, and observer responses can be easily specified in three dimensions. Any background field or target can be uniquely specified as a point in the 3-dimensional space (X, Y, Z). The linear difference between the background and target coordinates along a given axis ( $\Delta X$ ,  $\Delta Y$ , or  $\Delta Z$ ) defines the contrast of the target along that axis. A transform of the distance between a target and a background field along any arbitrary axis in this space provides a measure of detectability of that target when viewed against that background field; the larger the distance in this space, the greater the visibility. For a standard measure of detectability such as threshold, the loci of target coordinates that are just noticeably different from the background trace out a three-dimensional surface. The size and shape of a surface centered at a given point provide information about the relative detectability of targets that are viewed against a given background. Variations in the size and shape of the threshold surface across different center points provide information about how backgrounds influence detectability.



2) Combining Information from Different Dimensions. The second concept is one of information combination across the three primary dimensions of the measurement space. Detection thresholds can be measured along the luminance dimension or along any arbitrarily selected axis in the equiluminous XZ plane. The question here is how thresholds vary when targets vary along more than a single dimension. Once combining rules are specified, the surface shape of the threshold contour is predictable from only three measures. That is, the detectability of any arbitrary target on a given background can be predicted from performance along the relevant primary axes.

MacAdam (1942) derived discrimination thresholds for 2 deg stimuli lying along different axes in the XZ plane and plotted his results in the normalized chromaticity space (i.e., the xz plane). Each set of thresholds defined the locus of stimuli that were just noticeably different from a single standard stimulus (analogous to the background in the present discussion). In all cases, the threshold locus approximated an ellipse, although the lengths of the axes of the ellipse and the orientation of the axes relative to the axes of the space varied from one part of the plane to the other. Nevertheless, the elliptical shape of the threshold locus suggests two things. First, discrimination among different stimuli in the XZ plane is mediated by two independent mechanisms (presumably the red-green and blue-yellow opponent mechanisms); and second, information from the two mechanisms is combined according to a Euclidean metric (see Guth, Massof and Benzschawel, 1980, for a formal statement of this interpretation).

Guth and his associates (Guth, Donley, and Marrocco, 1969; Guth and Lodge, 1973; Guth, Massof, and Benzschawel, 1980) and Olzak and Wandell (Olzak and Wandell, 1983; Wandell and Olzak, 1983) have considered the results when targets vary simultaneously along the luminance dimension and both chromatic dimensions. They conclude that for large targets ( $> 1$  deg) the information along these dimensions is also combined according to a Euclidean metric, providing the stimulus exposure is not brief. For brief exposures, little information combination is observed. The original data of the Guth group were gathered with targets viewed against dark backgrounds. However, Guth et al. (1980) have used their conclusions to postdict the detectability of targets seen against various chromatic backgrounds. The detection targets of Olzak and Wandell were viewed against chromatic adapting backgrounds.

To summarize, the available data suggest that the locus of targets that are just noticeably different from a given background is defined by a constant Euclidean sum of the detectabilities of the targets with respect to the luminance and chromatic dimensions. For stimuli that vary only in chromaticity, the threshold loci are described by an ellipse, provided the data are normalized (i.e., expressed in terms of xyz coordinates). However, the orientation and semi-diameters of the ellipse may vary with background. Further, as discussed in the

next section, the relative magnitudes of the luminance and chromatic contributions to detectability may vary with adaptation.

It should be reiterated that most of the available data is based on measurements taken with relatively large targets (1-2 deg) with long exposure times (1 sec). Decreasing exposure time appears to change the combining rule; thus, it may be expected that Euclidean summation does not necessarily hold for very small targets, either.

3) Adaptation: The Effect of Background. The background against which a target is seen acts in part as an adapting stimulus that modifies the sensitivity of the visual system and of its component mechanisms. One aspect of adaptation is the familiar Weber's law relationship: in any type of intensity discrimination, the threshold rises as the intensity of the background rises. At moderate to high intensities, the rise in threshold is roughly proportional to the background intensity. If sensitivity is defined as the magnitude of response to a fixed absolute change in stimulus, all mechanisms become less sensitive as background intensity increases.

There is much evidence that adaptation does not affect all mechanisms equally, even when the changes in background intensity are chromatically neutral, i.e., when only luminance changes. When detection thresholds for narrow-band lights are plotted as a function of the wavelength of the light, the shape of the function changes significantly as the luminance of the background is altered (Boynton, Kandel and Onley, 1959; Sperling and Harwerth, 1972). The apparent hues of many wavelengths in the spectrum change as the luminance of the wavelength changes (Purdy, 1929; Boynton and Gordon, 1965). Opponent process theorists have interpreted these effects as indicating that the sensitivities of the different opponent mechanisms are altered at different rates. Specifically, although the sensitivities of all mechanisms are reduced at high background intensities, the reduction is less for the chromatic mechanisms than for the luminance mechanism. Between the two chromatic mechanisms, reduction is less for the blue-yellow mechanism than for the red-green mechanism.

If the background is altered in chromaticity as well as luminance, the sensitivities of the mechanisms relative to one another can be drastically altered. The classic data here are those of Stiles (1978), who used chromatic backgrounds to selectively adapt individual mechanisms. The adaptation appears to act at both the receptor and the opponent process level (Olzak and Wandell, 1983; Stromeyer and Sternheim, 1981; Wandell and Pugh, 1980; Wandell, Welsh, and Maloney, 1982).

The import of these findings for the present research is that the locus of targets that are just discriminable from the background (the threshold ellipsoid) can be expected to change in

size, shape, and possibly orientation as the luminance and chromaticity of the background is altered. However, recent evidence (Nagy, et al., 1987) has suggested that this dependence may in part be due to the choice of the color space in which thresholds are represented, and may simply represent an artifact of the transformation to chromaticity coordinates.

4) Spatial Summation. The fourth concept is that of spatial summation, or the specification of how performance increases with increases in the size of a target. Within certain limits, the likelihood that a given target will be detected against a background increases as the retinal image of the target increases in size (Blackwell, 1946). The range of sizes over which this change is observed is greater at low than at high luminances (Blackwell, 1946; Barlow, 1958). The range is also large when the short wavelength cones play a dominant role in the detection process (King-Smith and Carden, 1976). The import of these phenomena is that the size, and possibly the shape, of the threshold ellipsoid will depend upon the size of the target used in threshold measurements. In general, the smaller the target, the larger the ellipsoid. However, the relationships between these changes in target size and changes in the parameters of the threshold surface will vary, depending upon the luminance and possibly the chromaticity of the background. For example, reduction in the retinal image size of the target from 30 minutes to 10 minutes of visual angle would be expected to have less effect against a high luminance background than against a low luminance background. Similarly, the consequences of changes in viewing distance, which alter the retinal image size, can be expected to vary, depending upon the luminance and possibly the chromaticity of the background.

5) The Psychometric Function. The final concept is that of the psychometric function, or how detection performance is related to some measure of stimulus strength. As the term is used here, the measure will be a transform of the distance between target and background in the CIE XYZ space. This concept allows basic detection data to be extrapolated to varying contrast levels.

Empirically, psychometric functions have been found to approximate a cumulative Gaussian or the closely related Weibull function. An important feature is that the shape of the function is independent of many spatial, temporal and chromatic variables (Thomas, 1982; Wandell, Sanchez and Quinn, 1982; Watson, 1979). Such variables only affect the slope of the function.

This property is important to the present research because it means that the entire psychometric function need not be measured for every combination of target size and background condition. Rather, only the slope need be established.

## B. DEVELOPMENT OF PREDICTIVE EQUATIONS

Overview. In this section, the concepts discussed above are expressed formally and combined to form the general equations used to predict detection performance. There are several steps in the development of the predictive equations. The first three steps involve characterization of threshold contours in three dimensions. First, the primary axes of the response, or contrast, space are identified and related to the original axes of measurement in XYZ space by rotational transformations. Second, the lengths of the primary response vectors (directional distances in the response space) are defined by scaling each of the transformed axes. Third, primary response vectors are combined to provide a total response distance for an arbitrary stimulus that varies in both chromaticity and luminance. Empirical values of parameters needed in these three steps are estimated from Experiment I (see Section IV). The fourth step extends the relationships among the variables from threshold levels of detection to other levels via estimates of the slope of the psychometric function. The empirical information needed in this step is estimated in Experiment II.

Theoretical Development. The basic form of the predictive equation is developed in the following paragraphs. To facilitate the logical flow and conceptual understanding of the model, subscripts have been omitted throughout the discourse as much as possible. However, it should be kept in mind that each of the model parameters has the potential to vary with the background field (i) and target size (j). Thus, each parameter contains the implied subscripts ij.

The initial step is to relate the probability of detecting a target -- located at CIE tristimulus values of X, Y, and Z, and viewed against a background located at  $X_i$ ,  $Y_i$ , and  $Z_i$  -- to a transform of the distance between the target and background in XYZ space. This defines the contrast, or response, space. There are three primary axes in the contrast space:  $c_1$ ,  $c_2$ , and  $c_3$ .

$c_1$  is defined as a luminance axis, and is determined from thresholds to targets that vary from the background only in luminance. For such targets,  $c_1$  is defined as:

$$c_1 = Y - Y_i = \Delta Y \quad [7]$$

$c_2$  and  $c_3$  are chromatic axes, and are determined from thresholds to targets that only vary in the XZ (chromatic) plane. These are defined as rotations of the original chromatic axes X and Z:

$$c_2 = [(X - X_i) \cos \theta] + [(Z - Z_i) \sin \theta] \quad [8]$$

$$c_3 = [(Z - Z_i) \cos \theta] - [(X - X_i) \sin \theta] \quad [9]$$

where  $X$  and  $Z$  are tristimulus coordinates of a target at threshold visibility, and  $\theta$  is an empirically determined angle that may vary as a function of the background (i) and target size (j).

If  $\theta$  is determined to be 0, no rotational transformations are necessary, and Eqs. [8] and [9] reduce to the form of Eq. [7]; i.e.,

$$c_2 = (X - X_1) = \Delta X \quad [8a]$$

$$c_3 = (Z - Z_1) = \Delta Z \quad [9a]$$

In the second step, the distance transform is completed by determining the scaling parameters  $a_k$  ( $k=1$  to 3) that correspond to each of the response axes:

$$d_1 = a_1(c_1) \quad [10]$$

$$d_2 = a_2(c_2) \quad [11]$$

$$d_3 = a_3(c_3) \quad [12]$$

where  $a_k$  may depend upon the background (i) and target size (j).

When the target differs from the background only in luminance, detection is entirely determined by the distance along the  $c_1$  axis, i.e., by  $d_1$ . It is assumed that this distance is unity when the target is at the threshold of visibility. Thus, at threshold,

$$1 = d_1 = a_1(c_1)$$

Substituting from Eq. [7],

$$1 = a_1(\Delta Y)$$

and

$$a_1 = \frac{1}{\Delta Y} \quad [13]$$

When the target and background lie in the same XZ plane, detection is entirely determined by the distance between them in that plane. If  $\theta$  in Eqs. [8] and [9] is not 0, the primary axes of the response space  $c_1$  and  $c_2$  do not correspond to the  $X$  and  $Z$  axes of the measurement space. The parameters  $a_{12}$  and  $a_{13}$  cannot then be empirically determined from thresholds to stimuli that only vary along a single axis of the original measurement space. Instead, estimation of these parameters relies on the assumption that responses of the two chromatic mechanisms combine in a Euclidean metric. That is, on the basis of literature

summarized in the previous section, it is assumed that at threshold, the locus of just detectable targets is an ellipse centered on the background. The parameters of the best-fitting ellipse provide estimates of the primary response vector lengths, with axes  $c_2$  and  $c_3$  and semi-diameters  $a_{ij2}(c_2)$  and  $a_{ij3}(c_3)$ .

If  $\theta$  is determined to be 0 in both Eqs. [8] and [9], then axes  $c_2$  and  $c_3$  are defined by Eqs. [8a] and [9a], respectively. The scaling parameters  $a_{ij2}$  and  $a_{ij3}$  can then be estimated directly from empirical data, as in equation [13]:

$$a_2 = \frac{1}{\Delta X} \quad [14]$$

$$a_3 = \frac{1}{\Delta Z} \quad [15]$$

The third step evaluates how the three different response components  $d_1$ ,  $d_2$ , and  $d_3$  are combined. Together with the axis identification and distance transforms of steps 1 and 2, this step determines the shape of the three-dimensional response surface at threshold for a given target size/background combination.

On the basis of previous studies, it is assumed that information is combined across the two chromatic mechanisms according to a Euclidean metric:

$$d_c = (d_2^2 + d_3^2)^{1/2} \quad [16]$$

This assumption forces the shape of the response surface in the chromatic plane to be an ellipse. That is, if the three-dimensional response surface is sliced along any isoluminant plane, the resulting contour is elliptical.

When the target differs from the background in both luminance and chromaticity, detection is determined by a combination of responses along all three axes. The combination of information across luminance and chromatic mechanisms may vary with the background or target size. Furthermore, it may or may not be Euclidean, as determined by the combining parameter,  $p$ . The value of  $p$  remains to be estimated from empirical data, and determines the shape of the response contour when it is sliced along the XY or YZ plane.

The total response,  $d_t$ , is related to the component responses:

$$\begin{aligned} d_t &= [(d_1)^p + (d_c)^p]^{1/p} \\ &= [(a_1(c_1))^p + [(a_2(c_2))^2 + (a_3(c_3))^p]^{p/2}]^{1/p} \quad [17] \end{aligned}$$

As already indicated, the values of  $a_1$  are determined from thresholds for stimuli that differ from the background only in luminance, and the values of  $a_2$  and  $a_3$  are determined from thresholds that differ from the background only in chromaticity (i.e., lie in the same XZ plane). The value of the exponent  $p$  can be determined from thresholds for stimuli that differ from the background in both luminance and chromaticity, and its value may vary with background and/or target size. Again, the assumption is made that  $dt$  equals unity at the detection threshold.

The final step is to define the function that relates the probability of detecting the stimulus to the combined distance measure,  $dt$ . The function is assumed to have the form

$$z(\text{detect}) = b(d_t)^q \quad [18]$$

where  $z(\text{Detect})$  is the standard normal deviate corresponding to the probability of detection;  $b$  is a constant that depends upon the criterion adopted for the threshold judgments; and  $q$  is an empirically determined constant. The value of  $q$  is determined in a separate series of observations (Experiment II) in which the probability of detection is related to  $dt$ , calculated on the basis of the parameters obtained in the threshold observations (Experiment I). The value of  $q$  is given by the slope of the function that relates  $\log z(\text{Detect})$  to  $\log dt$ . As with the other estimated parameters, the value of  $q$  may vary with the background and target size.

Summary. Together, these equations provide a model to interrelate the probability of detection to target size (or distance for a target of fixed size), target chromaticity and luminance, and background chromaticity and luminance. The final form of the model, and the actual parameter estimates, are presented in Section V of this report.

For each possible background condition and target size, there are 9 parameters that must be estimated or identified in order to predict the detectability of a target. The three primary response axes ( $c_1$ ,  $c_2$  and  $c_3$ ) must be identified, and the angle that determines the orientation of each response contour ( $\theta$ ) must be estimated. Next, values must be estimated for the three scaling parameters that correspond to each response axis ( $a_1$ ,  $a_2$ , and  $a_3$ ). Finally, values must be estimated for two exponents: the combining exponent for information processed by chromatic and luminance mechanisms ( $p$ ), and the slope of the psychometric function ( $q$ ). Each parameter value has the potential to vary with the background and target size, and the values may vary in complex ways depending upon the particular combination of stimulus values.

In the worst case, each unique combination of target and background characteristics results in a different set of parameter values, and predictions must be obtained from a series

of nomograms that illustrate these complex interrelationships. However, to the extent that some parameters are constant across stimulus dimensions, or do not interact with each other, the model simplifies. Thus, an important part of this effort is to determine how each of these parameters varies with the target and background characteristics, and to assess the separability of these stimulus dimensions for predictive purposes. This information is presented in the next section.



#### IV. EMPIRICAL STUDIES

##### A. OVERVIEW

In this section, two empirical studies are described. These experiments generated the empirical information necessary to determine parameter values for the predictive model described in Section IIIB. Extensive analyses were performed in order to determine how these values varied with stimulus conditions; these results and their interpretation are described here. The final parameter estimates and model form are presented in Section V.

Experiments. The first experiment measured detection thresholds by a method of adjustment procedure for targets of 3 different sizes on 8 different adapting backgrounds. For each of the 24 resulting size/background combinations, 26 threshold measures were taken for targets that varied from the background in luminance, chromaticity, or both. The 26 measures defined the three-dimensional threshold surface for each of the size/background combinations. Each set of 26 measures provided the basic empirical information needed to determine the axes  $c_1$  and  $c_2$  of the transformed response space, to define the scaling constants  $a_{ijk}$  for each of the primary response axes, and to estimate the value of the exponent  $p$ , which defines the combining rule for responses to targets that vary in both luminance and chromaticity. Comparisons across the three target sizes on a given background provided information about how detection performance increases with increasing target size (the spatial summation function). Comparisons across backgrounds assessed the influence of adapting backgrounds on each of the model parameters.

The second experiment was performed to determine the slope of the psychometric function,  $g$ , that relates detection performance to target contrast (chromatic or luminance). A signal detection rating method was used to provide precise estimates of target visibility.

All psychophysical measurements, data analyses, and parameter estimation procedures were performed in the Visual Psychophysics Laboratory of the UCLA Department of Psychology. Stimuli were generated by a computer equipped with digital color-graphics capabilities, and were displayed on a high-resolution color monitor. To ensure precise identification of stimulus tristimulus coordinates (XYZ values), extensive calibration techniques were developed and implemented. Because the digital generation and display of color stimuli is a relatively new technique, the theory and procedures developed for calibration are included in this report as an appendix. Also included as appendices are techniques developed for fitting optimal ellipses to detection data and procedures for estimating combining rule parameters. Common statistical analyses such as the analysis of variance were performed by computer using existing software.

Apparatus. Stimuli for all experiments were displayed on a BARCO CDCT 5137 color graphic display, driven by a CAT 1631 graphics system installed in a Cromemco RS-2 computer. The BARCO display is a high-resolution RGB monitor (276 mm x 200 cm display area) that accepts analog input signals via separate RGB channels. The monitor is equipped with normal persistence red phosphors (32 ms decay to 10% of maximum), normal persistence green phosphors (110 ms to 10%), and short persistence blue phosphors (approximately 200 usec to 10%). The x,y,z chromaticity coordinates of the red, green and blue phosphors are, respectively, (.62,.33,.05), (.21,.675,.115), and (.15,.06,.79).

The CAT graphics system provides a 512x512 pixel display signal to the monitor. Color and luminance are controlled via three 256-level look-up tables corresponding to 256 possible luminance values for each of the red, green, and blue guns. The display was masked on three sides by a sheet of translucent plexiglass (930 mm x 420 mm), backlighted by multiple white light sources to provide a uniform surround that approximately matched the display in luminance.

Observers viewed the display binocularly from a distance of 3 m. At this distance the display subtended 5.26 x 3.97 deg of visual angle. With the surround, the entire configuration subtended 17.62 x 8.01 deg.

Calibration. Calibration of the color monitor was performed in accordance with steps outlined in Cowan (1985). A detailed discussion of the procedures and results is presented in Appendix A. They are briefly summarized here.

Calibration of the BARCO monitor was performed against a Gamma Model 220 Standard Lamp Source A (incandescent tungsten, 2854 deg. K, 342.6 cd/m<sup>2</sup>), equipped with three removable Kodak Wratten filters. The Wratten filters closely approximated the manufacturer-specified chromaticity coordinates of the red, green, and blue monitor phosphors. They were used to calibrate the photometer in the appropriate chromaticity region.

Calibration measurements were taken with a Spectra Pritchard photometer (Model 1970-PR), equipped with filters closely proportional to the  $\bar{x}$ ,  $\bar{y}$ ,  $\bar{z}$  functions. The integration time of this photometer approximates that of the human eye, making it an appropriate instrument for measuring the intermittent light generated by the monitor. A 2-degree aperture was used in all full-field measurements. A 1-degree aperture was used in small-spot measures.

Luminance levels were found to be independent of both the gun combination and the field size, assuring that color mixture equations could be used to create arbitrary chromatic stimuli from the three monitor phosphors. The chromaticity coordinates of each phosphor were measured to validate the accuracy of the manufacturer's specifications. These coordinates serve as the

primaries in color-mixing equations; thus, it is important that they be accurately determined. Gamma correction measurements, relating voltage to relative luminance, were taken at closely-spaced voltage increments. Higher order power-law functions were then fit for each gun. Finally, gun balance values were computed by measuring the Y tristimulus value of each gun at its maximum level and dividing by the corresponding y chromaticity coordinate.

These measures provided the basis for the functions relating tristimulus values (X, Y and Z) to gun voltage levels. The functions and errors for each gun are presented in Figures A1-A6 of Appendix A.

## B. EXPERIMENT I

### Methods

This experiment established threshold detection values for square targets that varied in size (3 levels), and luminance and chromatic composition (26 levels). Targets were viewed under different chromatic and/or luminance adapting conditions (8 backgrounds levels), for a total of 624 different threshold measures. A method of adjustment procedure was used. Five observers each repeated the measurements 5 times, for a final data base of 16,500 threshold measures. These served as the basic empirical data from which a majority of model parameter estimates were made.

Observers. Four females and one male participated in Experiment I as paid observers recruited from the UCLA student population. All were found to have 20/20 or better acuity (corrected) when tested with a Snellen acuity chart, and no observer showed evidence of color defects when tested with Ishihara (1964) plates. Observer ages ranged from 19-24. Observer NT was a male emmetrope. Observer KAB was a female emmetrope. Observers MRS, SJS, and PJM were female myopes, corrected to normal with spectacles. Observers participated in the experiment for 1 hour per day, five days per week, over a period of approximately 8 months.

Stimuli. The stimuli were small square targets centered on the background display. Three target sizes were used, subtending either 3, 10 or 30 minutes of visual arc. Eight backgrounds (adapting conditions) were chosen to span a range of chromaticity space. Six of the backgrounds were equiluminous, differing only in chromaticity. These constituted the basic set of background fields. The hues of the six backgrounds corresponded roughly to the colors pink, blue, turquoise, green, orange, and gray. They were presented at a luminance level of  $18.85 \text{ cd/m}^2$ . The six backgrounds are plotted in the xy chromaticity plane in Figure 1.

The two additional backgrounds were isochromatic with the gray background of the basic set, but were presented at higher

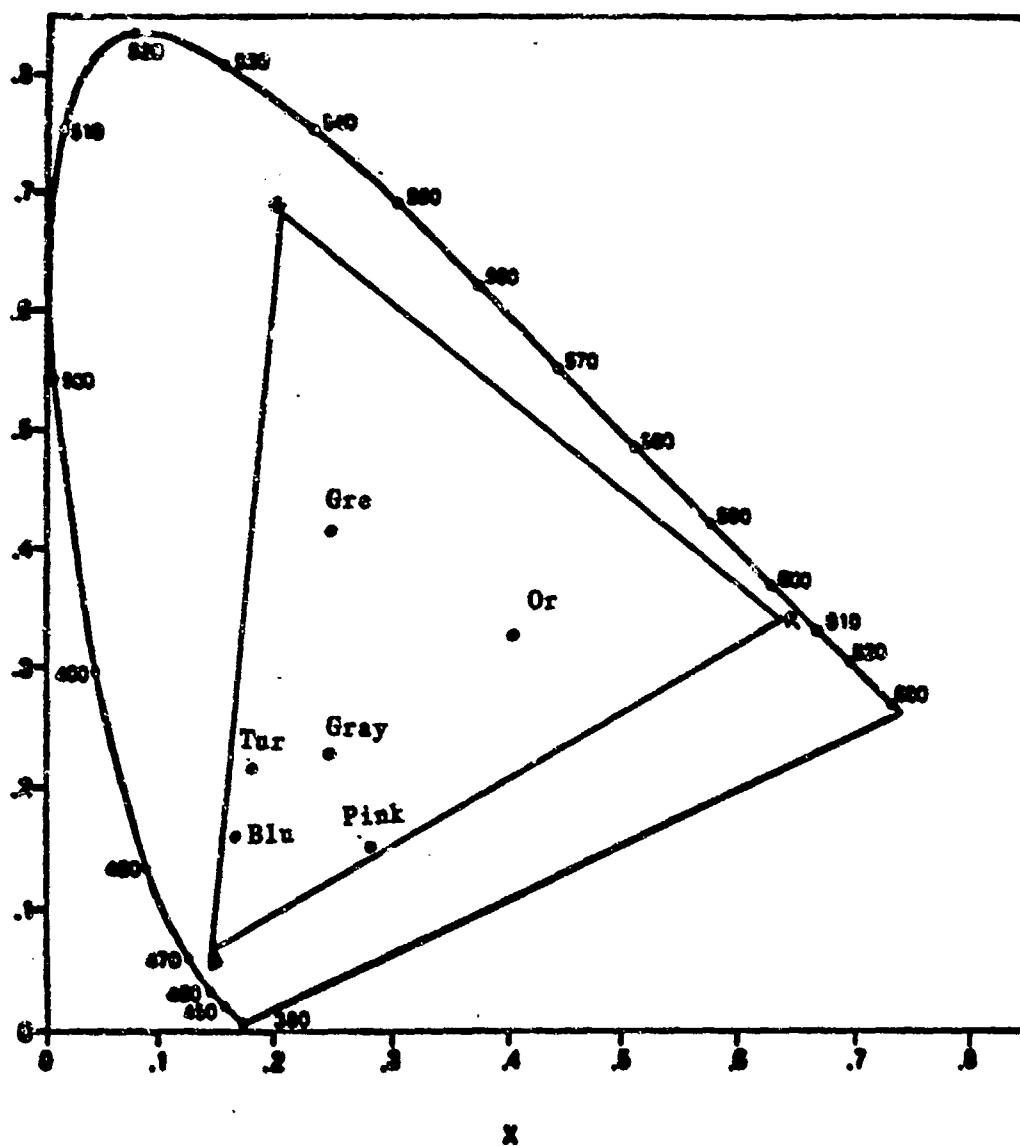


Figure 1. Six isoluminant background fields, plotted as locations in the xy plane of chromaticity space.

and lower luminance levels of 37.69 and 9.42 cd/m . These additional luminance-varying backgrounds were included primarily to provide supplementary information, and were excluded from some of the analyses.

Targets differed from each background in luminance only (i.e., varied in the +Y or -Y direction only -- 2 targets total); in chromaticity only (i.e., varied in the XZ plane only -- 8 targets total); and in both luminance and chromaticity (i.e., varied in the X, Y and Z directions -- 16 targets total). Thus, a total of 26 target directions were presented for each of the 24 target size/background combinations, resulting in 624 distinct stimuli. The contrast of each target was varied along a vector originating at the background location and pointing in the predefined direction. Thresholds were measured as distances along each vector, in XYZ tristimulus units.

The digital nature of stimulus presentation did not permit continuous variation along any arbitrary vector, but created a slightly zig-zag path. An algorithm was developed to minimize step size while simultaneously minimizing deviation from the desired vector. Checks ensured that deviations did not exceed threshold values in any direction; in most cases the deviations were a small percentage of threshold.

Procedures. In each experimental session, a single adapting background and target size was used. Each session consisted of 26 threshold measurements, corresponding to each of the 26 target colors. The 26 targets were presented in a different random order in each session. Target size/background combinations were also run in a random order for each observer. On a given day, either two or three sessions were run during the hour allotted for each observer, with the stipulation that no particular condition was run more than once in a single day. Each threshold measurement was replicated five times by each observer.

Each session began with a two-minute adaptation period, during which observers adapted to the background display. Each trial consisted of two parts. The first was a preview condition, during which the target for that trial was presented at its highest possible contrast. The preview was found to be necessary to reduce significant color and location uncertainty. When the observer was satisfied with the preview, a button was pressed, and the target was erased for 1 second to remove any aftereffects from the high contrast target. The target then reappeared, concurrent with a short tone, at a random contrast.

A method of adjustment procedure was used to determine thresholds. By use of a response box, the observer could increase or decrease the contrast of the target, at one of two predetermined rates. Both rapid and fine-tune adjustment speeds were available to the observer. When the observer was satisfied that the target was just barely visible, a button was pressed. The computer then recorded the voltages of the red, green, and

blue guns, which were transformed into tristimulus values via the functions given in Appendix A.

## Results

Overview. The analysis of data from Experiment I was accomplished in several steps. Because of the complexity of these analyses, each step and the results are briefly summarized here. Details of the analyses and results for each step are discussed in subsections.

In the first step, the primary response axes  $c_1$ ,  $c_2$  and  $c_3$  were established for each target size and background. All eight backgrounds were included in this step of the analysis.

The primary luminance response axis,  $c_1$ , was defined as described in Eq. [7] of Section IIIB; that is, as the difference in the  $Y$  value between target and background, for targets that only varied along a luminance measurement axis. The chromatic response axes,  $c_2$  and  $c_3$ , were initially estimated by fitting ellipses to the 8 measures taken in the  $XZ$  plane for each size/background combination, and rotating the measurement axes,  $X$  and  $Z$ , by the empirically determined angle  $\theta$  (see Eqs. [8] and [9] in Section IIIB). Four findings of import were discovered here.

First, the data were adequately described by ellipses. This provides some confirmation for the assumption that the combining exponent for information processed by chromatic mechanisms does indeed follow a Euclidean metric (combining exponent = 2), at least to a first approximation. The second finding of import was that small but significant asymmetries were found in the data for some background/size combinations. Because ellipses assume symmetry along any axis that passes through the center, the asymmetries result in the overestimation of the rotation angle  $\theta$ , and may in some cases inaccurately estimate the lengths of the semidiameters. The third finding was that, even though the rotational angles were overestimated, they were found to be quite small (generally less than 6 deg). The fourth result was that no systematic differences in angle were found as a function of background or target size.

It was concluded from these analyses that although the elliptical shape (and therefore a combining exponent of 2) for chromatic information provided an adequate description of the data in the isoluminant plane, a more accurate and concise description was obtained by assuming that the rotational angle  $\theta$  was 0 for all size/background combinations. Thus,  $c_2$  and  $c_3$  could be defined according to the simplified equations [8a] and [9a] of Section IIIB. Another way of stating this result is that, in all cases, the primary axes of the response space correspond to those of the measurement space; they do not change with target size or the region in color space.

The second step in the analysis was to determine the scaling parameters  $a_{ijk}$  that determine the length of the threshold vectors in the response space ( $d_1$ ,  $d_2$  and  $d_3$  in Eqs. [10]-[12] of Section IIIB). The simplification that resulted from the first step of the analysis allowed these parameters to be estimated directly from the data, as described in Eqs. [13]-[15] of Section IIIB. An important component of this analysis was to determine how the values differed for different target sizes and backgrounds. Each of the three vector lengths could potentially depend upon the individual size/background combination. Furthermore, each vector, or direction in color space, could potentially depend upon these combinations in a different way. However, the results of this analysis determined that no such complexity was necessary; the majority of the variance was accounted for by three different vector lengths that varied with the target size only.

The way in which each vector length depended upon size was nearly the same for all directions in color space. That is, the spatial summation function was the same for the two mechanisms that process chromatic information as it was for the mechanism that processes luminance information. This result suggests that the three-dimensional response surface does not change its shape in any significant way in different regions of color space. Instead, the shape simply expands in a linear way as target size decreases.

The third step of the analysis was an estimation of the parameter  $p$ , the combining exponent for information processed by the two chromatic mechanisms, on the one hand, and the luminance mechanism, on the other. Several different criteria were used to obtain estimates of the best fitting combination rule. Initially, estimation procedures were performed separately for each of the 24 target size/background combinations. There was some variation in the estimates obtained, and the different criteria did not always agree. However, no systematic differences in the estimate were found as a function of either variable, indicating that the combining rule was the same regardless of the target size or adapting background. The data were therefore collapsed across these two variables to provide the most stable estimate of  $p$ . For this final estimate, all criteria pointed to an identical value of  $p = 3$ . A value of 3 indicates that information is not combined across mechanisms that process chromatic and luminance information, except for probability summation. This result is in contrast to the combining exponent of 2 (Euclidean summation) found for the two mechanisms that process only chromatic information.

In the following subsections, the analyses and results outlined here are presented in detail.

Step 1. Determination of the Primary Response Axes in the Chromatic Plane. The first step of the analysis was to determine the transformed chromatic axes for each target/background combination  $c_2$  and  $c_3$ . This analysis

considered only those data for the 8 targets that varied in the XZ (chromaticity) plane. The primary measurement axes in this plane are X and Z; four targets (+X, -X, +Z, and -Z) varied along these axes. The remaining four targets varied along the diagonals of the measurement space, representing equal combinations of X and Z variation (+X,+Z; +X,-Z; -X,+Z; and -X,-Z). Across the 5 observers, 5 replications, 3 target sizes and 8 backgrounds, there were 600 data sets of 8 points each involved in this analysis.

Each set of raw threshold tristimulus values was subtracted from the background coordinates to express threshold as a deviation coordinate ( $\Delta X$ ,  $\Delta Z$ ) from the adapting background. The absolute value of each deviation defines a standardized threshold distance from each adapting background. The greater the distance, the higher the threshold.

Discussion of Individual Data. Data were first analyzed for the five replications from each individual observer in each of the 24 target size/background conditions (120 separate XZ threshold contours). In Figure 2, a representative set of these contours for an individual observers is plotted in the XZ plane. The plot represents the raw deviation data from all five replications performed by an individual observer for the indicated target/background combination. The adapting background is represented at the center of the plot.

An additional selection of these plots is presented in Appendix C (Figures C-1 through C-11). Note there that different scales are used for targets of different size. This was done to clearly present all the data, since the range of target sizes (3 min arc to 30 min arc) produced thresholds that varied on the order of 7 to 1, with the largest thresholds obtained for the smallest targets.

There are several points to note about these raw data plots. As in Figure 2, one trend that is clearly visible across all plots is that thresholds are maximal along the Z axis (roughly a blue-yellow axis of modulation), and minimal along the X-axis (roughly a red-green axis of modulation). This implies two things. First, to the extent that these axes represent different response levels in two different chromatic mechanisms, it is clear that there are large differences in the sensitivity of the two mechanisms. Second, the result implies that this sensitivity difference is not dependent upon target size, adaptation level or individual differences. That is, the orientation of the threshold contour for chromatic stimuli is quite constant across individuals, and does not change with changes in the adapting background or target size. Specifically, the orientation is such that the major semiaxis of the contour is on or near the Z measurement axis, indicating poorest sensitivity to targets that differ from any background along this axis.

A second point to note is that despite the rather coarse sampling of 8 data points, the threshold contours are roughly elliptical in shape. This implies that, at least to a first



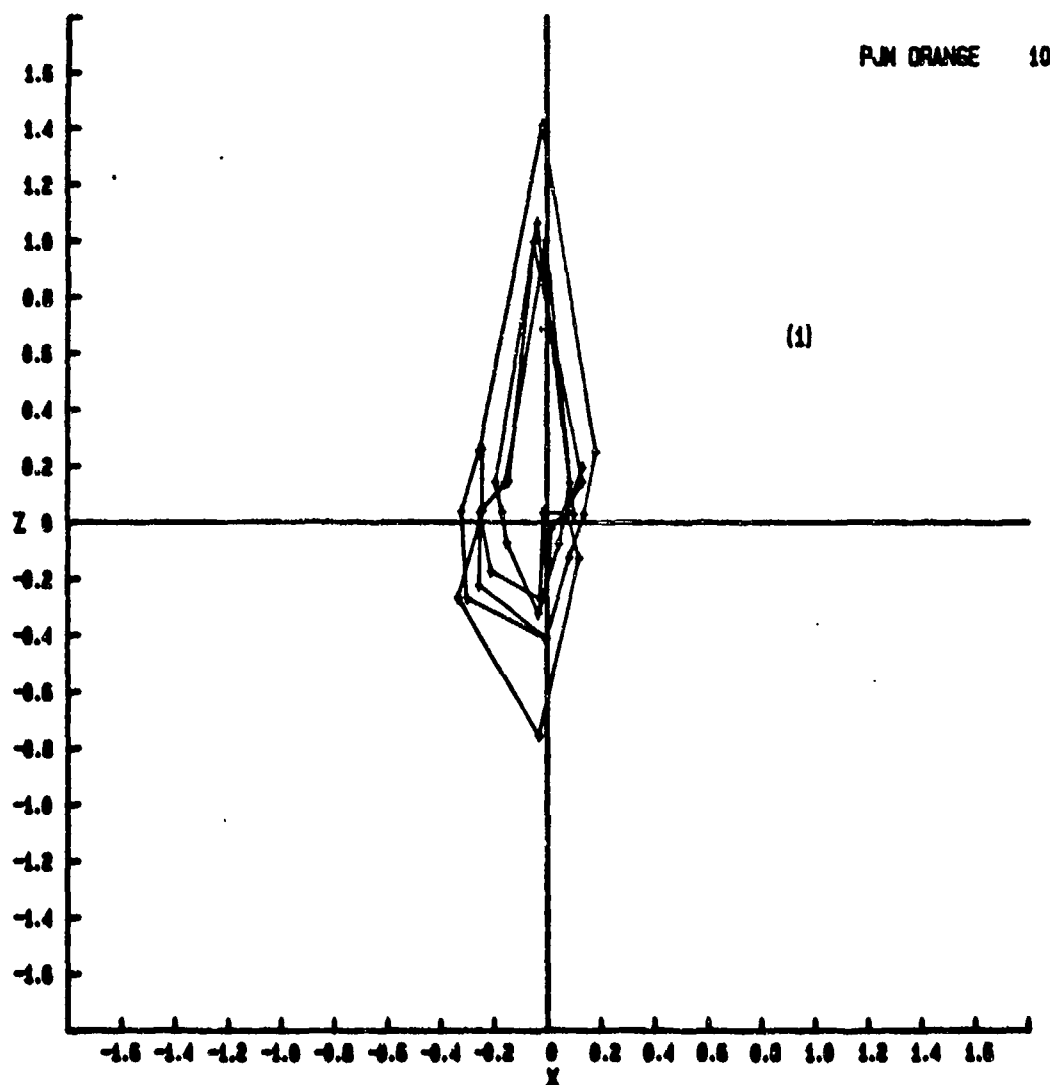


Figure 2. A representative individual threshold deviation contour in the isoluminant (XZ) plane. The adapting field is located at the center of the figure. Each point represents a daily threshold deviation from the adapting field for targets that vary along the primary measurement axes (X and Z) or along combinations of the two. Each contour represents one of the five replications performed by the designated observer with the background and target size shown in the figure legend. Data for observer RJM. Targets were 10 minarc in size, and viewed against an orange background. See Appendix C, Figures C-1 through C-11 for additional plots.

approximation, responses to targets that vary in both X and Z coordinates do appear to reflect a Euclidean combining rule for information processed by two chromatic mechanisms.

A third point is that there are relatively small, but clear, asymmetries in some threshold contours. These asymmetries are consistent across observers, but were not present for all adapting backgrounds and all target sizes. This result has implications for fitting ellipses to the data, because symmetry about a given axis is assumed when an elliptical contour is centered on the adapting background. This result is analyzed further in a later section.

In addition to these important trends, there is also evidence for variation in thresholds across observers, and day-to-day variations in thresholds within observers. The contribution of variation across observers is assessed in a later section. Within observers there is fair amount of day-to-day variation in thresholds, although the degree of such variation depends upon the individual observer. No formal analyses were performed to investigate the source of this variation, but the data were informally examined for obvious trends across days. In general, thresholds decreased over the five replications, suggesting that practice effects may be of some import in this detection task. Further examination of this effect suggested that practice effects were quite specific to a condition; practice with one adapting background or target size, for example, did not necessarily stabilize the data in another.

Ellipse Fitting. Ellipses were fit to data from each individual separately. For each of the 24 target size/background combinations, data from the five replications performed by each observer were used, so that each ellipse estimate was based on 40 data points. In total, 120 ellipses were fit (24 conditions x 5 observers). The fitting procedure used a least-squares criterion, and tested to ensure that the data were adequately described by an ellipse. The parameters of each ellipse,  $a$  (length of the major semiaxis),  $b$  (length of the minor semiaxis), and  $\theta$ , were estimated by the fitting procedure. The theory and methods of the ellipse fitting procedure are presented in detail in Appendix B.

In Figure 3, a typical set of data is plotted together with the estimated ellipse. (Additional plots are included in Figures C-12 through C-22, presented in Appendix C.) Points for plotting the ellipse were generated by calculating 360 XZ coordinates from each set of estimated ellipse parameters.

The fitted ellipses generally confirm expectations based on examination of the raw data plots. The major and minor axes of each ellipse lie on or near the primary axes of measurement, X and Z, indicating relatively less sensitivity to modulations along the approximately blue-yellow axis than along the approximately red-green axis. The orientation of the ellipses

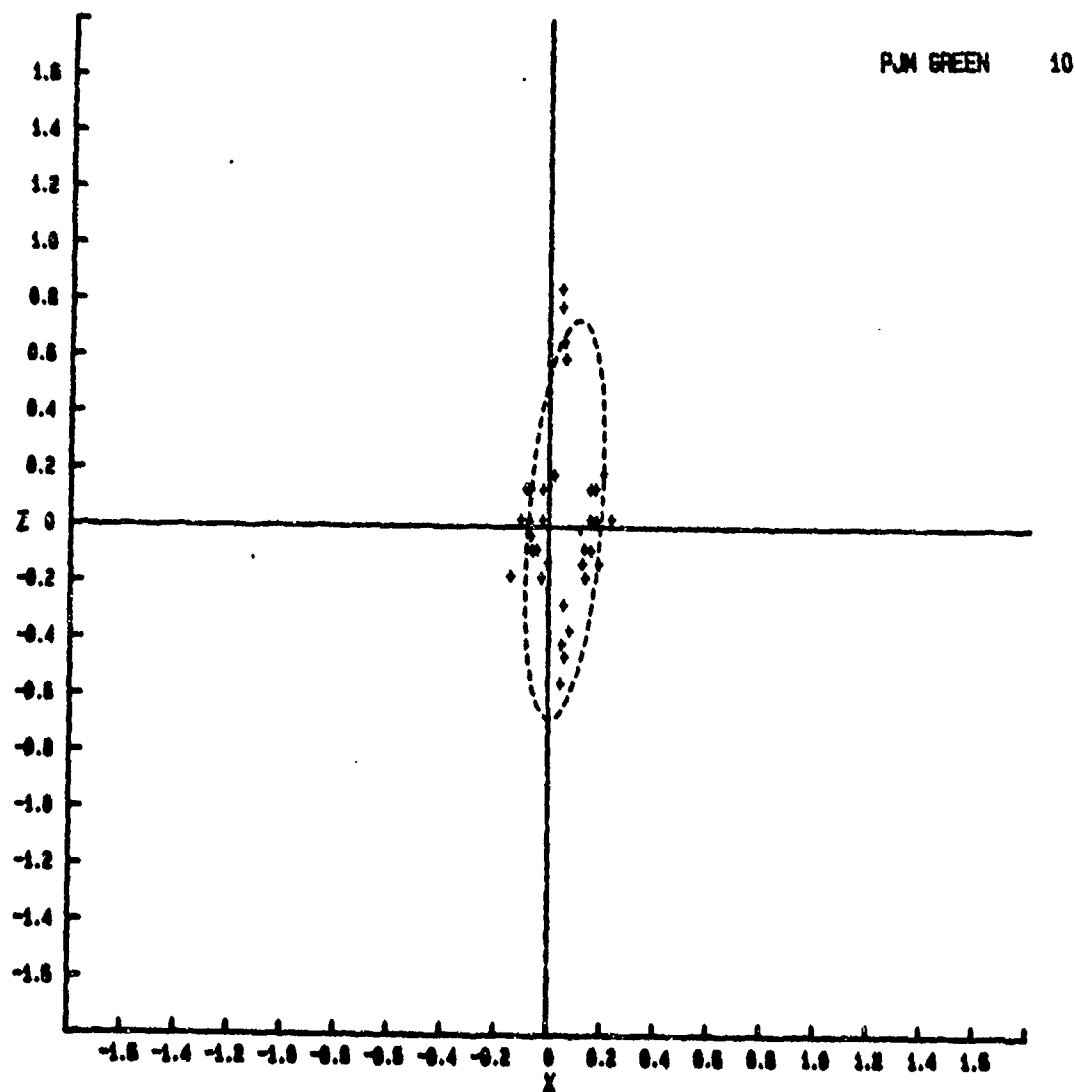


Figure 3. A representative plot of individual threshold deviation points in the isoluminant (XZ) plane together with individually fit ellipse. Data for observer PJM. Targets were 10 minarc, viewed against a green background. See Appendix C, Figures C-12 through C-22 for additional plots.

does vary consistently across different adapting backgrounds or target sizes. The lengths of the semiaxes do not show any strong dependencies on adapting background, but they clearly grow in size as target size is reduced. However, the fitted ellipses did not characterize all data sets as well as expected on the basis of previously reported results.

An examination of Figures C-12 through C-22 suggest that some of the individual data sets are not described very well by ellipses. Two problems are immediately evident. First, the predicted ellipses do not always bisect the data point clusters that arise from repetitions of the same target. Instead, more empirical points seem to fall inside the predicted ellipses than outside. Second, the predicted ellipses for some data sets are rotated slightly, while the data do not seem to reflect a rotation. These problems are most likely due to the asymmetries noted in the raw data for some data sets.

Because of these problems, it seemed unwise to use the parameters of the fit ellipses as the basis for predictive modelling. The alternative to using the fit parameters, as discussed in Section IIIB, is to assume that the rotational angle,  $\theta$ , is 0. This assumption forces the primary response axes  $c_2$  and  $c_3$  to be identical to the primary measurement axes  $X$  and  $Z$ . If this alternative is accepted, then vector lengths that describe thresholds in the response space can be estimated directly from threshold measures along those axes.

How valid is the assumption that the rotational angle is 0? The estimated angles were first subjected to a repeated-measures analysis of variance to determine if systematic differences in the rotational angle occurred as a function of the adapting background or target size. Neither of these variables was found to be significant (all  $p$ 's  $> .10$ ). The data were then collapsed across conditions, revealing a mean rotational angle of 6 deg. No statistical test was performed to determine whether this angle is significantly different from 0 because the variance estimate is based on both within-subjects and between-subjects variation. However, a rotation of 6 deg is very small. Furthermore, as noted previously, the rotation may well be an overestimated due to asymmetries in the data. The assumption that  $\theta = 0$  therefore seems reasonably valid.

It was concluded from the above analyses that the response axes  $c_2$  and  $c_3$  were best represented as being identical to the measurement axes  $X$  and  $Z$  in tristimulus space.

Step 2. Determination of Scaling Parameters. In this step of the analysis, the scaling parameters  $a_{ijk}$  that determine the lengths of the primary response vectors  $d_1$ ,  $d_2$ , and  $d_3$  were estimated. A major component of this step was to determine how the parameters varied with the adapting background and target size, as well as in relation to each other. The analysis was performed twice, using different subsets of data. The main

analysis included only those data from the 6 backgrounds that were equiluminous; it excluded the high- and low-luminance gray backgrounds. This analysis assessed the effects of chromaticity with respect to the background variable. The second analysis included data from all three gray backgrounds, and was performed primarily to verify that our procedures were sensitive enough to isolate small changes of the type expected with luminance variations.

The data used in both analyses were log deviation thresholds for targets that varied along the three primary response axes, X, Y, and Z. Because of the asymmetries noted in the XZ plane threshold contours, "increment" and "decrement" thresholds were treated as two levels of a new variable. That is, thresholds to targets that varied in the +X, +Y, and +Z directions were treated as increment stimuli, whereas thresholds to targets that varied in the -X, -Y, and -Z directions were treated as decrement stimuli. This new variable will be referred to as the "Sign" variable.

The raw deviation data for each individual were first averaged across replications to obtain the most stable threshold estimate. The absolute values of these mean deviations were then log transformed, and used as input to an analysis of variance procedure.

Main Analysis: Equiluminous Backgrounds. The data for the six equiluminous backgrounds were analyzed first in a  $6(\text{Background}) \times 3(\text{Size}) \times 3(\text{Axis}) \times 2(\text{Sign})$  repeated measures design. Data from all five observers were included. The results of the analysis, and the percent variance accounted for by each factor, are presented in Table 1. In this design the Subject factor, and interactions with the Subject factor, cannot be statistically tested, since they are used as error terms for the other effects.

Two main effects, two 2-way interactions, and two 3-way interactions were significant. The majority of the variance in thresholds (52%) was accounted for by the two significant main effects: the size of the target, and the axis of modulation. These two effects were subjected to a series of pairwise comparisons, to determine their nature. For targets that vary along any axis of modulation, threshold is highest for targets that are small, and decreases as target size increases. For targets of any size, threshold is highest to targets that vary along the Z (blue-yellow) axis of tristimulus space. Thresholds are lower to targets that vary along either the luminance axis or the X (red-green) axis of tristimulus space. The latter two thresholds are similar, but the threshold is slightly lower for targets that vary along the X axis.

Although not testable, idiosyncratic factors (Subjects and interactions with the Subject variable) accounted for an additional 34% of the variance. Nearly 10% of the variance was accounted for by the main effect of Subjects, suggesting that subjects primarily differ in their absolute ability to detect

**Table 1. SUMMARY OF EQUILUMINOUS-BACKGROUNDS ANOVA AND  
PERCENT OF VARIANCE ACCOUNTED FOR BY EACH FACTOR.**

<u>Conditions</u>	<u>p values</u>	<u>% variance</u>
SUBJECT	---	9.65
BACKGROUND	NS	.68
SIZE	<.01	28.52
AXIS	<.001	22.99
SIGN	NS	1.24
SUBJECT X BACKGROUND	---	1.32
SUBJECT X SIZE	---	4.78
SUBJECT X AXIS	---	0.35
SUBJECT X SIGN	---	0.80
BACKGROUND X SIZE	NS	0.26
BACKGROUND X AXIS	.001	1.18
BACKGROUND X SIGN	.01	2.10
SIZE X AXIS	NS	0.22
SIZE X SIGN	NS	0.28
AXIS X SIGN	NS	0.13
SUBJECT X BACKGROUND X SIZE	---	1.51
SUBJECT X BACKGROUND X AXIS	---	1.17
SUBJECT X BACKGROUND X SIGN	---	1.54
SUBJECT X SIZE X AXIS	---	0.72
SUBJECT X SIZE X SIGN	---	0.66
SUBJECT X AXIS X SIGN	---	0.42
BACKGROUND X SIZE X AXIS	NS	0.39
BACKGROUND X SIZE X SIGN	<.05	1.44
BACKGROUND X AXIS X SIGN	<.001	5.00
SIZE X AXIS X SIGN	NS	0.59
SUBJECT X BACKGND X SIZE X AXIS	---	2.82
SUBJECT X BACKGND X SIZE X SIGN	---	2.49
SUBJECT X BACKGND X AXIS X SIGN	---	2.10
SUBJECT X SIZE X AXIS X SIGN	---	1.02
BACKGND X SIZE X AXIS X SIGN	NS	0.96
SUBJ X BACK X SIZE X AXIS X SIGN	---	2.69

targets. Although this effect reduces the accuracy in predicting absolute detection levels, it does not affect conclusions about the relative detectability of targets.

Such large individual differences are typical in visual psychophysics, and reduce the predictive power of any model. Individual differences arise from a variety of sources, including sensitivity differences in sensory capabilities and more cognitive factors such as differences in decision rules. These may in turn be differentially influenced by effects such as practice or stimulus uncertainty. The observers who participated in this experiment all had normal acuity and color vision; thus, sensory differences among subjects cannot be easily identified. Analysis of other possible effects are beyond the scope of this project.

Each of the four significant interactions accounts for only a few percent of the total variation. Therefore, although each is statistically significant, none is important for the purposes of prediction. Three of the four significant interactions contain the Sign and Background factors, indicating that they arise from the asymmetries noted in some of the threshold contours. However, the effects are very small and quite complex to interpret. Because no main effect of Sign was found, it is unlikely that these asymmetries arise from some fundamental property of visual processing. Instead, they are likely to be dependent upon very specific stimulus conditions. The fourth interaction, Background x Axis, suggests that thresholds for some axes may change slightly as a function of the adapting background. However, the effect is not large enough to warrant its inclusion in a predictive model, as it accounts for less than 2% of the variance.

A most important finding for the present purposes was that the adapting background was not a significant factor; in fact, it accounted for less than 1% of the variation in thresholds. This result was somewhat unexpected, since previous studies have indicated that chromatic adaptation effects can significantly change the sensitivity of responding mechanisms (MacAdam, 1942; Olzak and Wandell, 1983; Wandell and Olzak, 1983). However, a recent reanalysis of the MacAdam data by Nagy et al. (1987) suggests that the apparent changes in sensitivity are primarily a function of the space in which the data are plotted. The Nagy et al. reanalysis concludes, as we do, that thresholds do not vary across isoluminant regions of color space.

The results of this analysis can be summarized as follows. When backgrounds vary in chromaticity -- but not in luminance -- the two major variables of interest for predictive purposes are: (a) the axis along which a target varies from its background (its  $\Delta X$ ,  $\Delta Y$ , and  $\Delta Z$  values), and (b) the size of the target. These two effects account for over 50% of the variance. Idiosyncratic factors (subject effects) contribute significantly to variation in thresholds; when these are included, over 85% of the variance can be accounted for. Subject effects, however, are

not easily predicted from standard measures of color vision or acuity, and thus cannot be readily included in a predictive model. Result (a) implies that the actual chromaticity of the background is of no importance; it is only the deviation of the target from the background that is predictive. Result (b), together with the fact that the Axis x Size interaction was not significant, indicates that each of the primary response vector lengths increases with decreasing target size at the same rate. That is, the spatial summation function for the three primary response mechanisms is the same.

Interpretation of Results from Main Analysis. Result (a) above can be restated as suggesting that for a given background luminance level, the three dimensional response surface to targets that vary in all directions of color space has the same shape across all chromaticity regions and target sizes. For a target of a given size and for backgrounds in any isoluminant plane of color space, the shape, size, and orientation of the response surface is identical across various regions of color space. The axis of least sensitivity (major axis) lies along the Z axis of tristimulus space. The X and Y axes yield response vectors of approximately equal length (slightly shorter along the X axis), and both are shorter than the Z axis. Thus, sensitivity is about equal for targets that vary only in luminance and targets that vary along an approximately red-green axis, and is better than sensitivity to targets that vary along an approximately blue-yellow axis of modulation. Furthermore, as the target size decreases, the response surface grows but maintains the same constant shape.

These results are evident in Figures 4 through 6, which plot the three two-dimensional slices of the response surface (averaged across observers) for one adapting field. The remaining conditions are presented in Appendix C, Figures C-23 through C-37. It can be seen in these figures that for any given plane, the shape and orientation of the response contours are quite similar, while the dependency upon size is regular and independent of background field.

In terms of model parameters, the results of this analysis indicate that the scaling parameters  $a_{jk}$  differ for the three different response axes, and depend upon the target size. However, the effect of the target size is the same for all axes, indicating that axis and size are separable dimensions. This point is taken up again in Section V, where the estimated values of  $a$  are presented.

Secondary Analysis: Luminance Variations in Backgrounds. It is known from previous research results that the spatial summation function does vary with the luminance of the adapting field. However, this effect is primarily of importance at very low luminance levels, where color vision itself deteriorates and where the results of the present study would not be expected to



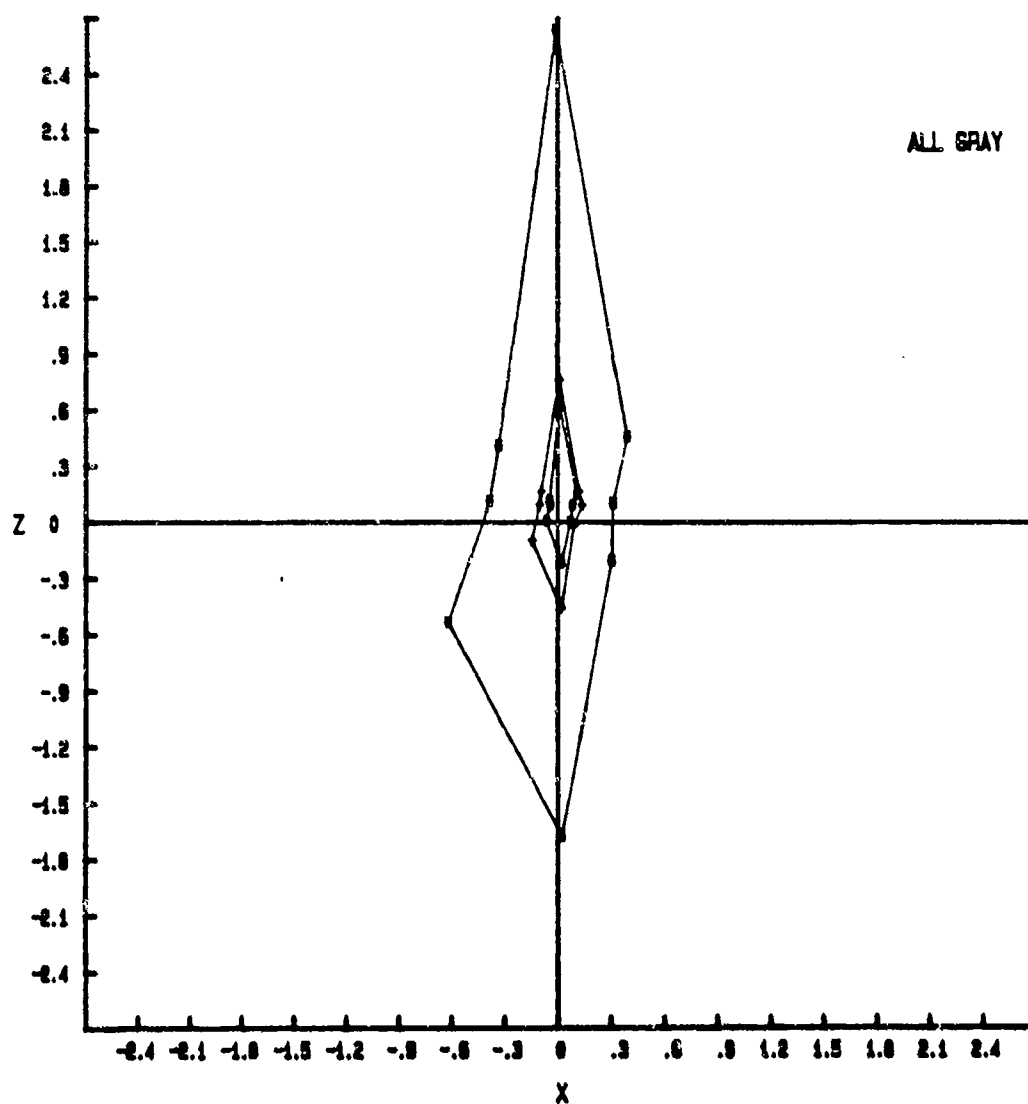


Figure 4. A two-dimensional slice of the three-dimensional response contour obtained for the standard-luminance gray background. This plot shows contours that result from targets varying only in chromaticity (the XZ plane). The figure plots the three contours for different target sizes; larger contours result from smaller targets, indicating the need for greater target contrast. Points are averaged over five observers and five replications. See Appendix C, Figures C-23 through C-27 for additional plots.

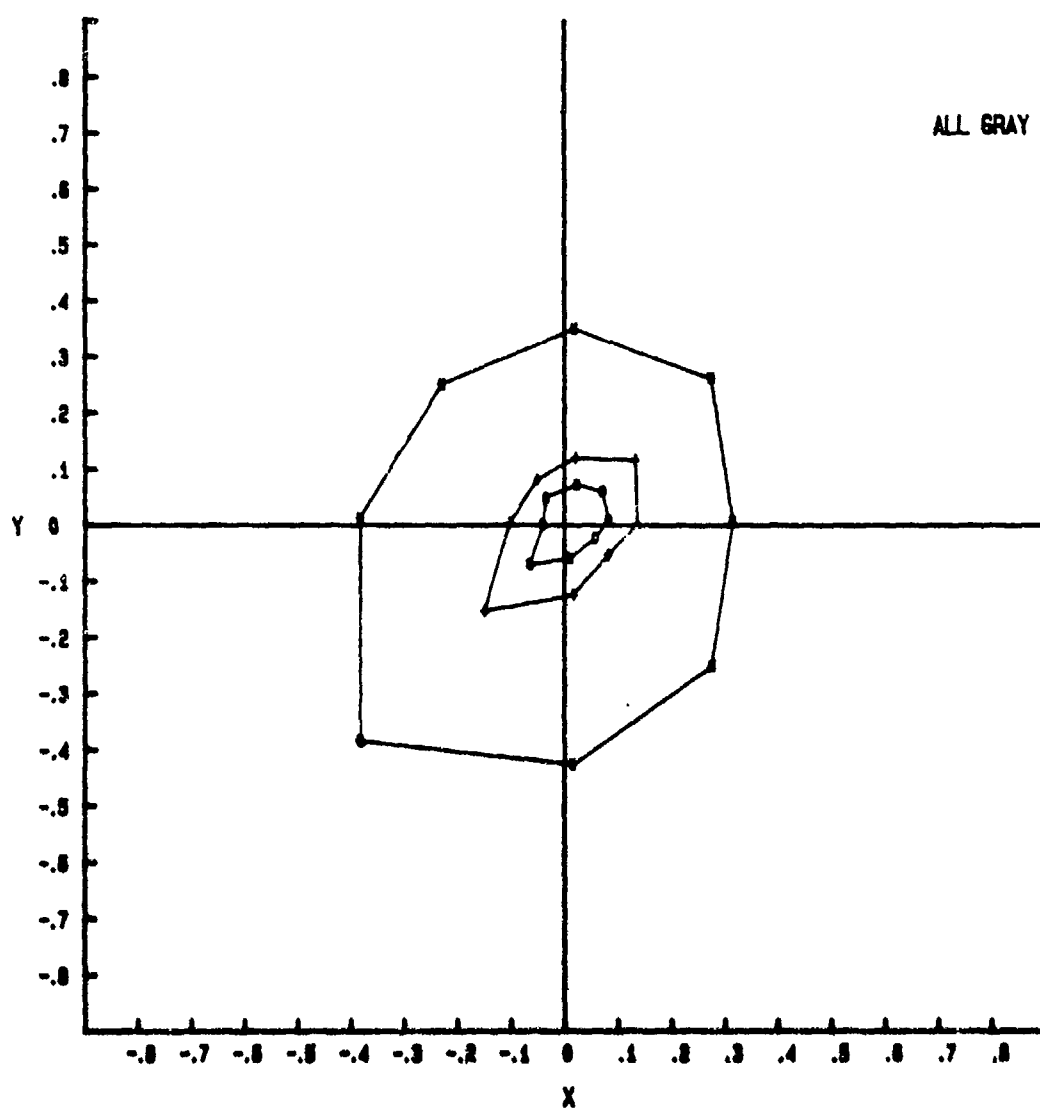


Figure 5. A two-dimensional slice of the three-dimensional response contour obtained for the standard-luminance gray background. This plot shows contours that result from targets varying in luminance and chromaticity along the X-axis (the XY plane). The figure indicates the three contours for different target sizes; larger contours result from smaller targets. Points are averaged over five observers and five replications. See Appendix C, Figures C-28 through C-32 for additional plots.

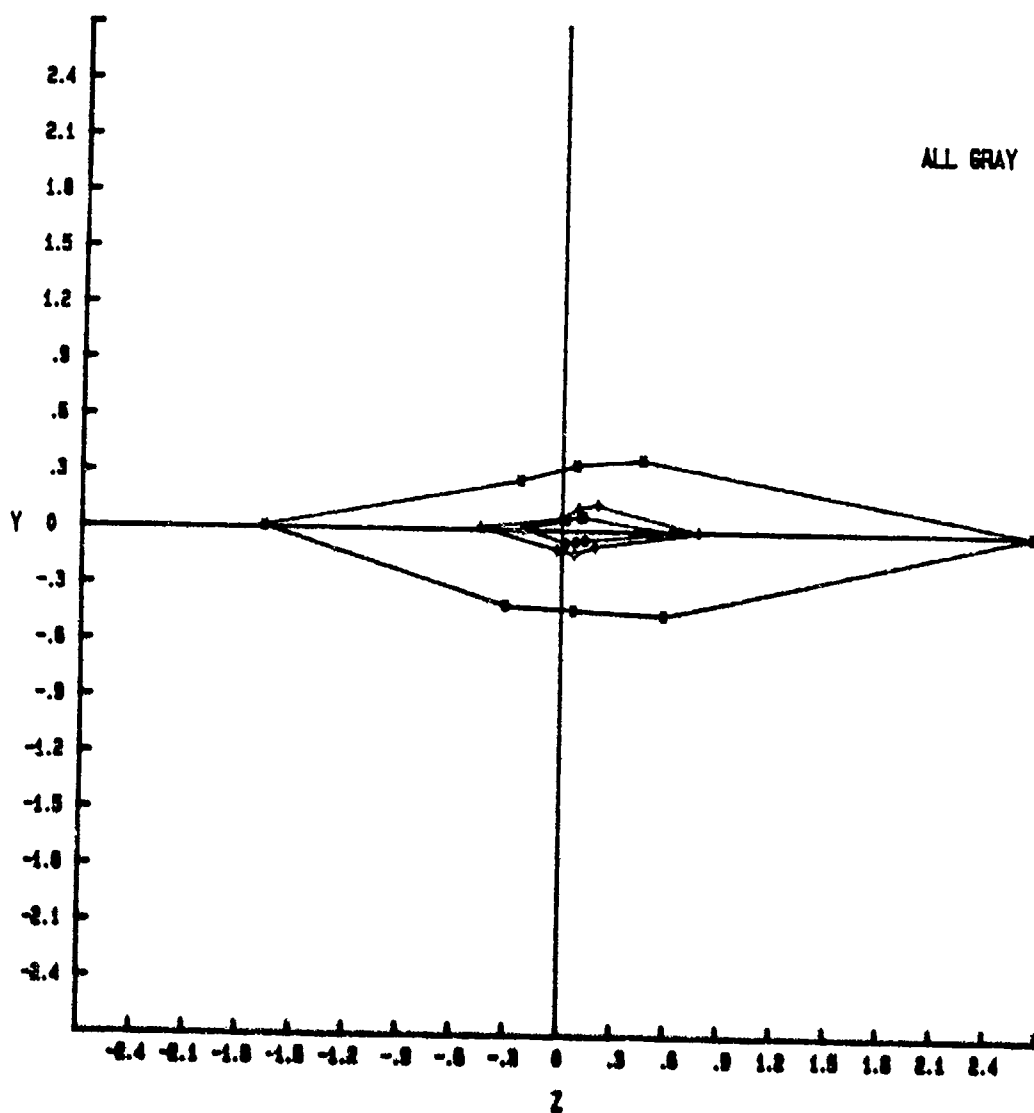


Figure 6. A two-dimensional slice of the three-dimensional response contour obtained for the standard-luminance gray background. This plot shows contours that result from targets varying in luminance and chromaticity along the Z-axis (the YZ plane). The figure indicates the three contours for different target sizes; larger contours result from smaller targets. Points are averaged over five observers and five replications. See Appendix C, Figures C-33 through C-37 for additional plots.

hold (See Blackwell, 1946; Hood and Finkelstein, 1986). At the higher luminance levels typical of daylight conditions (the luminance levels used here), the effect is very small.

Despite the small effect of background luminance, this variable was briefly assessed in the current study. In part, the inclusion of this variable serves as a way of assessing how sensitive our study was to small background effects. This is of particular importance in assessing the validity of the conclusion that the chromaticity of the background field is not a significant variable.

The analysis described above was repeated for data collected on the three gray backgrounds that differed only in luminance. As in the main analysis, target size and axis of modulation were found to be significant factors and account for a major portion of the total variance. Thresholds changed across levels of these variables in the same way as in the main analysis. Thus, the main conclusions of the study hold at slightly higher or lower luminance levels.

As expected, background luminance was found to be a significant factor. In general, thresholds increased for targets viewed against a higher-luminance background field. Despite their significance, these changes were very small, accounting for only a small percentage of the variance. This result indicates two things. First, the data generated by the experimental procedures and the analyses performed were indeed sensitive enough to indicate statistically significant differences across backgrounds in which they were expected to exist. This suggests that the lack of significance found with chromatically varying backgrounds is real; it is not due simply to a lack of power in the statistical test, nor is it due to noise in the data. The second implication of this result pertains to the small magnitude of the effect. Across the range of luminance levels likely to be encountered in daylight conditions, only small variations in thresholds are to be expected. In other words, within the range of photopic luminance conditions expected for daylight viewing, the luminance of the background is not an important predictive variable.

Two interactions were found to be significant in this secondary analysis: Background x Size, and Background x Sign. The first interaction reflects the small changes expected in spatial summation as a function of background luminance level, while the second interaction suggests that the small asymmetries noted in the data change character with the luminance level. However, since neither interaction contributes significantly to the amount of variance accounted for, both can be safely ignored for predictive purposes.

Step 3. Combining Rule for Chromatic and Luminance Information: Estimation of the Combining Exponent  $p$ . The third step in the analysis concerned the determination of the exponent  $p$ .

Subjects can detect a stimulus when its distance from the background color exceeds some criterion. Equation 17 of section IIIB states that for targets that vary in both luminance and chromaticity (along either two or three axes in tristimulus space), this distance is obtained by combining the deviations of the stimulus from the background in the X-, Y- and Z-directions of CIE color space, using with a combining parameter of  $p$ . The value of  $p$  is unknown, but can be estimated from the available data. This requires finding the value of  $p$  for which the predicted and actual values of  $dt$  best agree with each other.

Only a few values of  $p$  are theoretically meaningful. If  $p=1$ , subjects are using the "city-block" method to combine the X-, Y- and Z-deviations. If  $p=2$ , subjects are using a Euclidean combining rule. If  $p=3$  or  $p=4$ , subjects are using some form of probability summation. Larger values of  $p$  suggest that subjects are not combining the distances at all; instead, they are simply attending to a single dimension (e.g., just the X-deviation). If subjects attend to a single dimension on each trial, but vary the particular dimension that is attended to from one trial to the next, probability summation results (see Olzak and Thomas, 1986).

It is assumed that the actual value of  $dt$  at threshold is unity, after the data have been normalized. The threshold data can therefore be used to estimate  $p$ , by selecting the value of  $p$  that yields either the smallest mean-squared deviation of the predictions from unity (i.e., the smallest mean-squared error), or the smallest mean absolute deviation of the predictions from unity, or the smallest overall deviation of any given prediction from unity. Other measures that can be used to evaluate the predictions from a given value of  $p$  include the mean prediction (which should be unity), and the variance of the predictions (which should be at a minimum).

The above measures were used to find the best value of  $p$  for each background color and target size. A separate prediction was made for each of the 26 stimuli (i.e., each direction). The overall accuracy of the predictions was then assessed using each of the measures described above. No pattern was evident: the best value of  $p$  varied in a nonsystematic fashion from one background to another, and from one target size to the next. The results also varied, depending upon the particular measure that was used to assess the accuracy of the predictions.

The logarithms of the predictions were then taken, to find the value of  $p$  that produced the logarithms that were closest to zero (since the logarithm of unity -- the expected prediction -- is zero). Once again, no pattern was evident: the best value of  $p$  varied in a seemingly haphazard fashion with the background color, the target size, and the particular goodness-of-fit measure that was adopted. This suggested that little could be gained by treating each background color and target size

separately. Furthermore, the best value of  $p$ , as determined by the closeness of the predictions to unity, often differed from the best value of  $p$ , as determined by the closeness of the logarithms of the predictions to zero, indicating that the sample sizes were too small to obtain stable estimates of  $p$  for each background color and target size.

The data from all backgrounds and target sizes were therefore combined. The best value of  $p$  was then estimated from this combined data set. All goodness-of-fit measures indicated that the best value for  $p$  was  $p=3$ . This result was obtained both for predicting the raw values of  $dt$ , and for predicting the logarithms of  $dt$  (Figure 7). Subjects therefore appeared to be using some form of probability summation in responding to deviations in the X-, Y- and Z-directions.

### C. EXPERIMENT II

The second experiment was performed to provide information needed to estimate the relationship between detection performance and some measure of stimulus strength (the psychometric function). These data lead to estimates of the parameter  $g$  in Eq. [18] of Section IIIB. Several stimulus conditions were evaluated to determine how the value of the exponent varies with the background, target size, and response axis.

#### Methods

A signal detection rating experiment was performed to provide precise estimates of the relative detectability of two targets that varied along a single primary axis in tristimulus space. The targets differed only in contrast along that axis; i.e., either in X, Y, or Z. The relationship between the physical contrast of the stimuli and measured performance levels provided estimates of the slope of the psychometric function. Estimates were taken for stimuli that varied along each of the three primary axes in the response space; i.e., the +Y axis for targets that varied in luminance only, or in one of two directions of the chromaticity plane (+X or +Z). The psychometric functions for each of these axes was further assessed on two different backgrounds, and with two different target sizes.

Observers. Two of the observers from Experiment I -- PJM and NT -- served as observers in this second experiment.

Stimuli. The stimuli were generated and configured as described in Experiment I. The gray and turquoise adapting backgrounds from that study were used, at the standard luminance level of  $18 \text{ cd/m}^2$ . Stimuli appeared at one of two target sizes (3 minarc or 30 minarc), and varied from the background along one of the three primary axes: luminance only, X, or Z. For each of the 12 target size/background/axis combinations, two targets were used

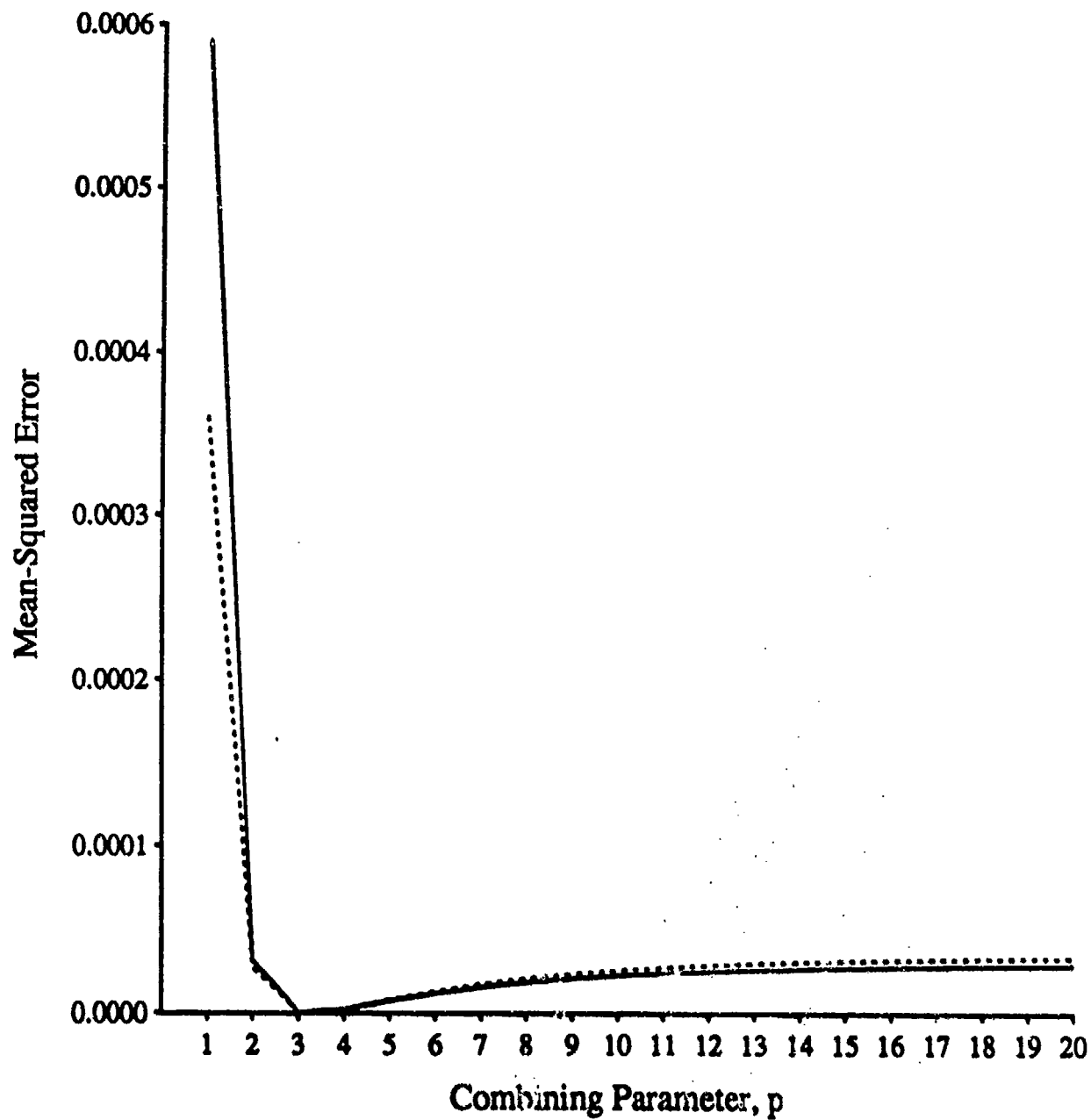


Figure 7. Mean-squared errors for different values of the combining parameter,  $p$ . The best fit (i.e., the minimum mean-squared error) occurs at  $p=3$ , both for predicting  $d_t$  (solid line) and for predicting the logarithm of  $d_t$  (broken line).

that differed in their contrast values along the axis. Contrast values were chosen individually for the two observers for each of the 12 conditions. The lower-contrast value was chosen to yield an area under the ROC curve of about 0.6, whereas the higher-contrast value was chosen to yield an area of about 0.9.

Procedures. In each experimental session, only a single adapting background, target size, and axis of modulation was used. The high and low contrast targets for that axis were intermixed with noise trials in a single session. Each observer participated in each of the 12 experimental conditions, and performed five replications of each condition.

Each session consisted of 150 trials. On 50 of the trials, no stimulus was presented (Noise). The remaining 100 trials were equally divided between the high-contrast target and the low-contrast target. Trial types were randomly intermixed throughout the session.

As in Experiment I, each session began with a two-minute adaptation period, followed by a preview condition. At the observer's signal, the series of 150 trials began. Each trial consisted of a 1-second period, during which a tone sounded, and one of the two signals (or noise, on blank trials) was presented concurrently. At the offset of the tone, there was a 2-second period of silence during which the observer responded. The next trial was then signalled by another tone. If no response was recorded during the 2-second period of silence, the trial was ignored and presented again at a later time in the session. Trials continued until 50 responses to each of the three trial types were made.

The observer's task was to rate, on a 6-point scale, his or her certainty that any target had been presented. A "1" rating indicated certainty that no target had been presented (Noise), whereas a "6" rating indicated certainty that one of the two targets had been presented.

The distribution of responses to each of the two target types was used, together with the distribution of responses to the noise trials, to generate an ROC curve for each target (see Green and Swets, 1964). The area under the ROC curve is a measure of detectability that approximates the proportion correct in a 2-alternative forced-choice experiment. ROC areas can range from 0 to 1.0 (perfect detectability); an ROC area of 0.5 corresponds to chance performance.

## Results

The normal transform of the area under the ROC curve (the z-score corresponding to the area) was used as the basic measure of detection performance. Stimulus contrast was measured as the difference between the target and the background along the relevant axis (e.g.  $X - X_1$ , or  $\Delta X$ ) in tristimulus coordinates. From each session, two target contrasts ( $\Delta i_{hi}$  and  $\Delta i_{lo}$ ) and



their corresponding performance levels ( $z(A)_{hi}$  and  $z(A)_{lo}$ ) were used to estimate  $g$ , which is the slope of the function relating detection performance to target contrast. The formula for  $g$  is

$$g = \frac{\log z(A)_{hi} - \log z(A)_{lo}}{\log \Delta i_{hi} - \log \Delta i_{lo}} .$$

The  $g$  parameter was calculated separately for each observer and each replication of the 12 experimental conditions, yielding 120 different estimates of  $g$ .

In one condition (modulation along the Z axis with the 3 minarc target on the turquoise background), neither observer could perform the detection task beyond a chance level at any contrast level obtainable by the equipment. The  $g$  parameter could not, therefore, be estimated for this condition. This reduced from 120 to 110 the number of estimated  $g$  parameters that could be analyzed.

An analysis of variance was performed on these data to assess the effects of background, target size, and axis of modulation on the slope. In order to obtain an estimate of interobserver variability, the analysis was performed as a 2(Subjects)x2(Background)x3(Axis)x2(Size) independent-measures analysis, with subjects as a random factor.

The results of this analysis, together with the percentage of variance accounted for by each effect, are shown in Table 2. No important effects were found to be significant, indicating that the slope of the psychometric function is constant across all the experimental conditions that were investigated. Both observers showed the same results.

Three higher-order interactions were significant. However, these were not considered to be important results for two reasons. First, each of the significant interaction terms contained the subject variable, indicating that the effects were idiosyncratic and unpredictable. Second, although the effects were statistically significant, none accounted for more than 3% of the variance. Thus, these effects were discounted for predictive purposes.

Since none of the important effects were significant, the single best estimate of  $g$  is obtained by simply averaging all 110 estimates. This yields a value of  $g=1.34$ .

Table 2. SUMMARY OF Q-ESTIMATE ANOVA AND PERCENT OF  
VARIANCE ACCOUNTED FOR BY EACH FACTOR.

SOURCE	p values	% variance
SUBJECT	NS	0.79
BACKGROUND	NS	15.48
AXIS	NS	11.74
SIZE	NS	0.11
SUBJECT X BACKGROUND	NS	0.39
SUBJECT X AXIS	NS	1.41
SUBJECT X SIZE	<.007	2.45
BACKGROUND X AXIS	NS	8.99
BACKGROUND X SIZE	NS	0.36
AXIS X SIZE	NS	9.62
SUBJECT X BACKGROUND X AXIS	NS	1.09
SUBJECT X BACKGROUND X SIZE	<.005	2.84
SUBJECT X AXIS X SIZE	<.013	2.89
BACKGROUND X AXIS X SIZE	NS	13.20
SUBJECT X AXIS X BACK X SIZE	NS	1.59
WITHIN CELL	---	27.04

## V. FINAL MODEL AND GUIDE TO ITS USE

### A. THE MODEL

#### Overview

In this section, the interpreted results of the empirical studies are applied to the general model developed in Section III, the parameter estimates are given, and a final equation is presented. The equation represents a single quantitative statement that describes the interrelationships among target detectability, target size, target luminance and chromaticity, and background chromaticity at photopic luminance levels. In this form, the equation predicts the relative detectability of various targets. A second form of the equation is derived in order to use these interrelationships to predict the distance at which an arbitrary target will be detected with some probability. We conclude the presentation with an example demonstrating the use of the predictive forms and the results of a short validation study.

#### Parameter Estimates

The general model can be expressed in its most explicit form by combining Eqs. [17] and [18] from Section IIIB and adding the subscripts omitted in that section:

$$z(\text{detect}) = b \times \{ [(a_{ij2} \times c_{ij2})^2 + (a_{ij3} \times c_{ij3})^2]^{p/2} + [a_{ij1} \times c_{ij1}]^p \}^{q/p} \quad [19]$$

where  $i$  is a subscript denoting background chromaticity,  $j$  is a subscript denoting target size, and  $k$  is a subscript (here explicitly taking the values 1, 2 and 3) that denotes the direction of the response axis. The use of the subscripts  $i$  and  $j$  implies that each of the parameter values may be dependent upon particular combinations of the background and target size. The parameter  $b$  is a multiplicative scaling factor (here taken to be 1.0) that depends upon the psychophysical task and the observer's criterion.

As indicated in Section III, the general model requires 9 parameters (and an estimate of  $b$ ) to fully interrelate the variables of interest: identification of the three primary response axes  $c_1$  (defined in Eq. 7), and  $c_2$  and  $c_3$ , which depend upon the angle  $\theta$ ; the value of the scaling parameters  $a_{..k}$ ; the value of the combining exponent  $p$ ; and the value of the slope of the psychometric function  $q$ . In the general model, each of these potentially takes different values, depending upon the particular combination of background and target characteristics.

The results of our studies indicate that such complexity is not necessary; many of the parameter values are constant across

all conditions, and others can be separated into independent dimensions. In this section, each of the 9 parameters is considered in turn, and the estimated values presented. For convenience, the values are summarized in Table 3.

Response Axes c1, c2 and c3 and the angle  $\theta$ . The empirical results of our studies indicate that the response space is not rotated from the tristimulus measurement space in any region of color space; the two spaces are isomorphic. Thus, angle  $\theta$  is estimated to be 0, and the primary response axes correspond to the measurement axes of tristimulus space: X, Y and Z. The response axes c1, c2 and c3 can be specified simply as  $\Delta Y$ ,  $\Delta X$  and  $\Delta Z$ , as shown in Eqs. [7], [8a], and [9a] of Section IIIB. These values are measured stimulus characteristics that characterize the contrast of the target (the difference between the target and background in tristimulus units) in three dimensions: luminance (c1) and two chromatic dimensions (c2 and c3).

Scaling Parameters  $a_{ijk}$ . As shown in Eqs. [13], [14], and [15] of Section IIIB, the values of these parameters are estimated from the threshold  $\Delta X$ ,  $\Delta Y$  and  $\Delta Z$  values of targets that vary only along the X, the luminance, and the Z axes in tristimulus measurement space. The value estimated for each response axis is determined by the reciprocal of the relevant threshold delta. In turn, the threshold values may depend upon the background chromaticity, the target size, or unique combinations of the two.

The empirical results indicated that log threshold values depended only upon the response axis and target size. These two dimensions are separable; that is, they do not interact. This result indicates that all values of the parameter  $a_{ijk}$  can be expressed as the product of only two terms, a size-dependent term ( $a_{.j.}$ ) and an axis-dependent term ( $a_{.k.}$ ).

The first term,  $a_{.j.}$ , takes on different values depending upon only the retinal size of the target. It does not depend upon the background or axis, and is therefore best estimated from data collapsed over these two variables. The functional relationship between target size and the parameter  $a_{.j.}$  is calculated for the three empirically measured target sizes according to Eqs. [13], [14], and [15] of Section IIIB, and scaled for mean detectability level. The three estimates for  $j=3$  minarc, 10 minarc, and 30 minarc are, respectively, .381, 1.097, and 2.368. Other values of  $a_{.j.}$  are given by linear interpolation among the empirically determined values (see Eq. [27]). The values used in Eqs. [27] reflect the most useful range of target retinal angles. Below 3 minarc (.05 deg), performance is limited by resolution factors, and only very high-contrast targets will be detectable. Above 30 minarc (.5 deg), performance will be close to perfect for targets that vary only minimally from the background; that is, within the limits of measurement error.

### Summary of Model Parameters

$$\Delta Z = Z - Z$$

$q = 1.34$

The second term,  $a..k$ , depends only upon the axis. In the model, there are only three primary axes of interest. Thus, only three values of this term must be specified. These are estimated directly from empirical data collapsed over the background and size variables. Because the  $a..k$  parameter terms are defined as the reciprocal of threshold contrast along a given axis, they are measures of sensitivity. The larger the value of the  $a..k$  term, the greater the sensitivity. The relative values of the three terms provide information about relative sensitivity to stimuli that vary along the primary axes.

The axis of least sensitivity is the  $c3$  axis, corresponding to modulation along the approximately blue-yellow  $Z$  dimension in tristimulus space. The corresponding  $a..3$  value has a value of 2.1. The remaining two axes,  $c1$  and  $c2$ , yield much greater estimates of sensitivity. For targets that vary only in luminance, the corresponding  $a..1$  value is 8.8. For targets that vary along the  $X$ -axis of tristimulus space, the corresponding  $a..2$  value is 9.2. This axis of greatest sensitivity is approximately a red-green axis of modulation. The color plates of Figures 8 through 13 show actual response contours for six backgrounds, plotted in the  $XZ$  plane of tristimulus space. The axis is printed in the color of the adapting background; threshold points are plotted in the color of the target (at a high contrast value for clarity).

Value of the Combining Exponent  $p$ . The value of the exponent that describes information combination between chromatic and luminance axes was found not to depend upon either background or target size. Thus, a single estimate of the exponent  $p$  suffices. This value was found to have the value 3.0. A value of 3 indicates that information is not combined across the luminance and chromatic axes except for probability summation.

Value of the Slope of the Psychometric Function  $q$ . The results of Experiment II indicated that the slope of the function that relates target contrast to the level of detection performance does not vary with background, target size, or axis. Thus, a single value suffices for the slope of the psychometric function. This slope was found to have the value 1.34.

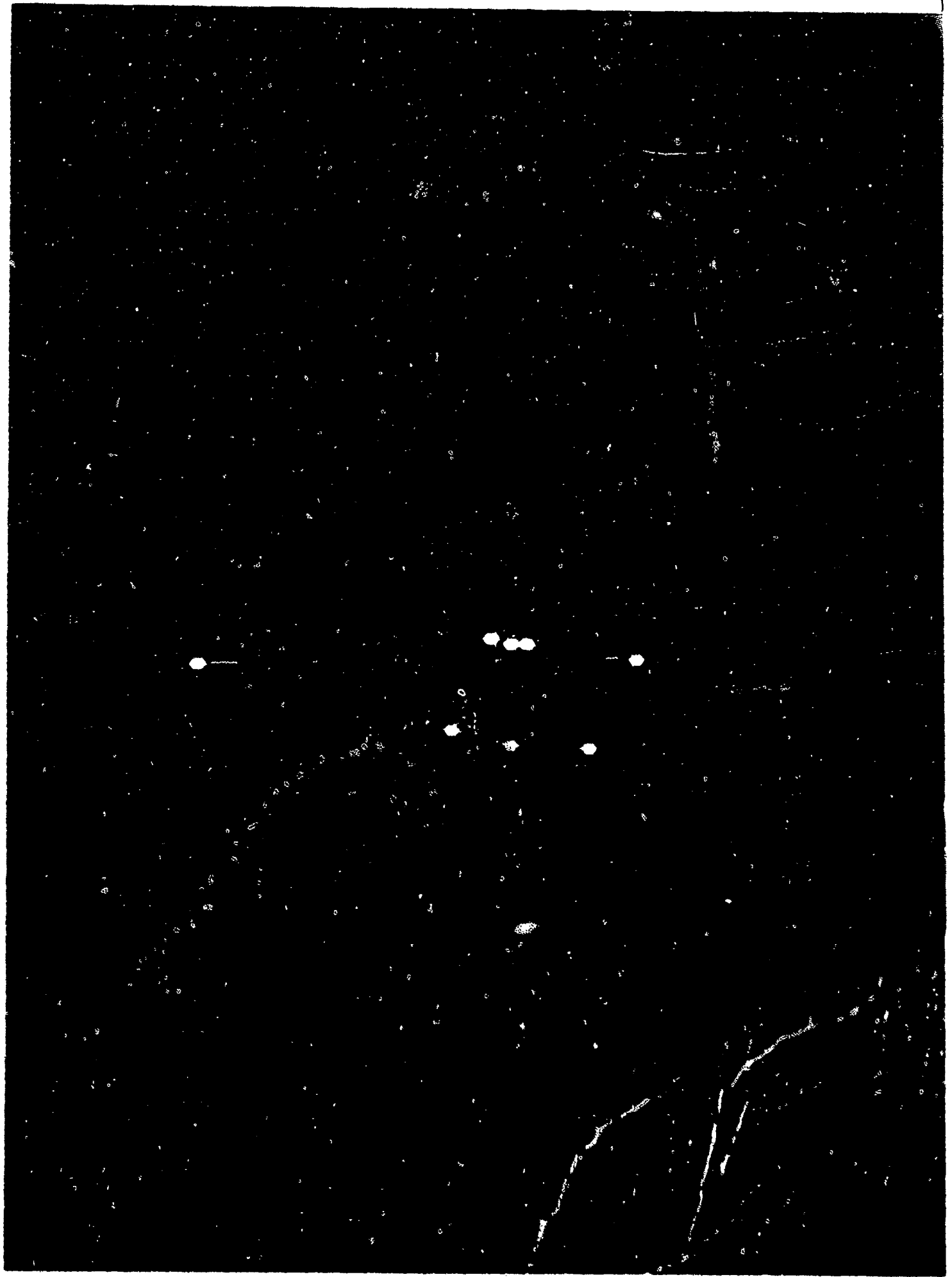
#### Predicting detectability of a Target

The general form of the model given in Eq. 19 can be reduced to a final form that incorporates the empirical results reported here:

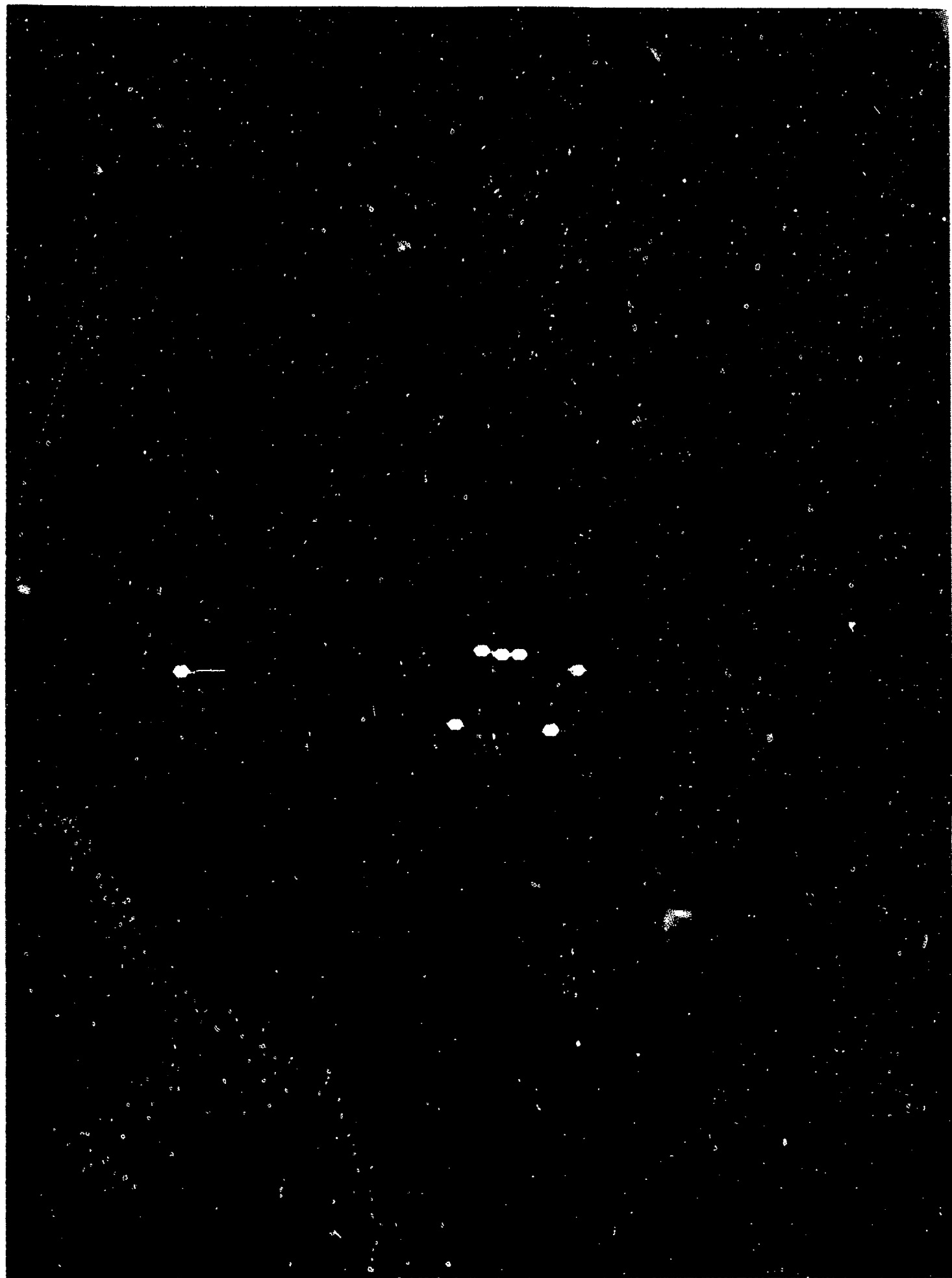
$$s(\text{detect}) = b \times \{ [(\Delta x \times a..2 \times a..j.)^2 + (\Delta z \times a..3 \times a..j.)^2]^{p/2} + [\Delta y \times a..1 \times a..j.]^p \}^{q/p} \quad (20)$$

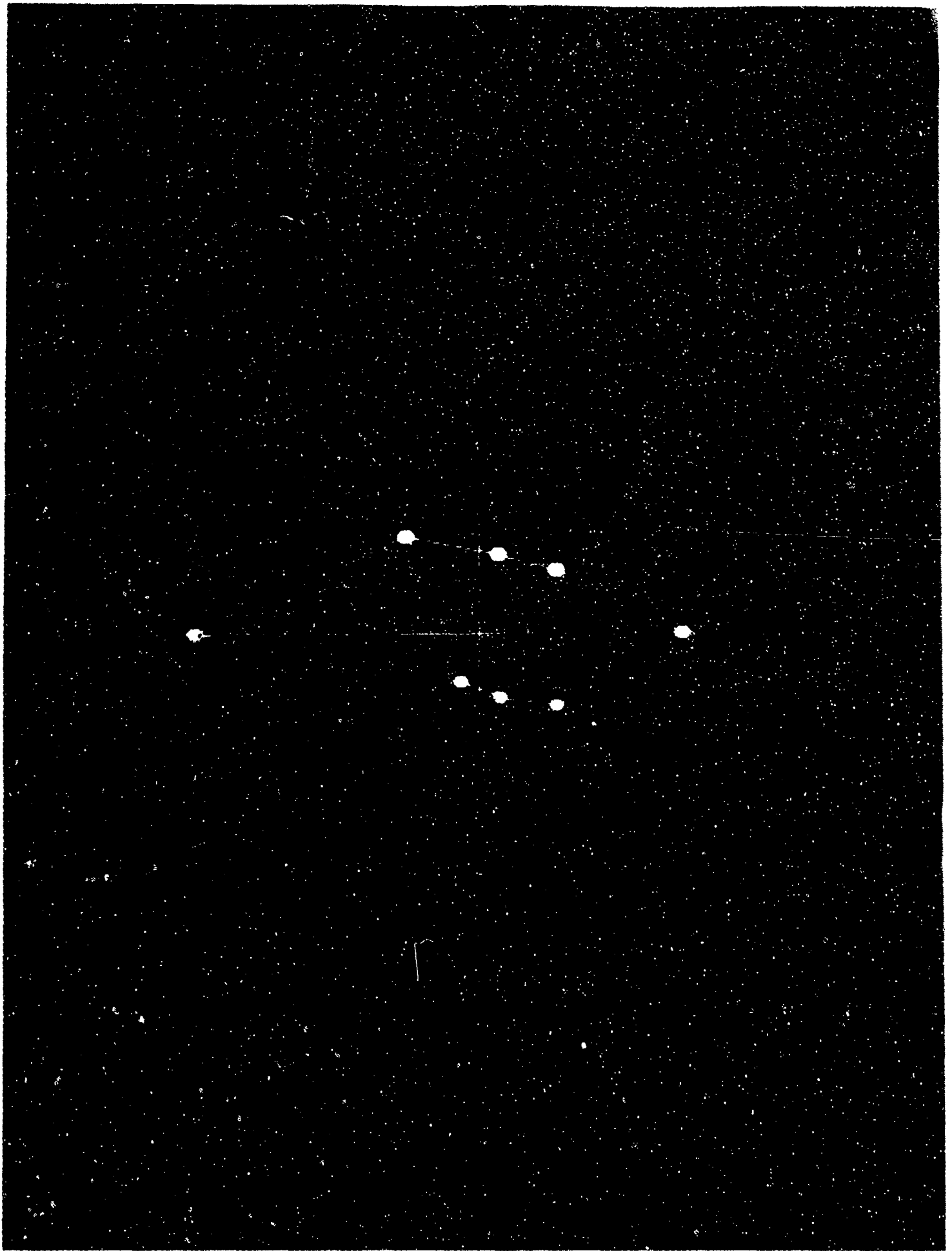
Figures 8 through 13. Color plates indicating shapes of threshold contours for targets that vary in the isoluminant (XZ) plane. Axes are plotted in the hue of the background field, whereas each point is plotted in the approximate hue of the target (at a high-contrast value). Note that some chromatic resolution has been lost in the photographic process. Data are for 3-minarc targets, but represent typical contour shapes for targets up to 30 minarc. Each point is the average of five observers and five replications.

These plates correspond to the 3-minarc contours shown in Figure 4 and Figures C-23 through C-27. To view, they should be rotated 90 degrees such that the bound edge is at the top. In this orientation, the vertical axis is Z (the axis of poorest discrimination and hence the major axis of the contour); the horizontal axis is X. Targets that increased in X and Z values are plotted to the right and top of the origin, respectively.

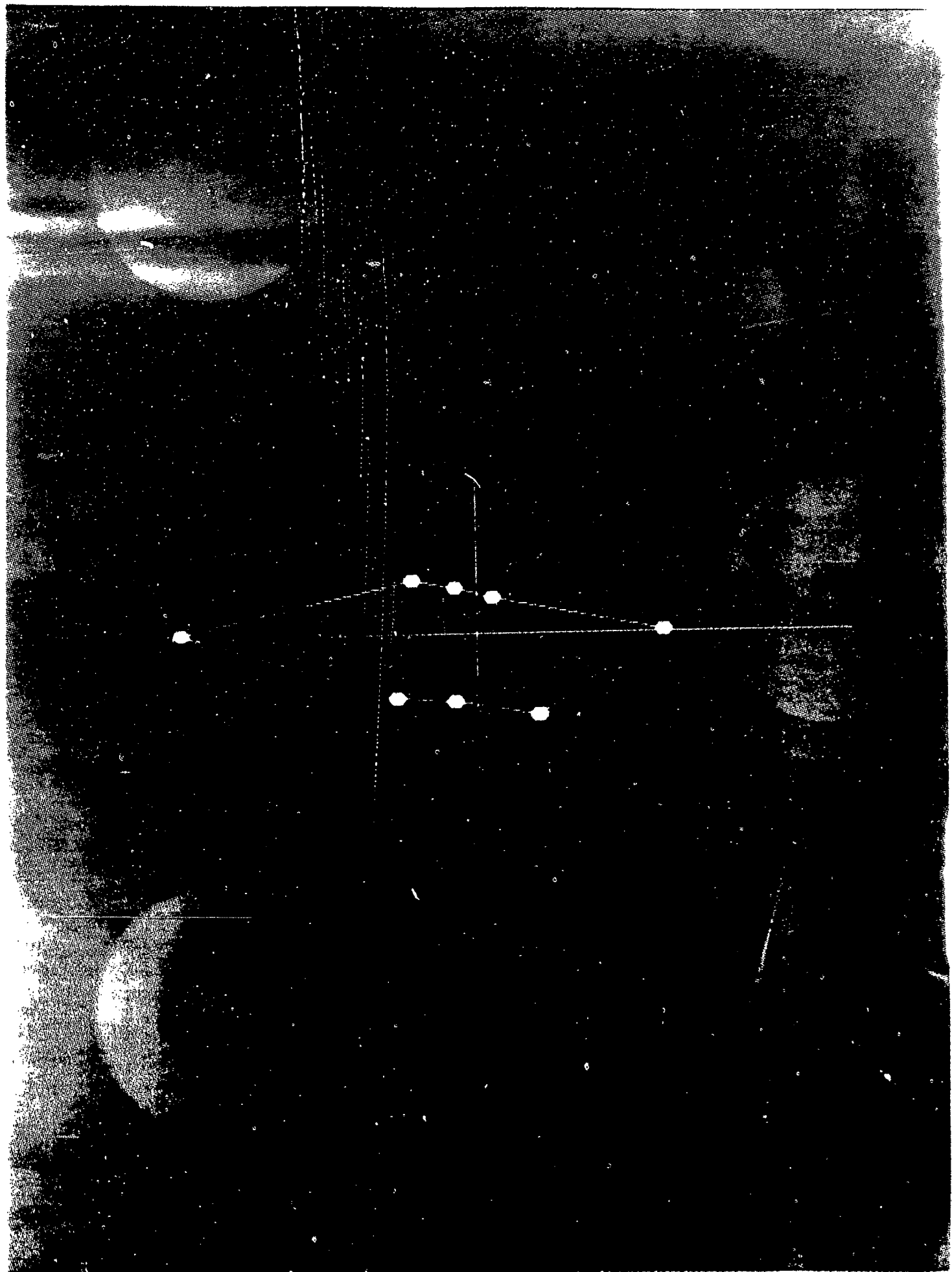


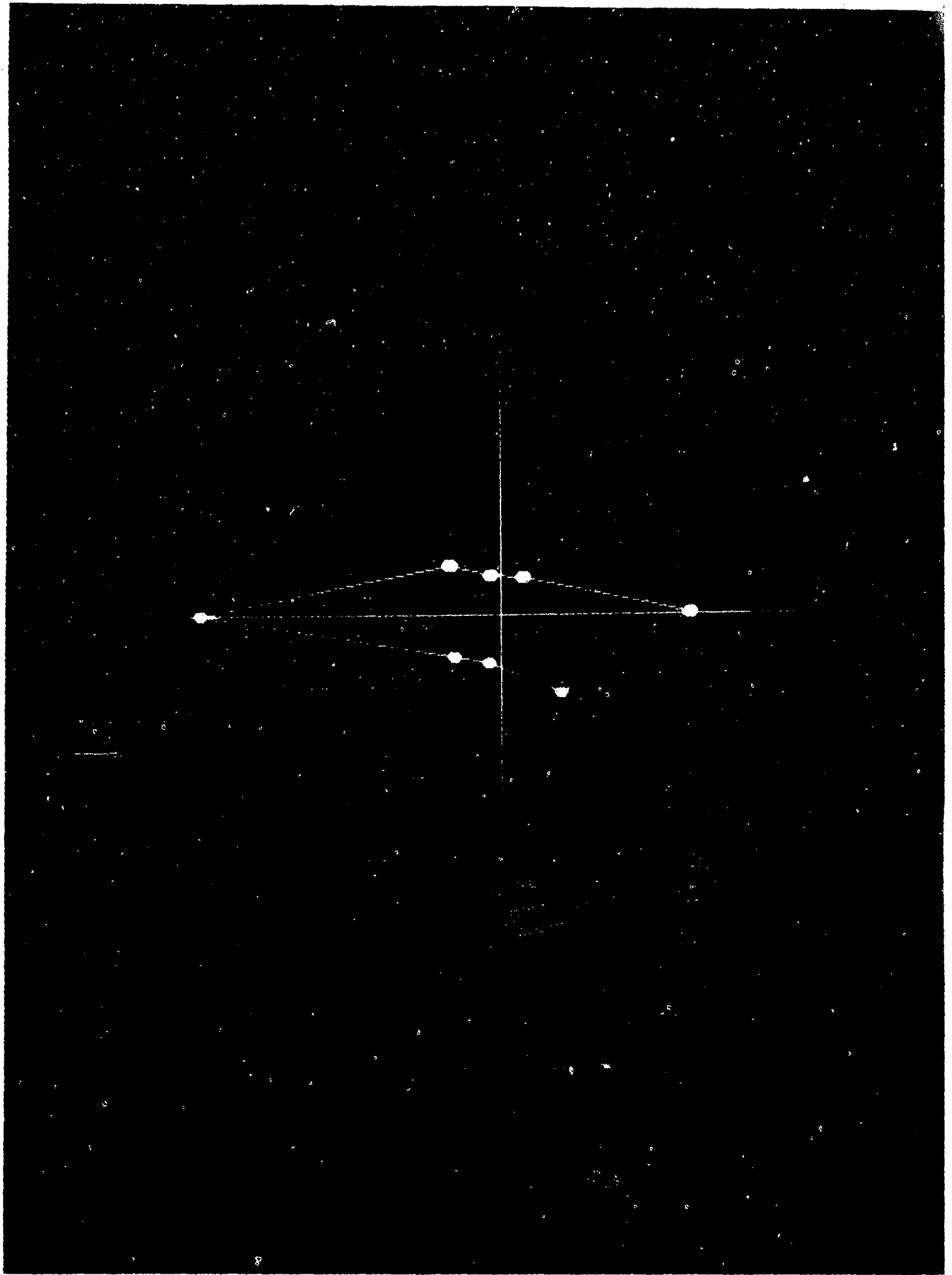












This model states that the detectability of a given target can be predicted (within a scale factor  $b$ , here assumed to be 1.0) by assessing the contrast of the target in  $\Delta X$ ,  $\Delta Y$  and  $\Delta Z$  coordinates, and by specifying the retinal size (in degrees of visual angle) of the target, which in turn determines the value of  $a.j.$ . The remaining parameter values are constants taking the values summarized in Table 3.

### Predicting Detection Distance

A second form of the model may be obtained by rearrangement of Eq. [20] in order to solve for the distance at which the target will be detected with a specified probability. In this form, the equation predicts an  $a.j.$  value:

$$a.j. = \frac{[z(\text{detect}) / b]^{1/q}}{[(\Delta x \times a_{..2})^2 + (\Delta z \times a_{..3})^2]^{p/2} + [\Delta y \times a_{..1}]^p]^{1/p}} \quad [21]$$

The calculated  $a.j.$  value can then be related to retinal size of the target by linear interpolation between measured points, and easily converted to viewing distance for a target of given diameter. As before, these will be relative distances. Determination of the parameter  $b$  is necessary for absolute prediction.

### B. USING THE MODEL

#### Predicting Detectability of a Specified Target.

The form of the model specified in Eq. [20] is used to predict the relative detectability of a specified target (size, luminance, and chromaticity) on a specified background (luminance and chromaticity). In order to use the model to predict absolute detection levels, the computed relative detection levels must be scaled by the parameter  $b$ , which depends upon the observer's criterion. Here,  $b$  is assumed to take the value 1.0.

Use of the model in this form requires four input values that characterize the target and background of interest: three measures of target contrast ( $\Delta X$ ,  $\Delta Y$ , and  $\Delta Z$ ) and an  $a.j.$  parameter value that is determined by target size. The remaining parameters are constant. When the constant parameters are entered into the model, Eq. [20] can be rewritten in a form convenient for use:

$$z(\text{detect}) = b \times (a.j.)^{1.34} \times [(84.64 \times \Delta x^2 + 4.41 \times \Delta z^2)^{1.5} + 681.47 \times \Delta y^3]^{0.4466} \quad [22]$$

The three target contrast values,  $\Delta X$ ,  $\Delta Y$  and  $\Delta Z$ , are obtained by measuring the luminance and chromaticity of the target in tristimulus coordinates (base ftL) (X, Y, and Z), and measuring the luminance and chromaticity of the background in the same units ( $X_i$ ,  $Y_i$ ,  $Z_i$ ). The three measures of target contrast are then determined by subtracting each target value from its corresponding background coordinate:

$$\Delta X = X - X_i \quad [23]$$

$$\Delta Y = Y - Y_i \quad [24]$$

$$\Delta Z = Z - Z_i \quad [25]$$

Parameter a.j. is determined as follows. First, the target of interest must be specified in terms of retinal angle, measured in degrees. This quantity is a function of the physical size of the target and the viewing distance, and can be calculated:

$$RA = (t * 57.3) / d, \quad [26]$$

where RA is the retinal angle in degrees, t is the target diameter, and d is the viewing distance. Both t and d must be measured in the same units. The parameter a.j. can be estimated by the following linear regression equation:

$$a.j. = .261 + 4.280 * RA \quad [27]$$

The four parameters are then entered into Eq.[22], which yields a value of z(detect). This is the normal transform of the area under the ROC curve. Its value will range from 0 to positive infinity, although values larger than about 3 all indicate virtually perfect detection performance.

Using any commonly available z-table, the area under the ROC curve is determined by the cumulative area under the normal curve up to the calculated z(detect) value. The area itself provides a measure of detectability that corresponds to the probability correct in a 2-alternative forced-choice experiment. Chance performance is given by an area of .5 (corresponding to z(detect) = 0); perfect detectability is indicated by values approaching 1.0.

#### Predicting Detection Distance.

The form of the model given in Eq. [21] is used to predict the distance at which a target of specified luminance and chromatic contrast will be detected with some specified probability. Eq. [28] gives the most convenient form of the

model for use, with constant parameters included:

$$a.j. = \frac{[z(\text{detect}) / b]^{0.746}}{[(84.64 \times \Delta x^2 + 4.41 \times \Delta z^2)^{1.5} + 681.47 \times \Delta y^3]^{0.33}} \quad [28]$$

Use of this form of the model again requires that the X, Y and Z values be calculated for the target of interest. In addition, the user supplies a measured or desired performance level: the z(detect) value. As discussed in the previous section, this value should range between 0 and about +3.

Eq. [28] results in a predicted a.j. value, which can then be related to the retinal angle of the target by the following linear regression equation:

$$RA = -.057 + .231 * a.j. \quad [29]$$

From the retinal angle, the relative distance at which a target of a given size will be detected is given by

$$\text{Distance} = t * 57.3/RA \quad [30]$$

Absolute distances can be calculated if the multiplicative parameter b is determined for particular viewing conditions.



## VI. VALIDATION OF THE MODEL

A short study was run in order to assess the validity of the empirical conclusions and of the model predictions. Threshold retinal sizes were determined for nine targets of fixed contrast, viewed against one of two backgrounds. For each background, six of the target contrasts were determined from the average threshold values obtained with the 10 min targets in Experiment I. These six targets varied along the X, the Y, the Z, the XZ, the XY, and the YZ axes of tristimulus space. It was predicted that, within a scaling factor dependent upon the particular psychophysical task (here, the method of limits), the threshold retinal angles for these six targets would be similar (about 10 minarc each). The remaining three targets were chosen to have equal delta values along the three primary axes of tristimulus space, X, Y, and Z. Here, it was predicted that the threshold retinal angle would be similar for the targets that varied along X and Y, reflecting the finding that sensitivity to targets that vary along these axes is similar. The targets that varied along the Z axis were expected to yield threshold retinal angles much larger than the other two, reflecting the lesser sensitivity to targets that vary along the Z axis.

### Methods

Observers. Twenty-six naive observers (11 males and 15 females) were recruited from a pool of students taking an Introduction to Psychology course at UCLA. Participation in experiments is a course requirement, and students received course credit for their time. All students were between 18 and 20 years of age. Each was individually tested for acuity using a Landolt-Ring chart, and only students with the equivalent of Snellen 20/20 vision or better (corrected) were accepted. Students were also tested for color vision, using the Ishihara (1968) book of plates. Two males were rejected as showing color vision anomalies.

Subjects were randomly assigned to view one of the two adapting backgrounds, pink or gray, so that 13 observers participated in each condition of the experiment.

Stimuli. Viewing conditions were identical to those described in Experiment I. Stimuli were identical in configuration, but were of fixed contrast and variable size. For each of two backgrounds (the gray and pink backgrounds of standard luminance from Experiment I), nine fixed-contrast targets were constructed.

Six of the targets were chosen to yield equal performance. These varied along the X, the Y, the Z, the XZ, the XY, and the YZ axes of tristimulus space. The values of  $\Delta X$ ,  $\Delta Y$  and  $\Delta Z$  that described each target were taken from the average results of Experiment I for the 10 min target. These stimuli (a) tested the

robustness of the conclusions from Experiment I, and (b) were used as input to the predictive model in order to test its accuracy. Thus, these stimuli were predicted to (a) yield similar retinal-angle thresholds (each near 10 minarc), and (b) yield similar predictions for the threshold retinal angle when their  $\Delta X$ ,  $\Delta Y$  and  $\Delta Z$  values were used in the predictive model.

The remaining three targets varied along the three primary axes of tristimulus space, X, Y, and Z. Contrast values for these targets were chosen to have equal  $\Delta X$ ,  $\Delta Y$ , and  $\Delta Z$  values. On the basis of conclusions from Experiment I, it was predicted that the X and Y targets would yield similar, small retinal-angle thresholds and predicted values. Threshold retinal angle to the Z-varying target was expected to yield much larger retinal-angle thresholds, and the model was expected to predict this relatively larger value.

The two backgrounds were used in order to again assess whether background is a significant factor in predicting detection performance.

Procedures. Each observer was run individually in a single session that lasted approximately 1/2 hour. Observers were read a standardized set of instructions that explained the method of limits procedure and instructed them in the use of the response box. The background adapting field was then displayed, and observers adapted for 2 minutes.

The first four trials were practice trials, followed by a series of experimental trials. Two thresholds for each of the nine targets were determined by the method of limits procedure, using one ascending series (increasing in size) and one descending series (decreasing in size) for each target. Thus, in addition to the four practice trials, there were 18 experimental trials per session. Experimental trials were presented in a random order that was uniquely determined for each observer.

On descending series trials, a large (30 min) target appeared on the screen with a concurrent tone. Observers were instructed to press the toggle-switch marked "yes" if they could see the target. The target was then replaced with a slightly smaller target (in one-pixel steps), and a new response was taken. On descending series, the shrinking continued until the observer's response changed to "no". The size of the target at that point was recorded as the threshold retinal angle.

On ascending-series trials, a small target (approximately 1 min) appeared with the concurrent tone. Observers were to press the switch marked "no" if they could not see the target. The target was then replaced with a slightly larger target, and the response was taken once again. When the observer's response changed to "yes", the size of the target was recorded as the threshold retinal angle.

## Results

The results from the two types of targets were analyzed separately. First, the six targets chosen to yield equal performance were analyzed. The threshold retinal angles for each of the observers were entered into a 2 (Background) x 2 (Series) x 6 (Axis of Modulation) mixed analysis of variance. Background was treated as the between-groups factor; Series and Axis were treated as repeated-measures factors.

The results of this analysis indicated that neither Background nor Series was a significant factor. Axis, however, was found to be significant ( $p < .001$ ). Furthermore, the Axis x Background interaction was significant ( $p < .05$ ). No other effects were significant.

The Axis and Axis x Background effects were explored by the use of post-hoc comparisons. Performance in each of the conditions was found to be equal, as expected, with two exceptions. These two exceptions were responsible for the significant effects in the main analysis. 1) On the pink background, the XY target yielded a threshold that was slightly larger than the thresholds to the Y target alone and the YZ target alone. It was not significantly different from the remaining three targets. 2) On the gray background, the XZ target was found to yield a threshold significantly higher than all other targets. It is not clear why these two targets yielded larger thresholds than the other conditions, based on the results from Experiment I.

Each of the  $\Delta X$ ,  $\Delta Y$ , and  $\Delta Z$  values was entered into the model to predict actual performance levels. A  $z(\text{detect})$  value of 1.8 was assumed, based on the results obtained in Experiment I. The predicted values were quite good for both the pink and the gray backgrounds, and results were similar between the two.

The individual thresholds for the gray background are plotted as points in Figure 14 for each of the six target conditions. In this figure, the solid line indicates the 10 min threshold expected on the basis of the results from Experiment I. Points denoted by the letter P show precise values predicted from Eq. [21]. It can be seen that, in general, the model predicts the thresholds quite well, always within the range of empirical values obtained.

It should be noted that the predicted values were based on an average  $z(\text{detect})$  value obtained from Experiment 1, which used a method of adjustment procedure and experienced subjects. No other scaling was done to reflect the differential criteria that might be expected with naive observers and the different (method of limits) psychophysical techniques. (However, the retinal angle was calculated by linear interpolation between the  $\Delta i$  values, rather than by the regression equation given in Eq. 29. The fit is slightly worse when Eq. 29 is used.) The fit might be

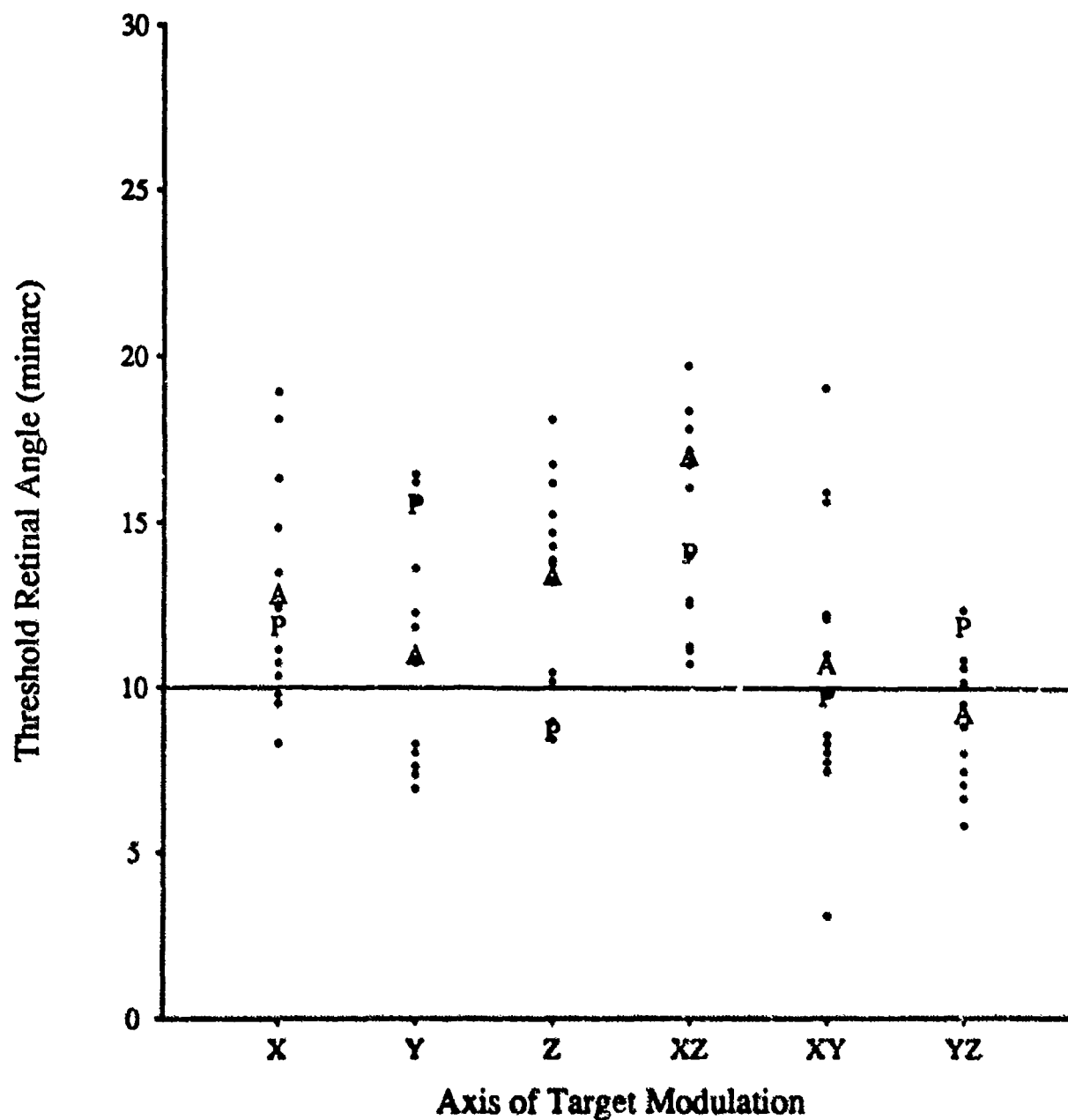


Figure 14 "Equal performance" results from the validation study, for the gray background. Thresholds from individual subjects are shown as dots. Mean thresholds across subjects are denoted by the letter "A," while predicted thresholds are denoted by the letter "P." The solid line at 10 minarc indicates the threshold expected on the basis of Experiment I.

improved by (a) assuming a different value for  $z(\text{detect})$ , or (b) assuming a value other than 1.0 for scaling.

The second analysis was performed on the remaining three targets as a 2(Background) x 2(Series) x 3(Axis of Modulation) mixed analysis of variance. For the gray background, each target varied along a primary axis with a delta value of 0.25. For the pink background, the deviations were smaller, having a value of 0.16. It was expected that for each background, the targets that varied along the X and Y axes would yield similar retinal-angle thresholds, whereas those that varied along the Z axis would yield significantly larger thresholds. It was also expected that the obtained thresholds would vary with the background, since the contrast of the targets on the gray background was larger than that on the pink background.

A problem was encountered with the data from the Z-axis modulations. In a large proportion of cases, the retinal angle thresholds exceeded the maximum size possible in the experiment (30 minarc). In order to complete the analysis, the maximum value of 30 min was used in these cases. This procedure clearly reduces the variability in these cells, which increases the likelihood of obtaining significant differences. However, since thresholds exceeded the 30 min limit, using 30 min reduces the potential difference between the Z and other conditions.

The results indicated that neither series nor background was a significant factor. The background result is somewhat surprising, but may indicate that the contrast difference between values of .16 and .25 is not great enough to be reflected in performance. As expected, the Axis factor was significant ( $p < .05$ ). No other factors were significant.

The Axis and the Axis x Background results were explored in a series of post hoc comparisons. As expected, the targets that varied along Z were significantly different from the X and Y targets. None of the remaining values differed significantly from one another, confirming the expectation that targets varying along the X and Y axes yield similar performance. No evidence was found to support the marginally significant Axis x Background interaction; thus, it was determined that this factor could be safely ignored.

In order to assess the validity of the model for prediction, the  $\Delta X$ ,  $\Delta Y$  and  $\Delta Z$  values were entered into Eq. [21]. Again, a  $z(\text{detect})$  value of 1.8 was assumed and linear interpolation was used in place of Eq. [29], but no further scaling was done. Figure 15 presents the obtained threshold retinal angles together with predicted values for each background. Recall that the obtained Z values are underestimated for points lying at 30 min. It can be seen that, as in the first analysis, the model adequately predicts the empirical data.

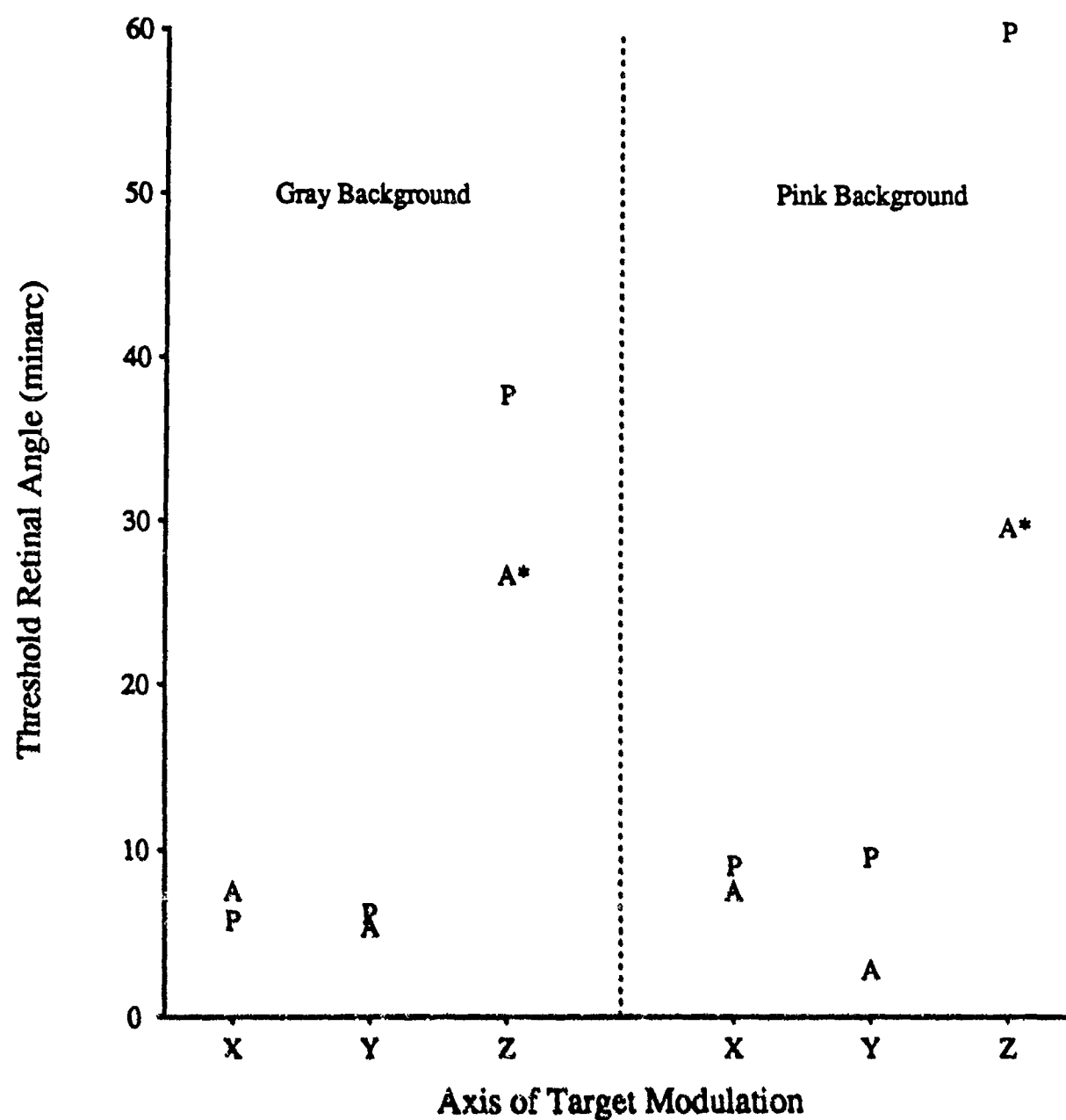


Figure 15 "Equal increment" results from the validation study. Mean thresholds across subjects are denoted by the letter "A," while predicted thresholds are denoted by the letter "P."

\* Underestimate due to equipment limitations (see text).

## VII. SUMMARY AND RECOMMENDATIONS

The model we have presented provides a quantitative statement relating target contrast to measures of detection performance. It has been presented in such a form as to be useful in predicting the relative detectability of specified targets in a limited set of viewing conditions, and has been briefly validated for laboratory conditions. Several limitations in the use of the model should be noted.

First, absolute performance predictions are only valid for method-of-adjustment laboratory conditions. For other psychophysical tasks or non-laboratory conditions, the model only predicts relative performance. In an actual field situation, the predictions must be scaled to reflect the particular task and observer criteria by determining the value of the parameter  $b$ . It is not currently known how robust the model is to different criteria and tasks, nor what the range of  $b$  might be. Additional research that relates the parameter  $b$  to other tasks is needed.

A second limitation of the model is that it has only been validated for a limited range of photopic luminance conditions. Although the model should theoretically be valid for a wide range of photopic conditions, the information is not available from the current studies. The limits of the model with respect to luminance range remain to be assessed.

Third, the current model was developed for an impoverished and limited viewing situation that does not adequately reflect a field viewing situation. It is known from previous research that uncertainty as to target location, target hue, and target contrast will reduce detection performance. In determining parameters of the model, no uncertainty was assumed. It is not known whether the reduction affects all parameters of the model equally, or whether the effects are complex. A related potential effect is one that will occur in any real viewing condition: the effect of other objects in the scene. The conditions assumed here did not allow an assessment of this effect, although it is known to affect detection performance.

Despite the limitations of any model developed in the laboratory, the results of this project represent a significant advance over previous work with chromatic/luminance contrast scales. The combined use of theoretical and practical considerations in developing the form of the predictive equation, the vast empirical data base upon which parameter estimates are based, and the extensive analyses performed have resulted in a concise model that accurately predicts the detectability of arbitrary targets and can be easily used in the field. In addition to its primary success in developing a predictive model, work on this project has also contributed to a more complete understanding of chromatic and luminance information processing in the visual system. It is hoped that this work will provide the foundation for further developments in the area.

## REFERENCES

- Barlow, H. B. Temporal and spatial summation in human vision at different background intensities. *J. Physiology*, 1958, 141, 337-350.
- Blackwell, H. R. Contrast Thresholds of the human eye. *J. Opt. Soc. Amer.*, 1946, 36, 624-643.
- Boynton, R. M. Color, hue, and wavelength. In E.C. Carterette and M. P. Friedman (Eds.) *Handbook of Perception*, Vol. 5. New York: Academic Press, 1975.
- Boynton, R. M. and Gordon, J. Bezolde-Brucke hue shift measured by color-naming technique. *J. Opt. Soc. Amer.*, 1965, 55, 78-86.
- Boynton, R. M. and Kambe, N. Chromatic difference steps of moderate size measured along theoretically critical axes. *Color Res. Appl.*, 1980, 5, 13-23.
- Boynton, R. M., Kandel, G. and Onley, J. W. Rapid chromatic adaptation of normal and dichromatic observers. *J. Opt. Soc. Amer.*, 1959, 49, 654-666.
- Commission Internationale de l'Eclairage. *CIE Proceedings 1931*. Cambridge, England: Cambridge University Press, 1932.
- Cowan, W. B. CIE calibration of video monitors. Unpublished preliminary version, Ontario, Canada: National Research Council of Canada, 1985.
- DeValois, R. L. and DeValois, K. K. Neural coding of color. In E. C. Carterette and M. P. Friedman (Eds.), *Handbook of Perception*, Vol. 5. New York: Academic Press, 1975.
- Green, D. M. and Swets, J. A. *Signal detection theory and psychophysics*. New York: Kreiger, 1974.
- Guth, S. L., Donley, M. J. and Marrocco, R. T. On luminance additivity and related topics. *Vision Research*, 1969, 9, 537-575.
- Guth, S. L., Lodge, H. R. Heterochromatic additivity, foveal spectral sensitivity, and a new color model. *J. Opt. Soc. Amer.*, 1973, 63 450-462.
- Guth, S. L., Massof, R. W. and Beneschawel, T. Vector model for normal and dichromatic color vision. *J. Opt. Soc. Amer.*, 1980, 70, 197-211.



Helwig, J. T. and Council, K. A. *SAS User's Guide*, 1979  
Edition Cary, NC: SAS Institute, 1979.

Hood, D. C. and Finkelstein, M. A. Sensitivity to light.  
In K. Boff, L. Kaufman, and J. P. Thomas (Eds.), *Handbook  
of Perception and Human Performance*, Vol. 1. New York:  
Wiley (1986).

Hurvich, L. M. and Jameson, D. Some quantitative aspects  
of opponent color theory. II. Brightness, saturation, and  
hue in normal and dichromatic vision. *J. Opt. Soc. Amer.*,  
1955, 45, 602-616.

Jameson, D. and Hurvich, L. M. Some quantitative aspects  
of opponent color theory. I. Chromatic responses and  
spectral saturation. *J. Opt. Soc. Amer.*, 1955, 45, 546-  
552.

King-Smith, P. E. and Carden, D. Luminance and the  
opponent-color contributions to visual detection and  
adaptation and to temporal and spatial integration. *J.*  
*Opt. Soc. Amer.*, 1976, 66, 709-717.

LeGrand, Y. Les seuils differentiels de couleurs dans la  
theorie de Young. *Rev. Opt. Theor. Instrum*, 1949, 28, 261-  
278.

MacAdam, D. L. Visual sensitivities to color differences  
in daylight. *J. Opt. Soc. Amer.*, 1942, 32, 247-274.

Nagy, A. L., Eskew, R. T. Jr., and Boynton R. M. Analysis  
of color-matching ellipses in a cone-excitation space. *J.*  
*Opt. Soc. Amer. A.*, 1987, 4(4), 756-768.

Olzak, L. A. and Thomas, J. P. Seeing Spatial Patterns. In  
K. Boff, L. Kaufman, and J. P. Thomas (Eds.), *Handbook of  
Perception and Human Performance*, Vol. 1. New York: Wiley  
(1986).

Olzak, L. A. and Wandell, B.A. Detection contours and  
field mixtures. Supplement to *Investigative Ophthalmology  
and Visual Science*, 1983, 24, 184.

Pokorny, J. and Smith, V. C. Colorimetry and color  
discrimination. In K. Boff, L. Kaufman, and J. P. Thomas  
(Eds.), *Handbook of Perception and Human Performance*, Vol.  
1. New York: Wiley (1986).

Purdy, D.M. Chroma as a function of retinal illumination.  
Unpublished Ph.D. dissertation, Harvard University, 1929.  
Cited in C. H. Graham, *Color: Data and theories*, In C.H.  
Graham (Ed.), *Vision and Visual Perception*. New York:  
Wiley, 1965.

Rodieck, R. W. *The Vertebrate Retina*. San Francisco, CA: Freeman 1973.

Schrodinger, E. Grundlinien einer Theorie der Farbenmetrik im Tagessehen. *Annual der Physik*, 1920, 53, 481. (English translation, Outline of a theory of color measurement for daylight vision. In D. L. MacLeod (Ed. & trans.) *Sources of color science*. Cambridge, MA: MIT Press, 1970.

Sperling, H. G. and Harwerth, R. S. Red-green cone interactions in the increment threshold spectral sensitivity of primates. *Science*, 1972, 172, 180-184.

Stromeyer, C. F. III and Sternheim, C. E. Visibility of red and green spatial patterns upon spectrally mixed adapting fields. *Vision Research*, 1981, 21, 397-407.

Thomas, J. P. Underlying psychometric function for detecting gratings and identifying spatial frequency. *J. Opt. Soc. Amer.*, 1983, 73, 751-758.

Vos, J. J. and Walraven, P. L. On the derivation of the foveal receptor primaries. *Vision Research*, 1971, 11, 799-818.

Wandell, B. A. and Olzak, L. A. Categorical color differences. *Supplement to Investigative Ophthalmology and Visual Science*, 1983, 24, 206.

Wandell, B. A. and Pugh, E. N. Jr. Detection of long-duration, long-wavelength incremental flashes by chromatically coded pathway. *Vision Research*, 1980, 20, 625-636.

Wandell, B. A., Sanchez, J. and Quinn, B. Detection/discrimination in the long-wavelength pathways. *Vision Research*, 1982, 22, 1061-1069.

Wandell, B. A., Welsh, D. and Maloney, L. Adaptation in the long-wavelength pathways. *Vision Research*, 1982, 22, 1071-1074.

Watson, A. B. Probability summation over time. *Vision Research*, 1979, 19, 515-522.

## APPENDIX A

### MONITOR CALIBRATION

In this appendix, calibration procedures and results are discussed. Precise calibration was necessary in order to (a) independently determine the chromaticity coordinates of the monitor phosphors as a check on manufacturer specifications, (b) determine the relative relationship between voltage input and luminance output of each electron gun (gamma correction) and to identify the usable linear range of each, and (c) to measure gun balance, the multiplicative constants that determine absolute luminance level. Once known, these three components allow the generation of arbitrary stimuli with known tristimulus values in CIE XYZ space, based on standard colorimetry concepts of metamerism and additive mixture.

In practice, principles of additive mixture applied to monitor calibration hold only to the extent that (a) phosphor chromaticity values are constant over their entire excitation range, and (b) the excitation produced by each gun is independent of excitation levels of the remaining guns. These assumptions were tested empirically as part of the calibration procedure. Additional measurements were made to ensure that these assumptions held for full-field stimuli as well as small spots at various locations on the display screen.

CIE calibration of the display monitor was performed in accordance with theory and procedures outlined in a short course on the Colorimetry of Video Monitors at the 1985 meeting of the Optical Society of America. A preliminary version of a publication based on the course is available from W. B. Cowan of the National Research Council of Canada (Cowan, 1985).

#### Equipment

Calibration of the BARCO monitor was performed against a Gamma Model 220 Standard Lamp Source A (incandescent tungsten, 2854 deg. K, 342.6 cd/m<sup>2</sup>), equipped with three removable Kodak Wratten filters. This source is certified by Gamma Scientific to be calibrated and standardized against their in-house standard source lamp, which in turn is calibrated against National Bureau of Standards Lamps No. NBS 7371 and NBS 5868. Chromaticity coordinates of the light emitted by the standard lamp source are provided in Table A1. Each Wratten filter was chosen to closely approximate the manufacturer-specified chromaticity coordinates of the red, green, and blue monitor phosphors, and used to calibrate the photometer to the appropriate chromaticity region. Specification of these filters is also given in Table A1.

Calibration measurements were taken with a Spectra Pritchard photometer (Model 1970-PR), equipped with filters closely proportional to the  $\bar{x}, \bar{y}, \bar{z}$  tristimulus functions. The

integration time of this photometer approximates that of the human eye, making it an appropriate instrument for measuring the intermittent light generated by the monitor. Care was taken to avoid momentary saturation of the photomultiplier dynodes in the photometer. A 2-degree aperture was used in all full-field measurements. A 1-degree aperture was used in small-spot measures.

Two computer programs were written to automate the calibration procedures as far as possible. The first program was used to check the critical assumptions of phosphor-excitation independence and gun independence (additivity) for full-field and small-spot stimuli. This program allowed the user to flexibly generate stimuli of various sizes, with any combination of gun excitation. A second program was written to automatically generate stimuli appropriate for gamma correction and gun-balance measurements. This program drove a single gun of choice, providing a full-field display that stepped in luminance by a fixed voltage increase automatically every 10 seconds.

### Procedures and Results

Gun and Field Size Independence. In order for principles of color mixture to be applied in generating colors on a video monitor, the primaries used in color mixing must remain unchanged when more than one primary is activated. In practical terms, this implies that to the extent that the electron guns in the display monitor are independent of one another, the voltage applied to one gun will be unchanged by voltages applied to either of the remaining guns. If this is true, then the luminance values measured for each gun alone should obey the principle of additivity. This assumption was tested by measuring the luminance output of each gun separately at the highest voltage levels (the worst case of power draw), then combining the guns in all possible combinations and comparing the measured value to that predicted by additivity. Each of the nine measurements was made both with full-field displays and with small spots just over 1 deg. of arc, and were repeated twice.

The results showed good agreement between luminance values obtained with full-field and small-spot stimuli. Of the eighteen measurements, only five did not yield identical values. Differences were on the order of a few percent, well within measurement error. Furthermore, differences obtained were not in consistent directions across the two replications.

Gun combination measurements showed a slight subadditivity, again on the order of a few percent. Although this is within the range of measurement error, the consistency suggests a small degree of gun interaction. Nevertheless, the small magnitude of the interaction is probably within the noise level for the present purposes.

Chromaticity Measurement of Phosphors. In order to accurately determine the chromaticity coordinates of an arbitrary stimulus, the coordinates of the primaries used to generate the stimulus must be precisely determined. For a video display system, the primaries are determined by the phosphors, which are assumed to be of constant chromaticity across the luminance range. Although phosphor chromaticities are provided by the manufacturer, the importance of their accuracy warranted an independent check of the specified values. Chromaticities were measured at several luminance levels to check the assumption of constancy.

The accuracy with which chromaticities can be measured depends in part upon calibrating the photometer to a known external standard whose coordinates are near those of the unknown sample. Thus, prior to measuring each of the red, green, and blue phosphors, the photometer was calibrated against the Luminance Standard equipped with the appropriate Wratten filter.

To calibrate the photometer, the meter was set to read 1.0 against the luminance standard of 100 ftL ( $342.6 \text{ cd/m}^2$ ). Each standard Wratten filter was measured using the three photometer filters approximating the  $\bar{x}$ ,  $\bar{y}$ , and  $\bar{z}$  tristimulus functions. This yielded three readings for each filter,  $R_x$ ,  $R_y$ , and  $R_z$ . The known chromaticity coordinates of the Wratten filter,  $x$ ,  $y$ , and  $z$ , were multiplied by the luminance photometric reading  $R_y$  to give tristimulus values  $X_0$ ,  $Y_0$ , and  $Z_0$  of the known sample. Correction constants  $k_x$ ,  $k_y$ , and  $k_z$  were then calculated according to formulae supplied with the Pritchard photometer:

$$k_x = 1/R_x (X_0 - 1.67 Z_0)$$

$$k_y = Y_0/R_y$$

$$k_z = Z_0/R_z$$

(The equation for  $k_x$  differs from others because the  $\bar{x}$  filter in the photometer does not have the secondary blue lobe required by the CIE system. It is approximated by a proportion of the reading of the  $\bar{z}$  filter).

Correction constants were calculated individually for each of the red, green, and blue filters. Then, the tristimulus values of each unknown phosphor were given by the new photometer readings  $R_{x1}$ ,  $R_{y1}$ , and  $R_{z1}$  as follows:

$$X = (k_x)(R_{x1}) + 0.167(k_z)(R_{z1})$$

$$Y = (k_y)(R_{y1})$$

$$Z = (k_z)(R_{z1})$$

Finally, chromaticity coordinates were calculated by the following standard equations

$$x = \frac{X}{X + Y + Z}$$

$$y = \frac{Y}{X + Y + Z}$$

$$z = \frac{Z}{X + Y + Z}$$

The chromaticity of each phosphor was measured at three luminance levels in order to get an estimate of measurement error. The values calculated according to the above procedures were compared to specified values in the lower part of Table A-1. As is evident, the results were in close agreement with the manufacturer specified values.

Gamma Correction. The goal of this measurement procedure was to determine the relative excitation function for each gun in the monitor; that is, to relate the voltage applied (determined by each of the 256 map locations) to the luminance output of each gun. For each of the three guns, 27 relative luminance readings were taken over the entire range (1-256) available, in equal decremental steps. Each measurement was repeated twice. Where discrepancies occurred, an average of the two was used to fit predictive functions.

Gamma functions (used to compute the tristimulus coordinates of the displayed stimuli from the voltages of the red, green and blue guns) were estimated by regressing the phosphor excitations on the gun voltage settings. Non-linear regressions were used: at small gun voltages, a simple quadratic function was used to compute excitation from the gun voltage setting. At higher voltages, a third-order power function was used, relating the logarithm of excitation to an expression that was quadratic in the logarithms of the gun voltage settings. The regression coefficients were constrained so that the simple quadratic function agreed with the third-order power function at the voltage that marked the transition from one regression equation to the other. Several different values were evaluated for this transition voltage setting; final values of 30 were chosen for the red and green guns, and 40 for the blue gun.

SAS procedure NLIN was used to estimate the regression coefficients (Helwig and Council, 1979). Figures A-1 to A-3 plot the computed functions, along with the actual measured values for the red, green, and blue guns. The computational formulae for the gamma functions are listed at the bottom of each figure. Figures A-4 to A-6 plot the gamma function errors on an expanded scale. Errors for the green gamma function (Figure A-5) appear to be worse than those for the other two gamma functions. However,

Table A-1  
 Manufacturer Specifications for Standard Source A, Monitor  
 Phosphors and Kodak Wratten Filters and Measured Chromaticity  
 Values for Phosphors.

#### MANUFACTURER SPECIFICATIONS

<u>Source</u>	<u>x</u>	<u>y</u>	<u>z</u>	<u>Dom</u>	<u>Pe</u>	<u>LT</u>
Standard Source A	.4476	.4075	.1449			
Red Filter #23A	.6498	.3498	.0004	605.5	100.0	36.3
Green Filter #60	.2249	.6616	.1135	520.0	59.5	20.7
Blue Filter #47	.1371	.0724	.7905	470.1	96.0	1.2
Red Phosphor	.62	.33	.05			
Green Phosphor	.21	.675	.115			
Blue Phosphor	.15	.06	.79			

#### MEASURED CHROMATICITIES

Red Phosphor	.63	.34	.03
Green Phosphor	.21	.66	.13
Blue Phosphor	.14	.07	.79

Note: For each source, chromaticity coordinates x,y, and z are provided. For filters, the dominant wavelength (Dom ), percent purity of excitation (Pe), and percent luminance transmission (LT) are also provided. The average standard deviation of measured values was approximately 0.01.

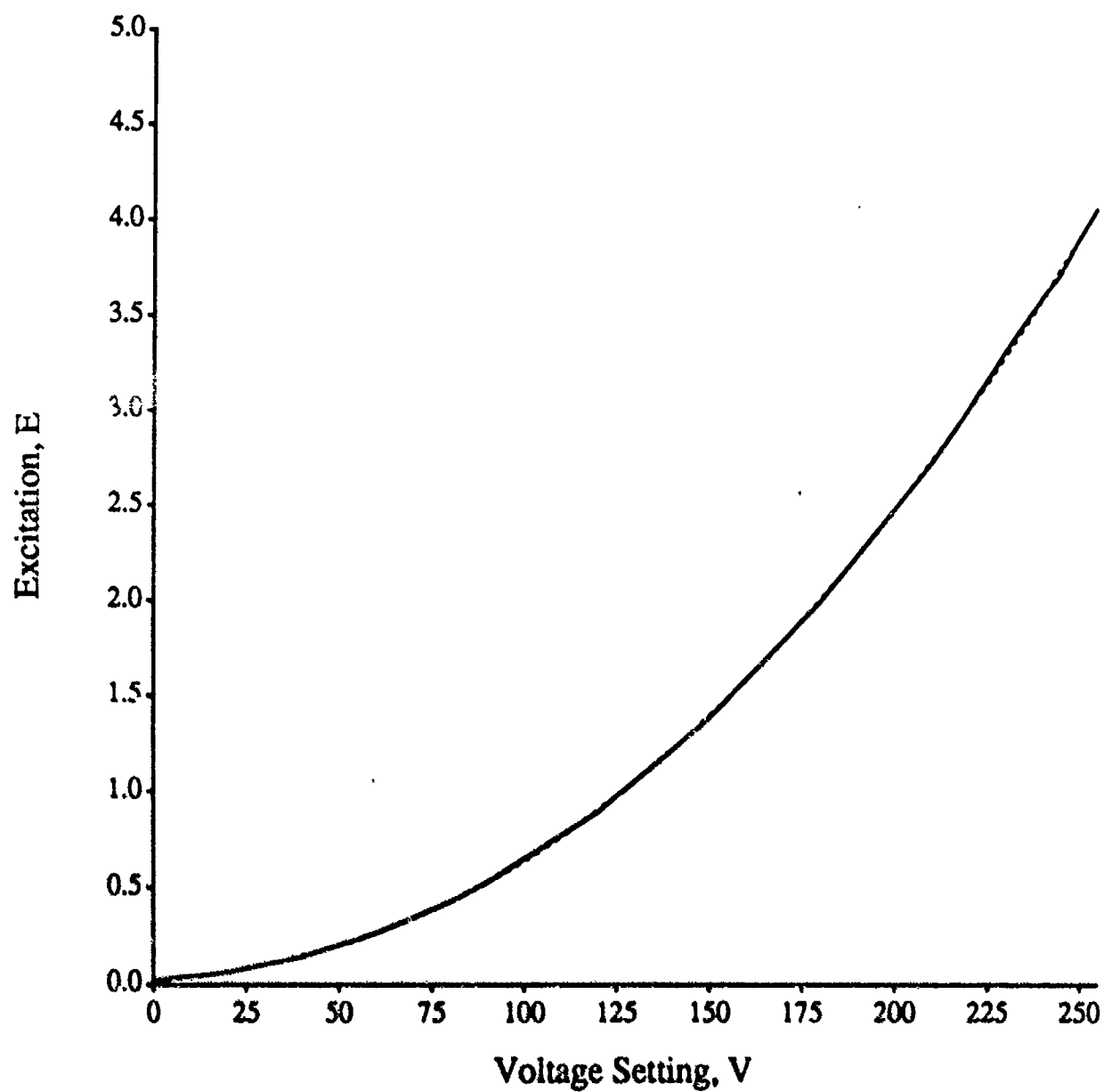


Figure A-1. Actual (solid line) and computed (broken line) red gamma function. Values are computed using the following equations:

$$E = 0.02155 + 0.00099 V + 0.00006 V^2 \quad \text{for } V \leq 30$$

$$E = \exp(1.26079 - 3.89026 \log(V) + 1.04862 [\log(V)]^2 - 0.06171 [\log(V)]^3) \quad \text{for } V > 30$$



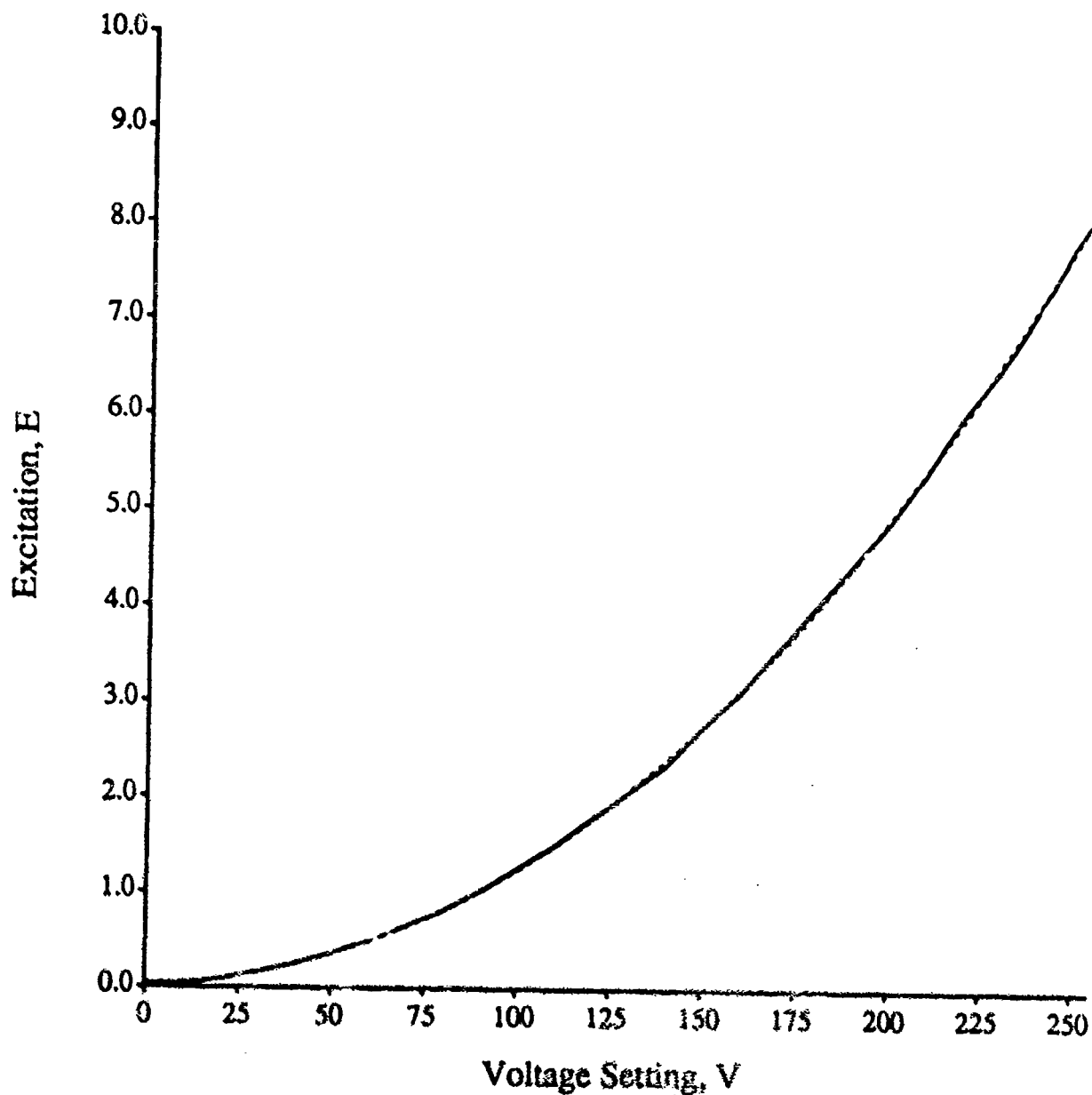


Figure A-2. Actual (solid line) and computed (broken line) green gamma function. Values are computed using the following equations:

$$E = 0.04318 - 0.00120 V + 0.00017 V^2 \quad \text{for } V \leq 30$$

$$E = \exp(-1.18499 - 2.27462 \log(V) + 0.77079 [\log(V)]^2 - 0.04576 [\log(V)]^3) \quad \text{for } V > 30$$

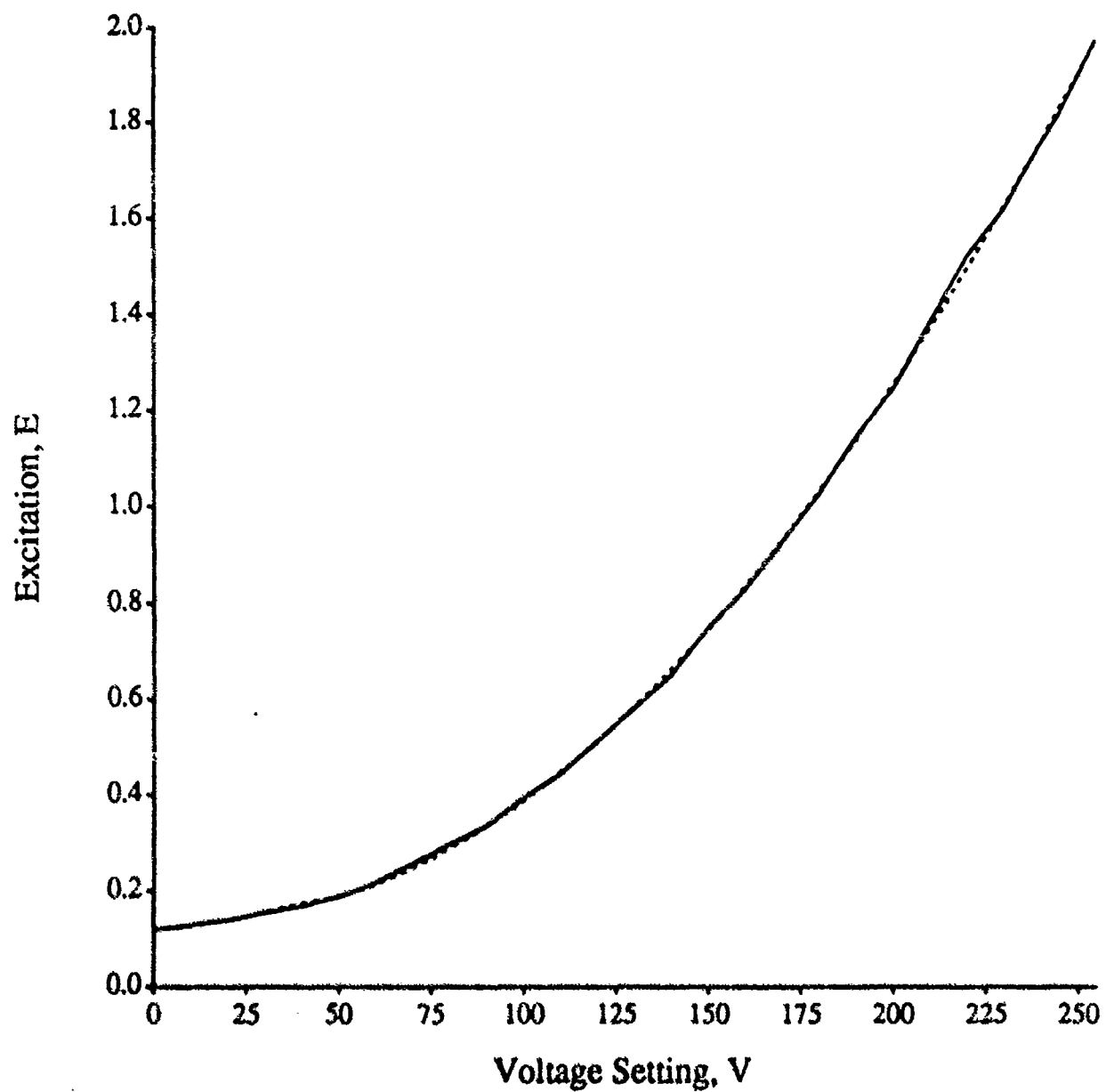


Figure A-3. Actual (solid line) and computed (broken line) blue gamma function. Values are computed using the following equations:

$$E = 0.11946 + 0.00061 V + 0.00002 V^2 \quad \text{for } V \leq 40$$

$$E = \exp(18.61655 - 13.49408 \log(V) + 2.77998 [\log(V)]^2 - 0.16763 [\log(V)]^3) \quad \text{for } V > 40$$

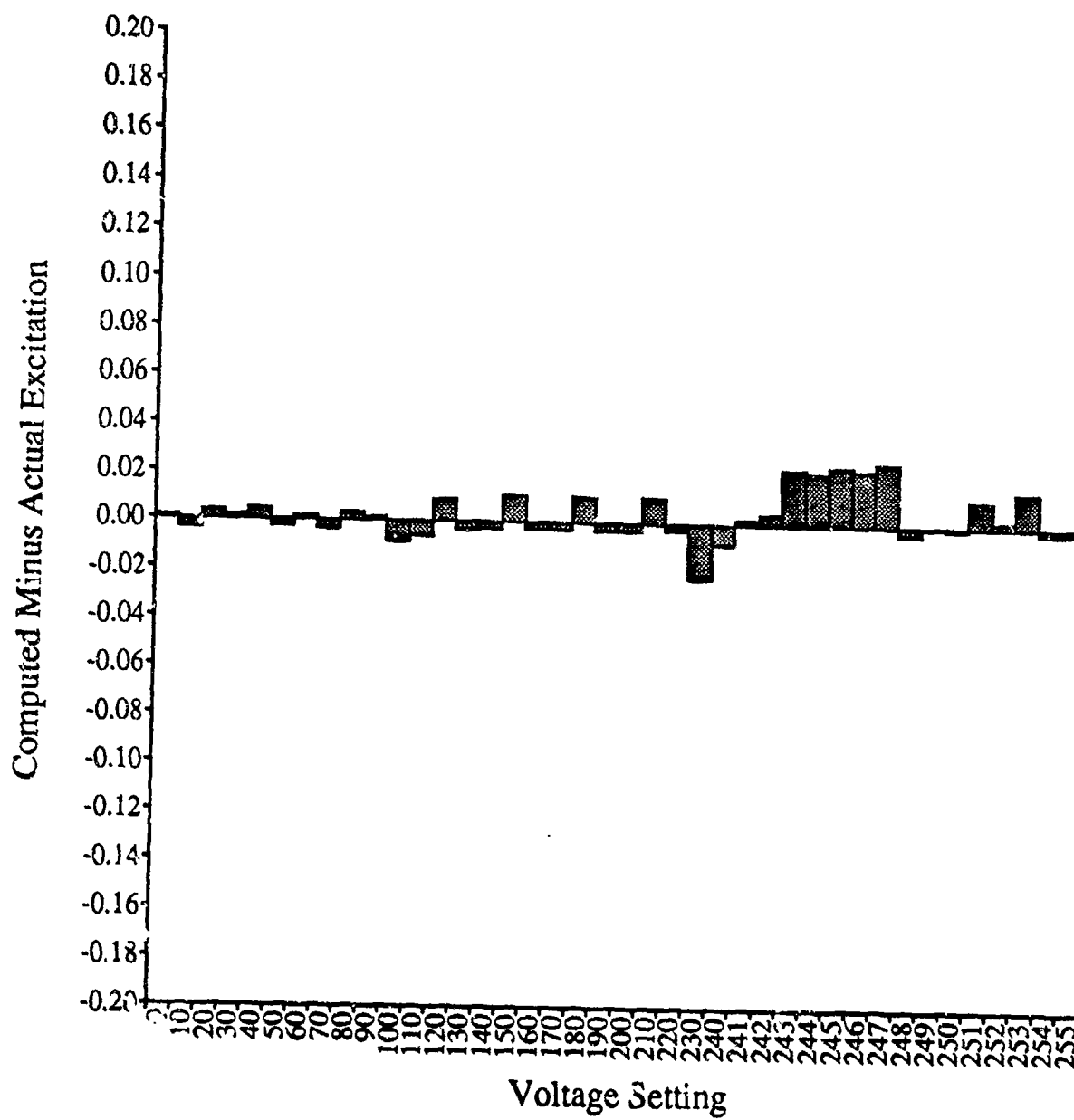


Figure A-4. Accuracy of the computational equations for the red gamma function.

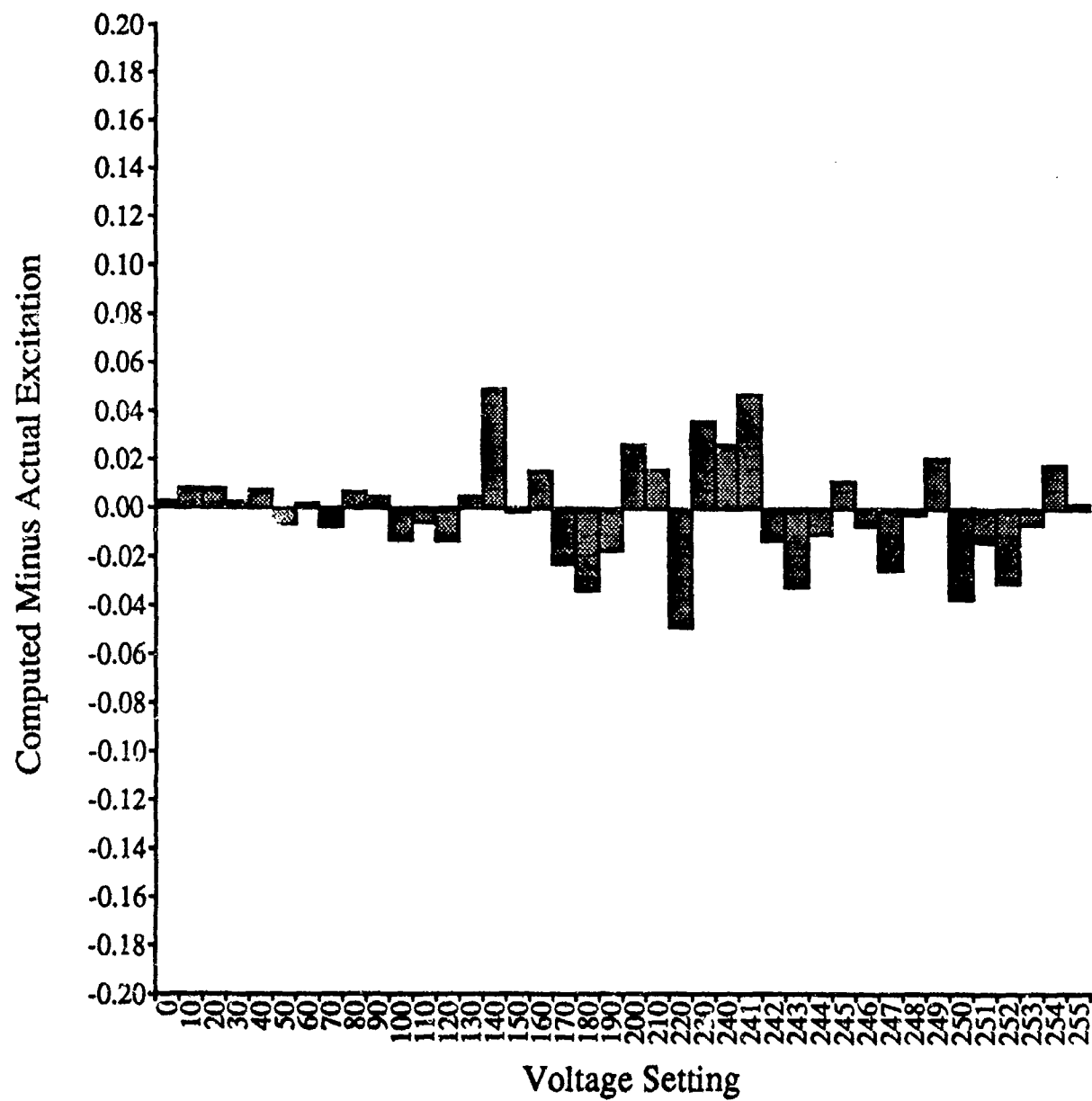


Figure A-5. Accuracy of the computational equations for the green gamma function.

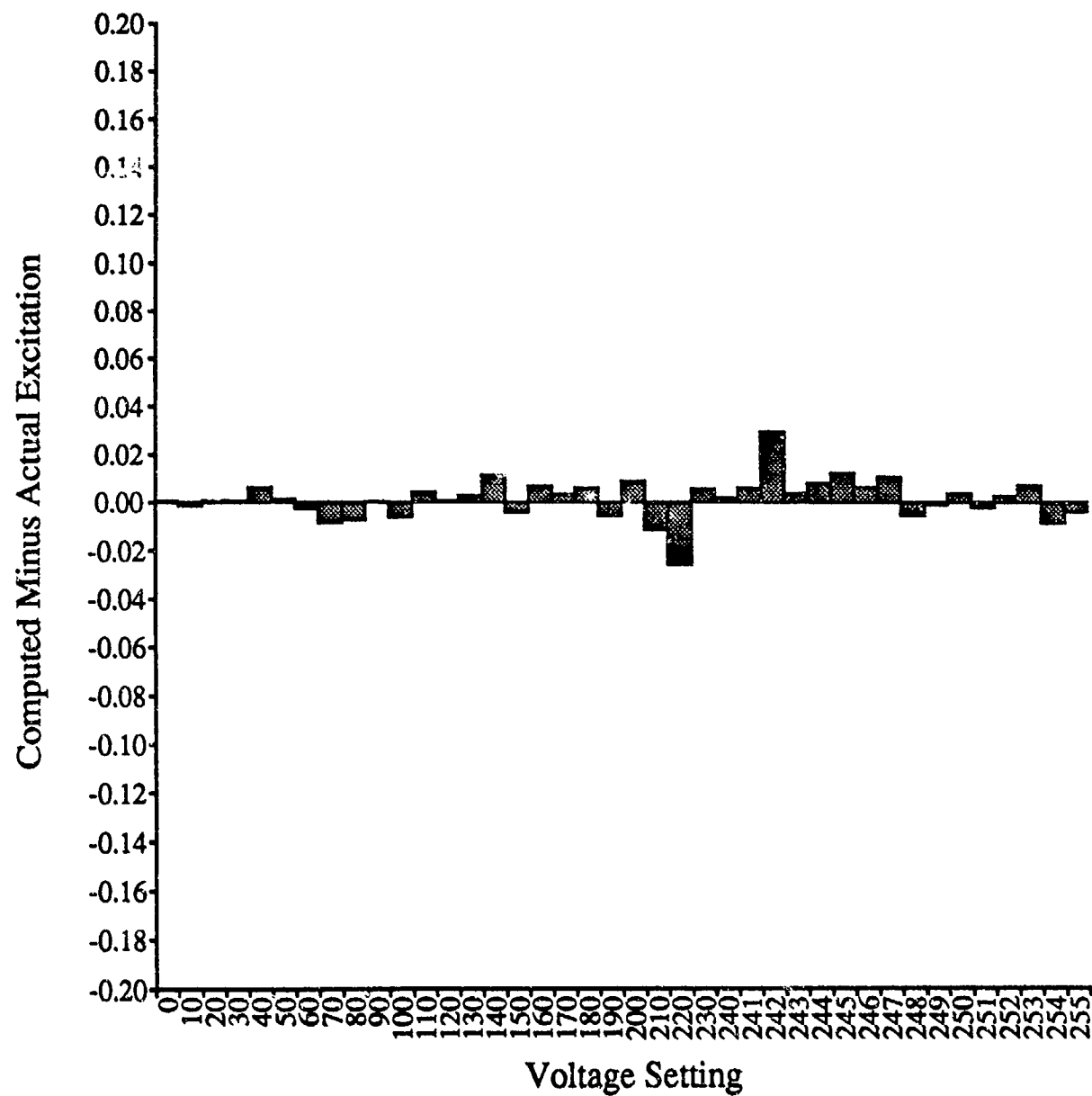


Figure A-6. Accuracy of the computational equations for the blue gamma function.

the maximal excitation for the green phosphors is much greater than that for the other two phosphors; in relative terms, the green gamma function is no less accurate than the red or blue gamma functions. All three gamma functions demonstrate close correspondence between the actual and computed excitations. This is critical, because stimuli were generated on the basis of the computed tristimulus coordinates.

Inverse gamma functions (used to compute the gun voltages needed to produce a stimulus with a particular tristimulus coordinate) were estimated in a similar fashion. The accuracy of these equations was of less concern, because the inverse gamma functions were used only to provide first-guess estimates of the gun voltages needed to produce a particular stimulus. A search was then made (by substituting gun voltages into the gamma functions and computing the actual tristimulus coordinates) for the gun voltages that came closest to producing the desired stimulus.

## APPENDIX B

### ELLIPSE FITTING PROCEDURES

#### Theory of Ellipse Fitting Procedure

The standard form of the equation for a horizontally oriented ellipse (major axis along the X-axis) centered at the origin is given by

$$(x_2/a^2) + (y^2/b^2) = 1 \quad [B-1]$$

where a is the length of the semimajor axis and b is the length of the semiminor axis. For a vertically-oriented ellipse, the equation becomes

$$(y^2/a^2) + (x^2/b^2) = 1 \quad [B-1a]$$

Eq. [1] may also be expressed in the more general second-order form as

$$A'x^2 + C'y^2 = 1 \quad [B-2]$$

(Primed notation is used here to indicate that these parameters have been transformed as outlined below).

The length of the semimajor axis is given by

$$a = A'^{1/2} \quad [B-3]$$

and the length of the semiminor axis is given by

$$b = C'^{1/2} \quad [B-4]$$

for a horizontally oriented ellipse. For a vertically oriented ellipse, the semimajor and semiminor axes are described by the parameters b and a, respectively.

For a general ellipse centered at the origin but not oriented to either the X- or Y- axes, the parameters a and b are supplemented by a third parameter, θ, that describes the angle of rotation with respect to the X-axis. (Two further parameters, k and h, are required if the ellipse is not centered at the origin; however, here the data sets were treated as deviations from a background value centered at [0,0].

In order to recover these three parameters from empirical data points, it is necessary to start with the generalized equation for conic sections, fit the necessary parameters of the equation

in that form, and rotate the empirical space to conform to the standard form required by Eq. [1]. Then, for any arbitrary point  $x'$ , Eq. [1] can be solved for the predicted  $y$  value by the equation

$$y' = \pm b (1 - x'^2)/a^2 \quad [B-5]$$

These standard-form predicted points are then re-rotated to conform to the original empirical space. These procedures are more fully described in the following paragraphs.

Any conic section (ellipse, parabola, hyperbola) can be described by a general equation of the second degree. Such an equation takes the form

$$Ax^2 + Bxy + Cy^2 + Dx + Ey + F = 0 \quad [B-6]$$

Under the constraints that  $A > 0$  and  $C > 0$ , and  $B^2 < 4AC$ , Eq. [6] describes an ellipse. However, before the parameters of Eq. [6] can be usefully related to the desired parameters (length of the semimajor axis,  $a$ ; length of the semiminor axis,  $b$ ; and angle of rotation,  $\theta$ ), several transformations must be performed in order to reduce the general equation to the standard form expressed in Eq. [2].

The first order terms,  $Dx$  and  $Ey$ , must be eliminated through translation of the axes  $X$  and  $Y$  to a new set of axes  $X'$  and  $Y'$ . Formally, this translation can be expressed for any data point  $(x,y)$  by two simple linear expressions.

$$\begin{aligned} x' &= x - h \\ y' &= y - k \end{aligned} \quad [B-7]$$

(In practice, this translation was made by expressing the empirical data points as deviations from the background location in CIE XYZ space, eliminating the terms  $Dx$  and  $Ey$  from Eq. [6] and obviating the need to perform the translational transformation.) The scaling constant  $F$  was set to  $-1$ , and added to each side of Eq. [6] to form the new equation

$$Ax^2 + Bxy + Cy^2 = 1 \quad [B-8]$$

Eq. [8] was fit to the empirical data points by a least-squares algorithm described below, to recover the parameters  $A$ ,  $B$  and  $C$ .

In order to reduce Eq. [8] to the general form of Eq. [2], a rotation of axes was performed. The rotation transforms the parameters  $A$ ,  $B$ , and  $C$  into  $A'$ ,  $B'$ , and  $C'$ , and the angle of rotation,  $\theta$ , is chosen to eliminate the crossproduct term; i.e.,



such that  $B'=0$ . The angle  $\theta$  is determined by the equation

$$\tan 2\theta = B/(A - C) \quad [B-9]$$

Then, the new parameters  $A'$ ,  $B'$ , and  $C'$  are determined by the equations

$$A' = 0.5(A + C + B^2 + (A-C)^2) \quad [B-10]$$

$$B' = B(\cos\theta - \sin\theta) - (A-C)(2\sin\theta\cos\theta) = 0 \quad [B-11]$$

$$C' = 0.5(A + C - B^2 + (A-C)^2) \quad [B-12]$$

transforming Eq. [8] to the general form given in Eq. [2].

In this form,  $A'$  and  $C'$  may be solved by Eqs. [3] and [4] for  $a$  and  $b$ , and predicted points may be generated by Eq. [5] for an arbitrary set of transformed  $x'$  points. In order to compare predicted ellipse points to obtained points, the  $x'$  and  $y'$  points may be re-rotated to their original CIE XYZ coordinate space according to the equations

$$x = x'\cos\theta - y'\sin\theta \quad [B-13]$$

$$y = y'\cos\theta - x'\sin\theta \quad [B-14]$$

and plotted against empirical data points.

#### Least Squares Fitting Algorithm

In this section, the rationale and equations underlying the algorithm implemented to fit parameters  $A$ ,  $B$ , and  $C$  of Eq. [6] (previous section) are presented. Given Eq. [6] and data at a series of  $n$  points  $(x_i, y_i)$ , the problem is to find values of  $A$ ,  $B$   $C$  that minimize the error function

$$E_i = Ax_i^2 + Bx_iy_i + Cy_i^2 - 1 \quad [B-15]$$

For a least-squares fit, we minimize the square of the errors summed over the  $n$  points

$$\phi = \sum_{i=1}^n E_i^2 = \sum_{i=1}^n (Ax_i^2 + Bx_iy_i + Cy_i^2 - 1)^2 \quad [B-16]$$

At the minimum,

$$\partial\phi/\partial A = \partial\phi/\partial B = \partial\phi/\partial C = 0 \quad [B-17]$$

giving the equations for three unknowns

$$\partial\phi/\partial A = \sum_{i=1}^n [A_i^2 + Bx_i y_i + Cy_i^2 - 1] x_i^2 \quad [B-18]$$

$$\partial\phi/\partial B = \sum_{i=1}^n [A_i^2 + Bx_i y_i + Cy_i^2 - 1] x_i^2 y_i \quad [B-19]$$

$$\partial\phi/\partial C = \sum_{i=1}^n [A_i^2 + Bx_i y_i + Cy_i^2 - 1] y_i^2 \quad [B-20]$$

or, in more compact matrix form (matrices M, P and T respectively):

$$\begin{array}{ccc} \Sigma x_i^4 & \Sigma y_i^2 x_i^2 & \Sigma x_i^3 y_i \\ \Sigma x_i^3 y_i & \Sigma y_i^3 x_i & \Sigma x_i^2 y_i^2 \\ \Sigma x_i^2 y_i^2 & \Sigma y_i^4 & \Sigma x_i y_i^3 \end{array} \begin{array}{c} A \\ B \\ C \end{array} = \begin{array}{c} \Sigma x_i^2 \\ \Sigma x_i y_i \\ \Sigma y_i^2 \end{array} \quad [B-21]$$

Thus, the least-squares equation can be expressed, in matrix notation, as

$$MP=T.$$

To solve for vector P containing the desired parameters A, B, and C, we multiply the inverse of the data matrix M by the total matrix T, resulting in the equation

$$P = M^{-1} T \quad [B-23]$$

The obtained parameters are then available for transformation as described above to obtain the final desired parameters a, b, and θ.

## APPENDIX C

### ADDITIONAL FIGURE SETS

In this section, three additional sets of figures are presented. The first, Figures C-1 through C-11, is a representative set of individual threshold deviation contours for various observers. Each figure legend describes the background condition, target size, and individual observer. The plots are constructed as in Figure 2 of the main text. Note that different scales are used for different target sizes.

The second set, Figures C-12 through C-22, is similar to Figure 3 of the main text. These figures are a representative set showing individual data points together with fit ellipses. Each figure legend describes the observer, target size, and background condition.

The final set, Figures C-23 through C-37, shows average contours, in two-dimensional slices, for each target size on backgrounds not presented in the main text. Figures C-23 through C-27 plot contours in the chromaticity (XZ) plane, and are similar to Figure 4 in the main text. Figures C-28 through C-32 plot contours for targets that vary simultaneously in the luminance and the approximately red-green axis of the chromaticity plane (XY plane), and are similar to Figure 5 of the main text. Figures 33-37 plot contours for targets that vary in the luminance and approximately blue-yellow axis of the chromatic plane (YZ). Larger contours correspond to smaller target sizes, indicating the need for greater target contrast with small or distant targets.

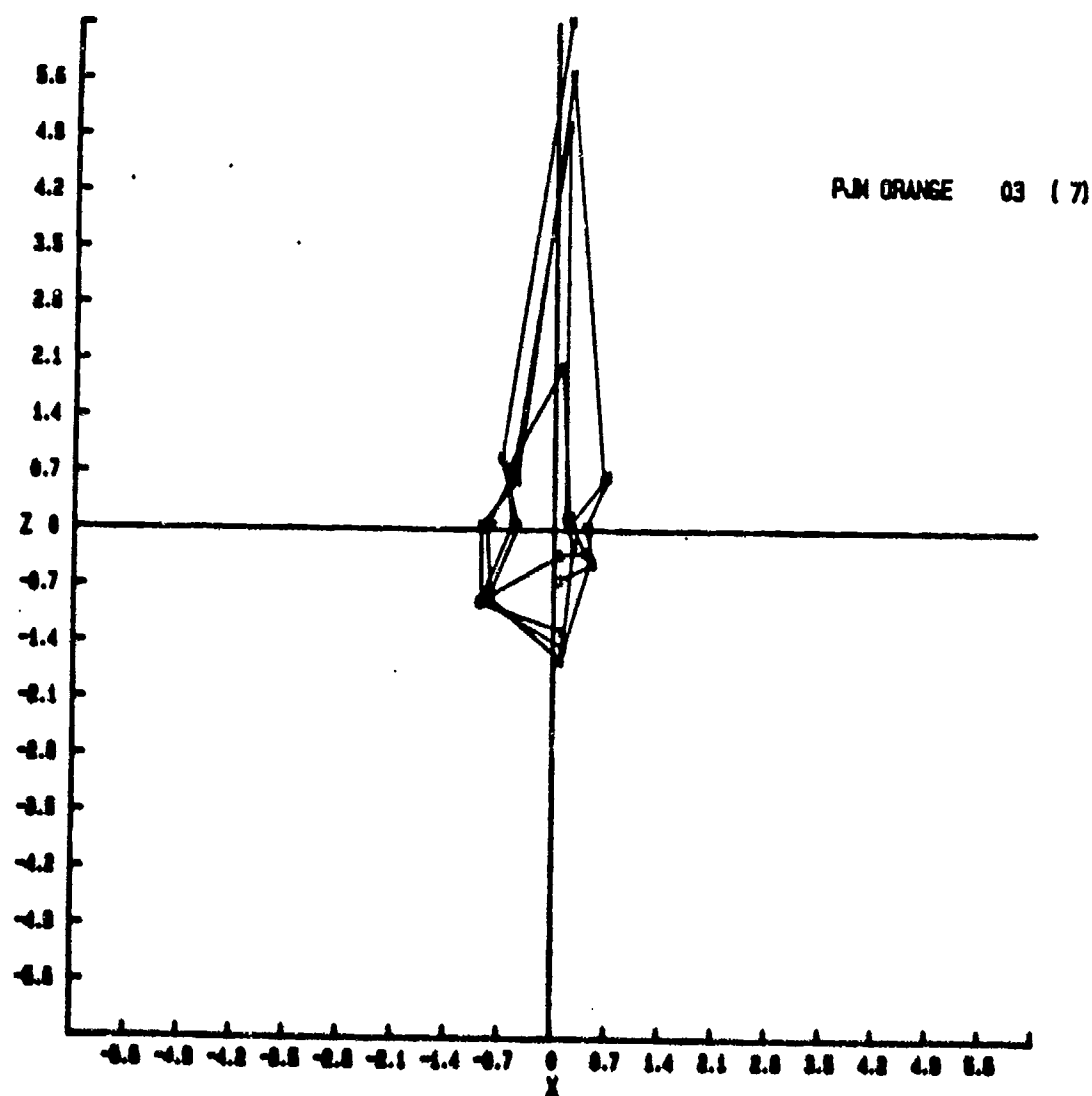


Figure C-1. Individual threshold deviation contour. Figure legend indicates observer, background condition, and target size.

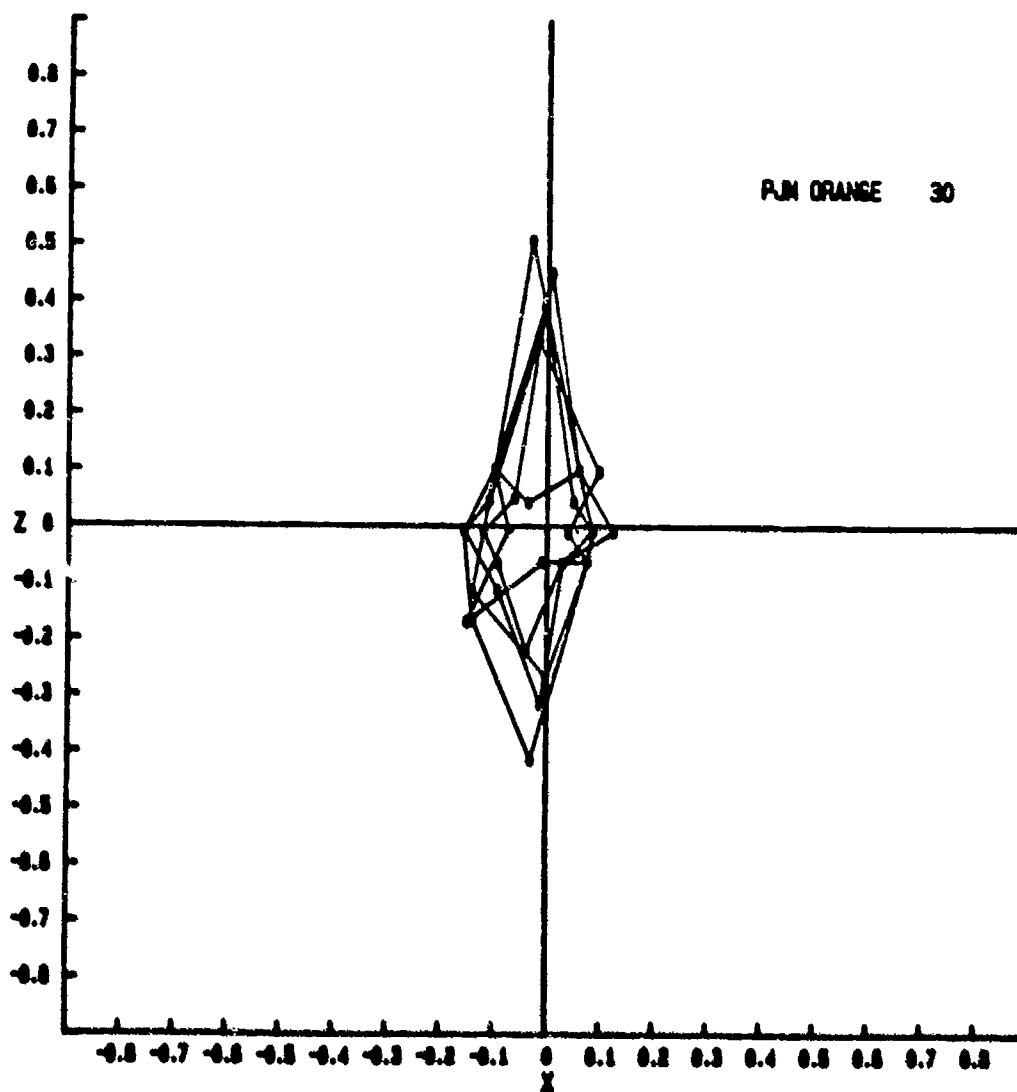


Figure C-2. Individual threshold deviation contour. Figure legend indicates observer, background condition, and target size.

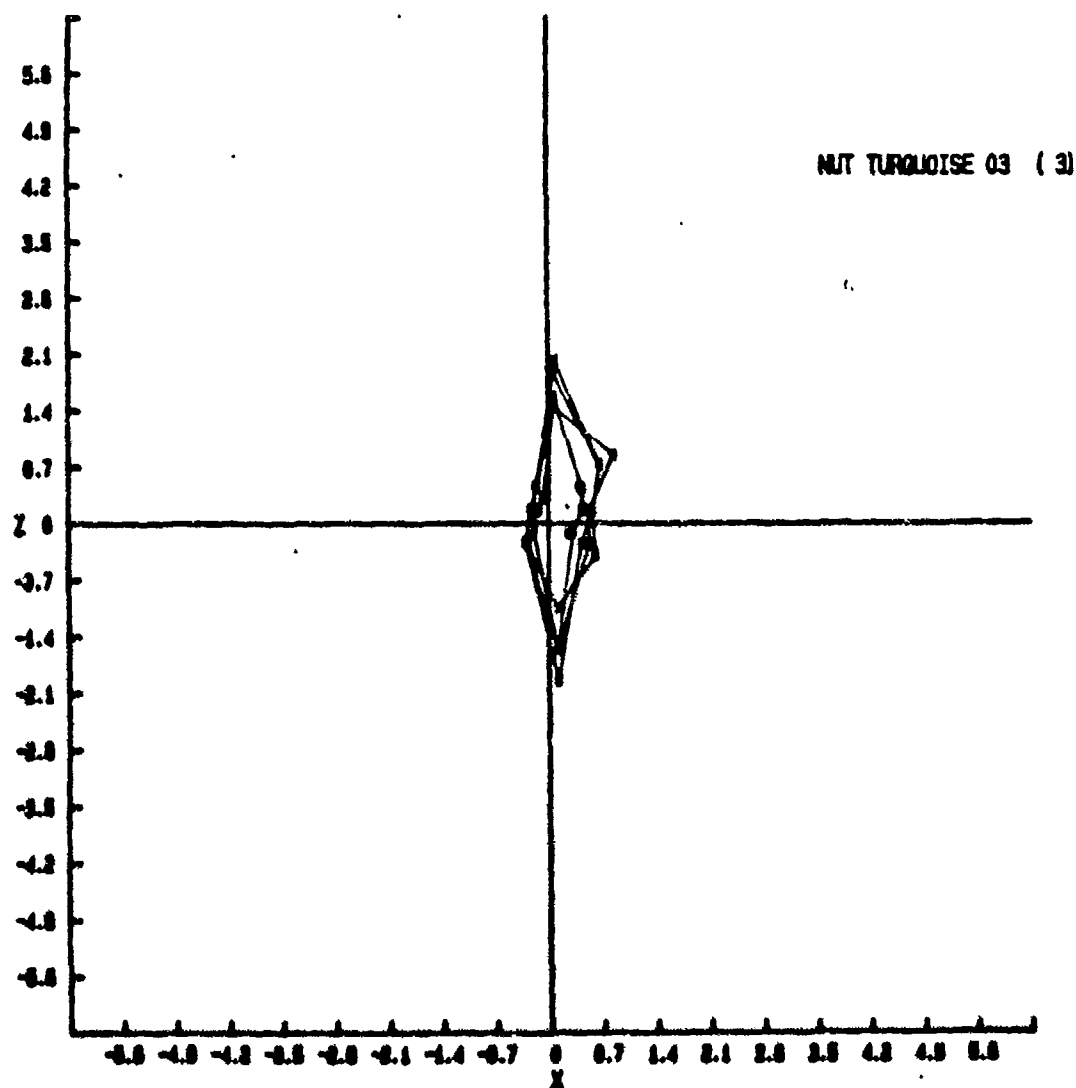


Figure C-3. Individual threshold deviation contour. Figure legend indicates observer, background condition, and target size.

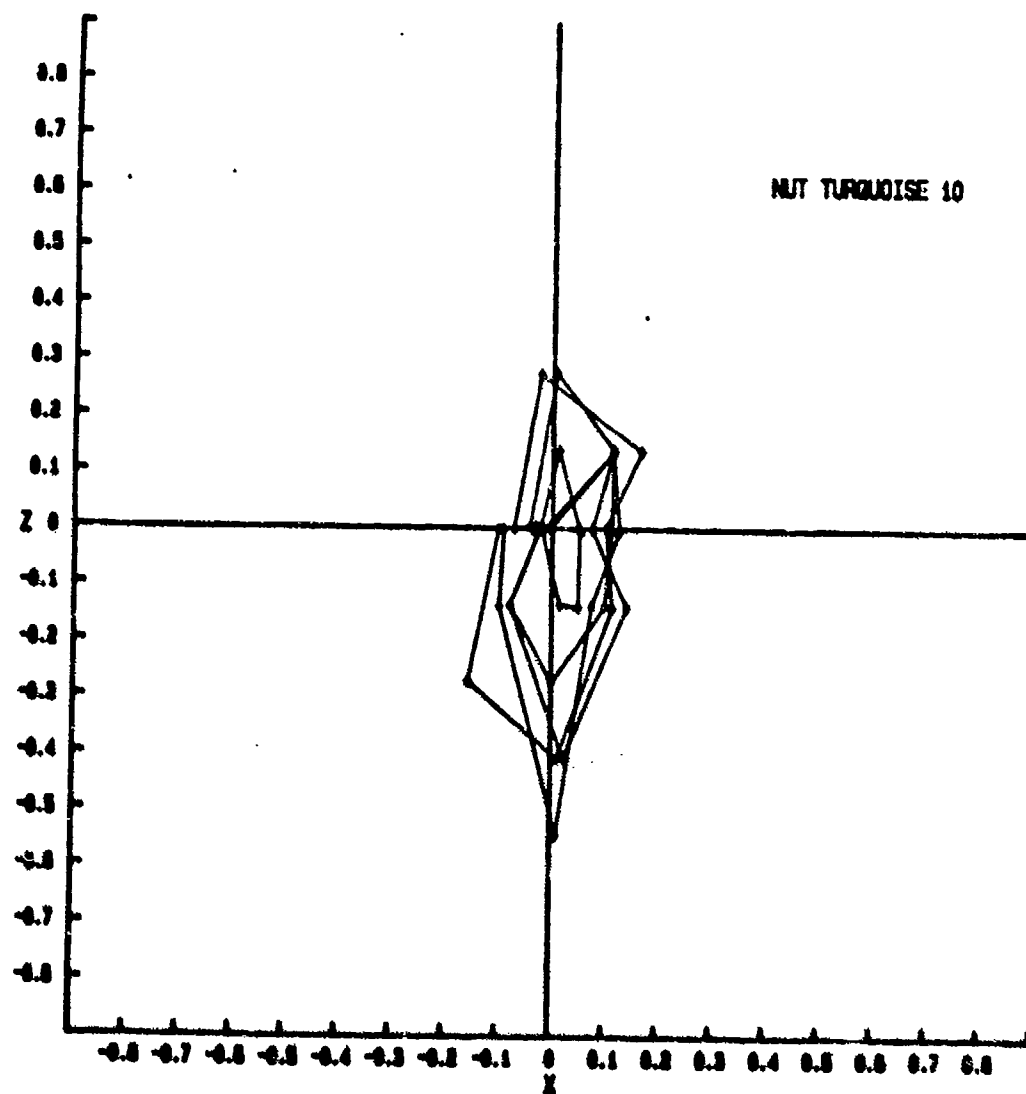


Figure C-4. Individual threshold deviation contour. Figure legend indicates observer, background condition, and target size.

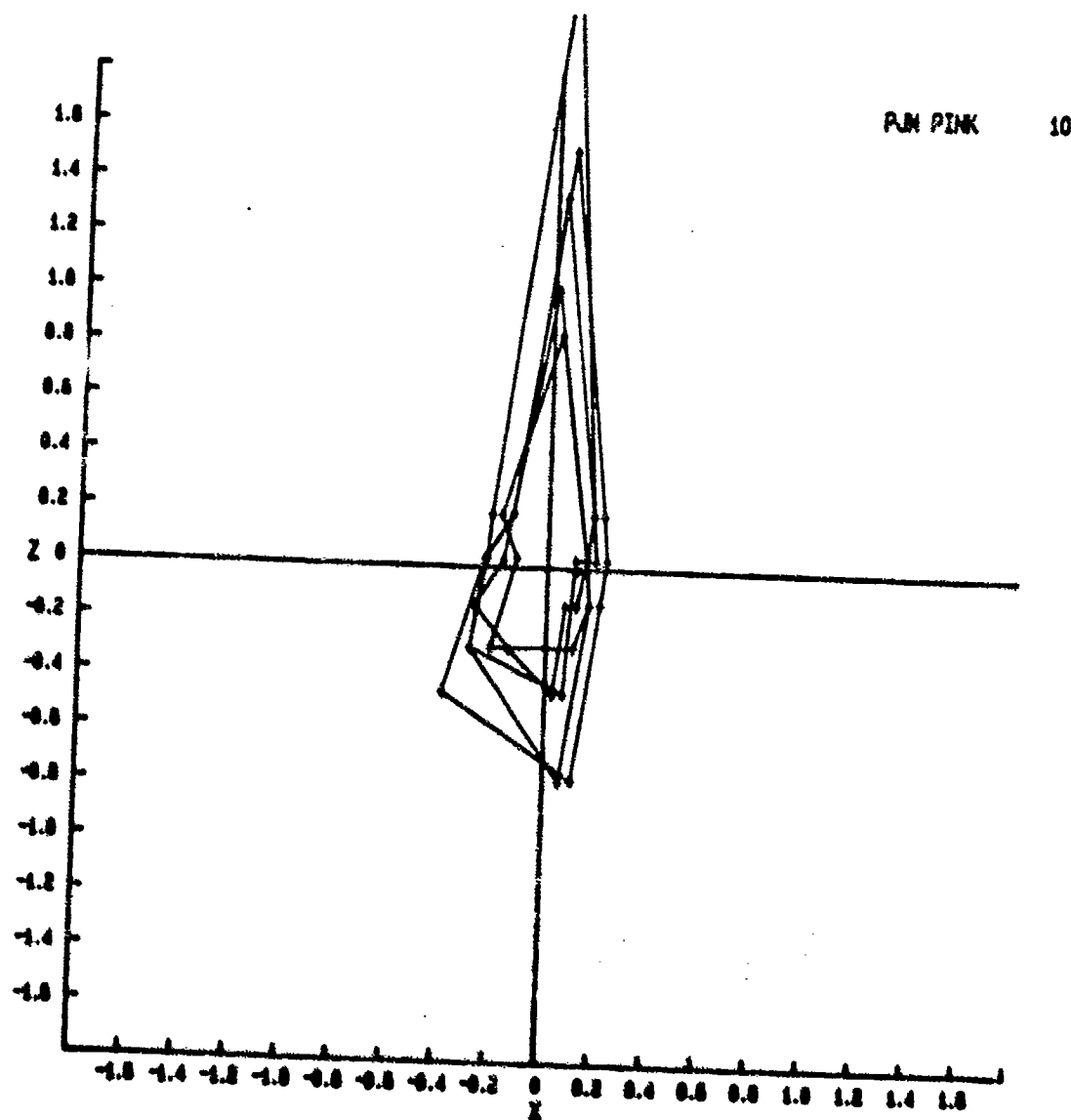


Figure C-5. Individual threshold deviation contour. Figure legend indicates observer, background condition, and target size.



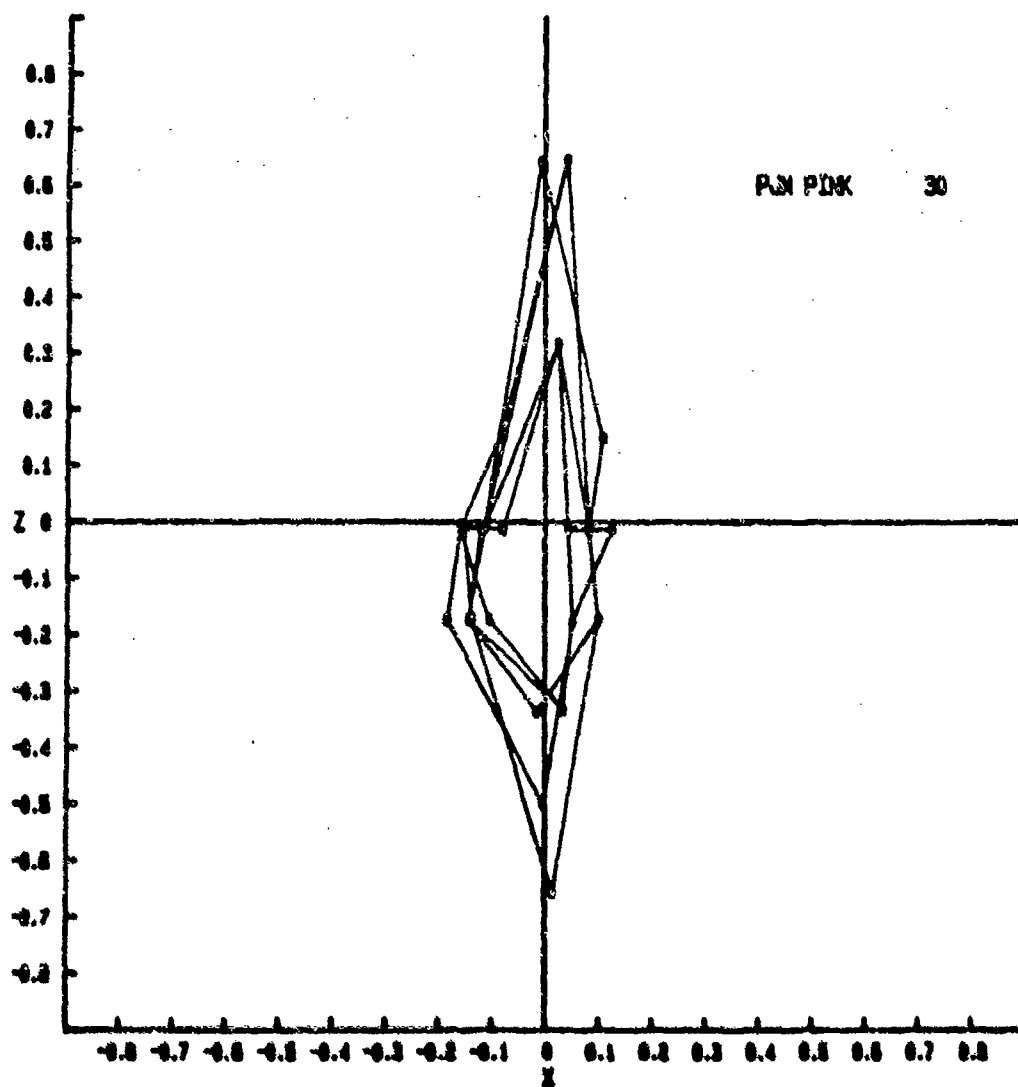


Figure C-6. Individual threshold deviation contour. Figure legend indicates observer, background condition, and target size.

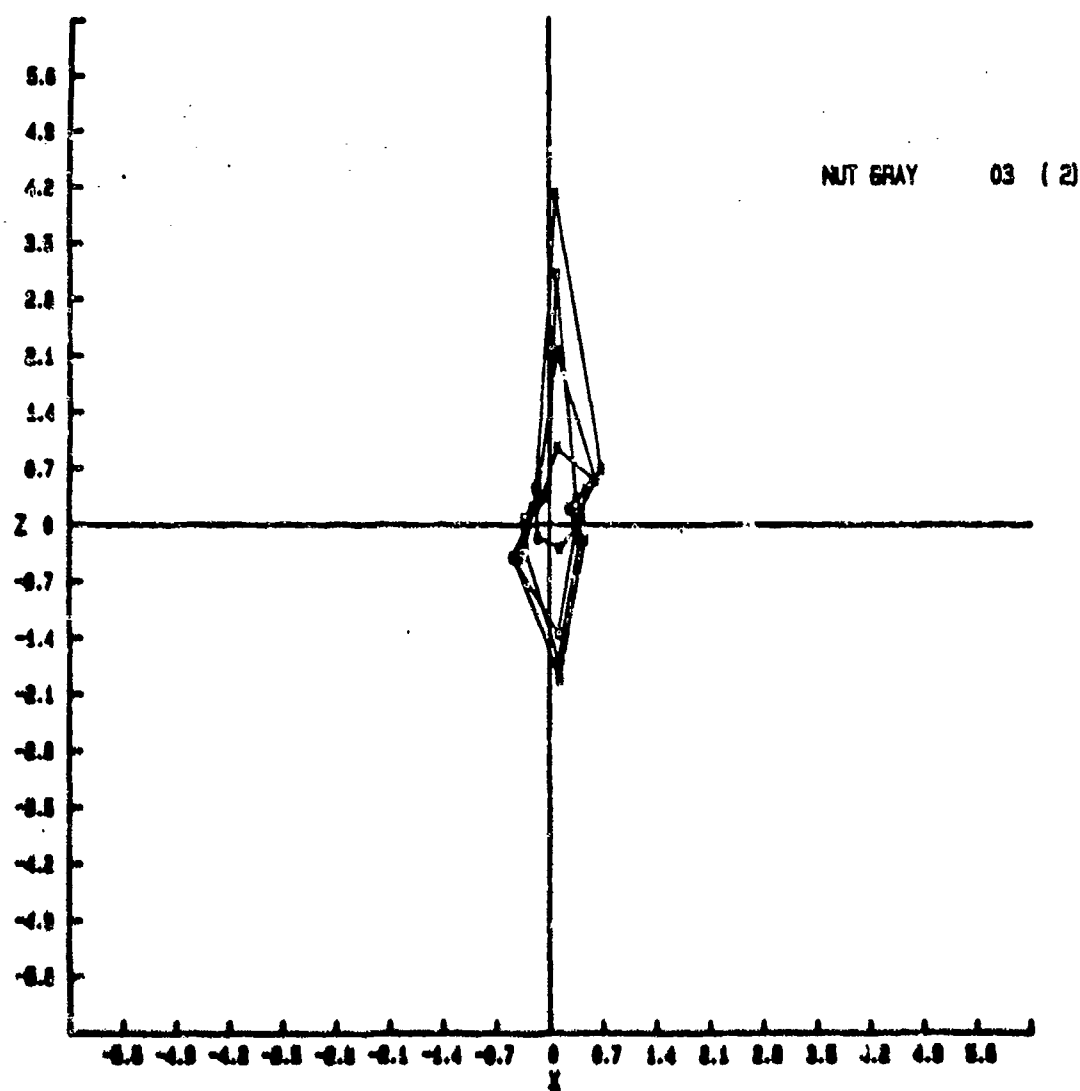


Figure C-7. Individual threshold deviation contour. Figure legend indicates observer, background condition, and target size.

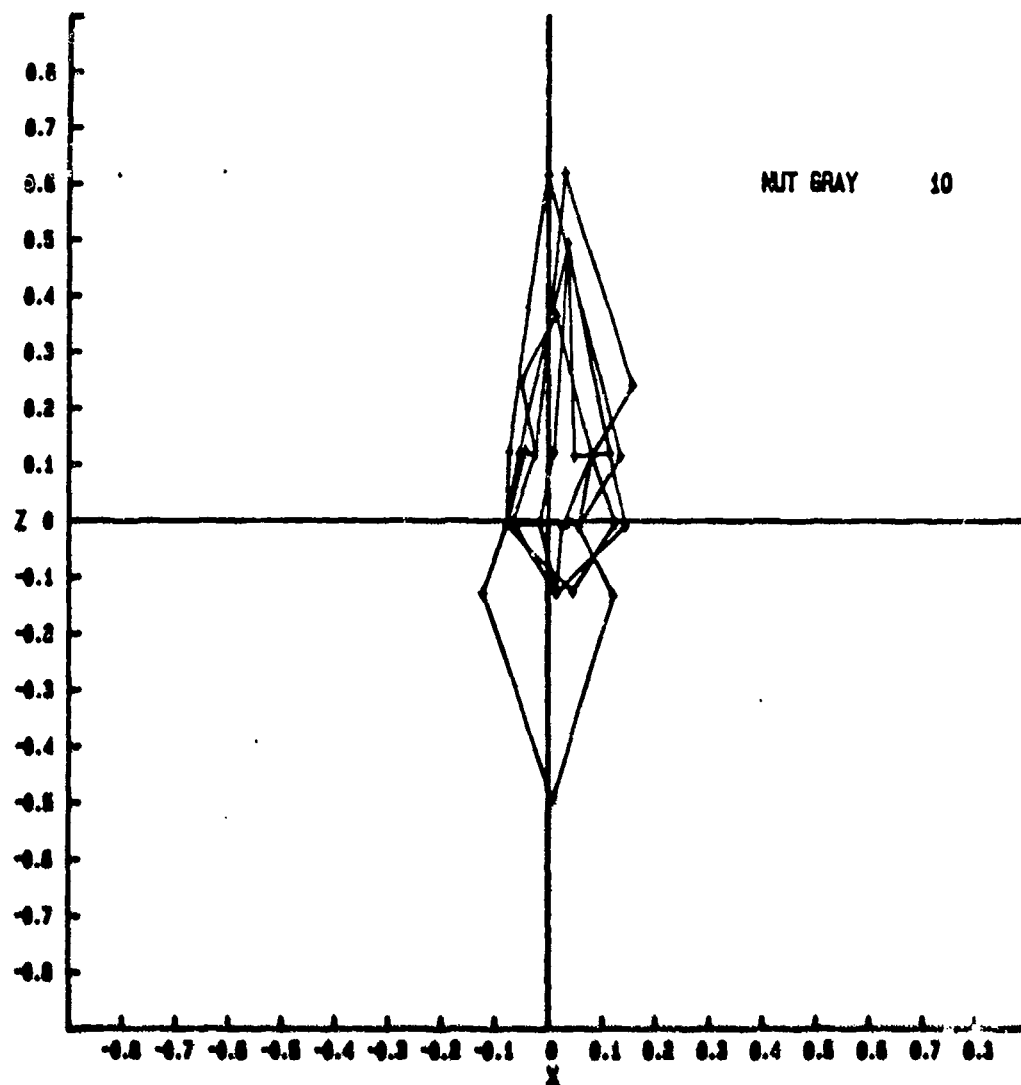


Figure C-8. Individual threshold deviation contour. Figure legend indicates observer, background condition, and target size.

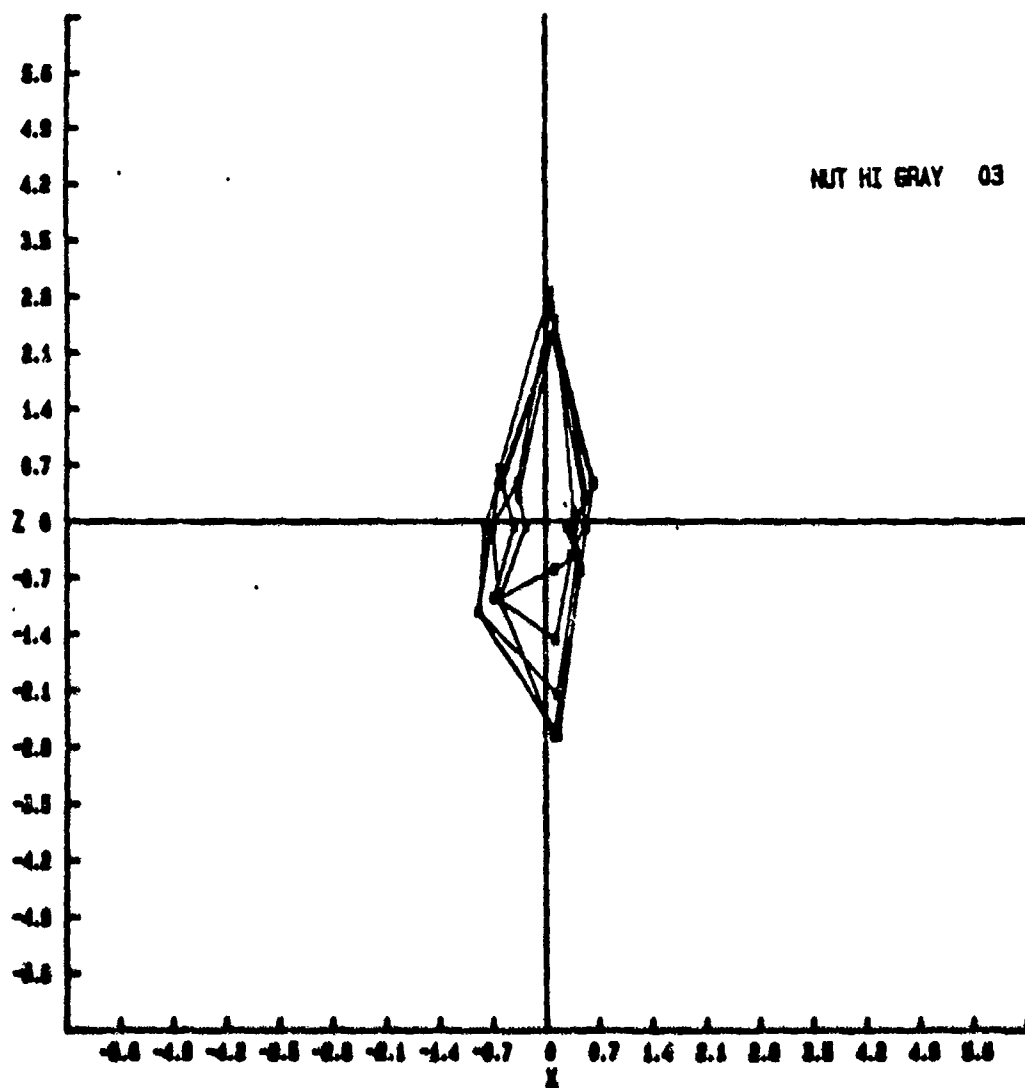


Figure C-9. Individual threshold deviation contour. Figure legend indicates observer, background condition, and target size.

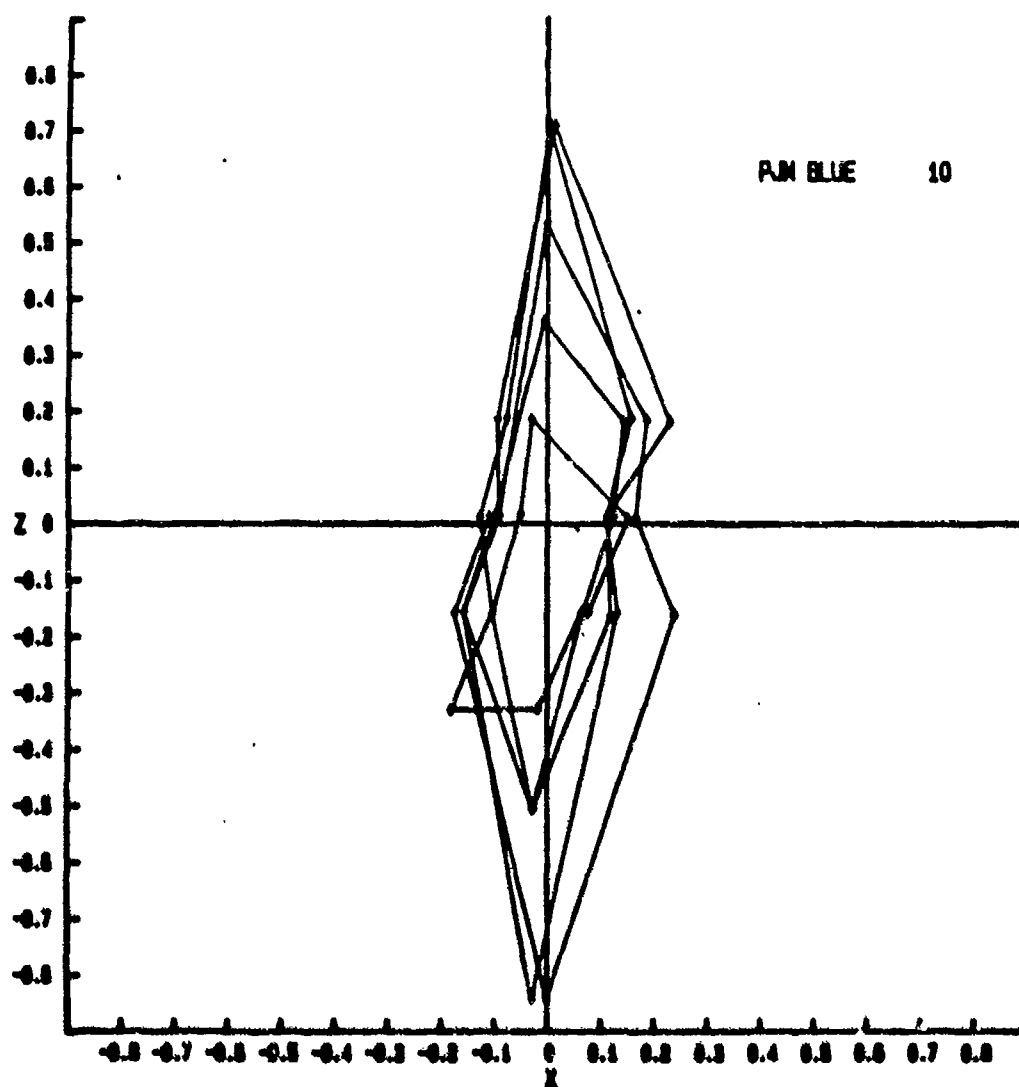


Figure C-10. Individual threshold deviation contour. Figure legend indicates observer, background condition, and target size.

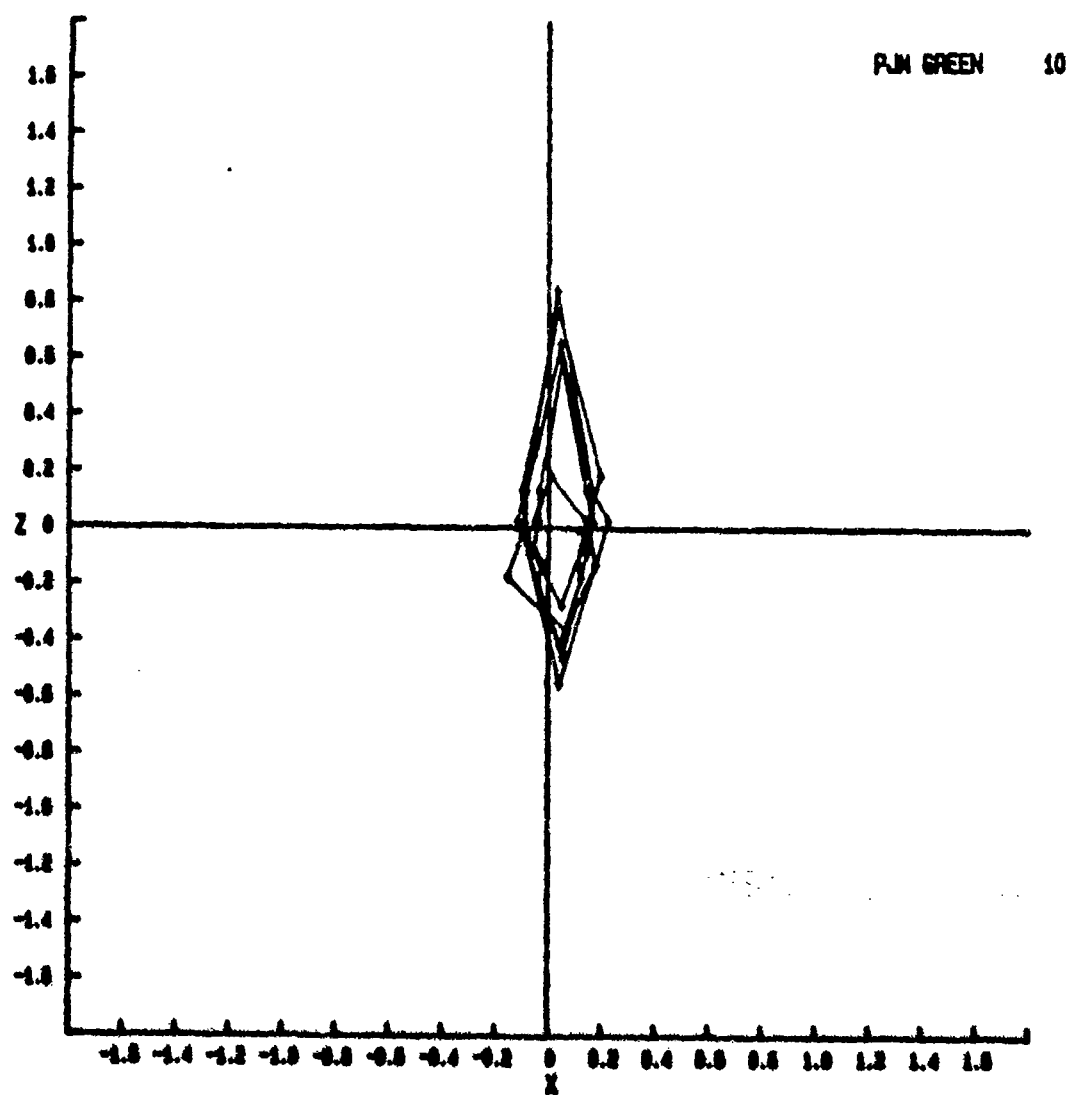


Figure C-11. Individual threshold deviation contour. Figure legend indicates observer, background condition, and target size.

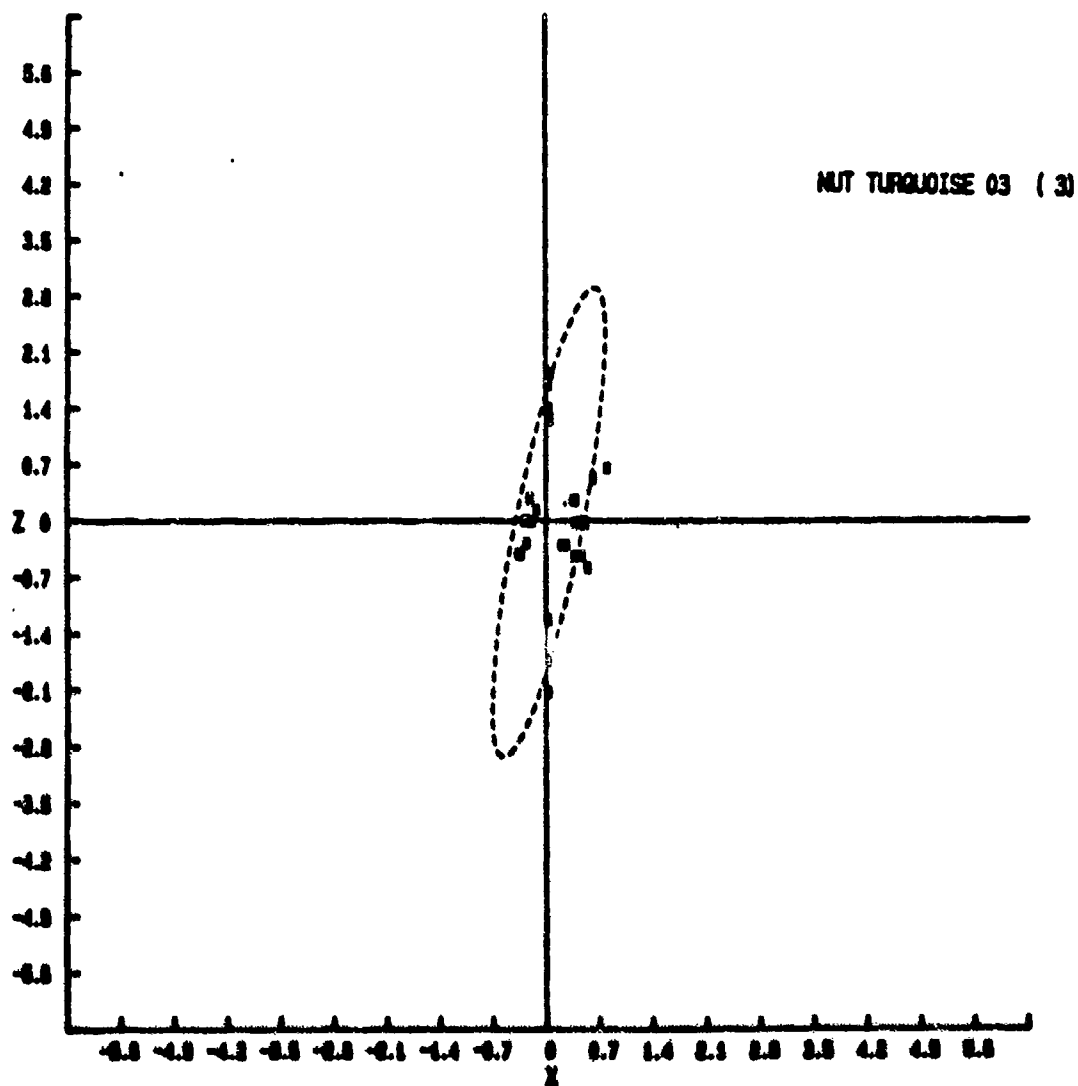


Figure C-12. Individual data points with fit ellipse. Figure legend indicates observer, background condition, and target size.

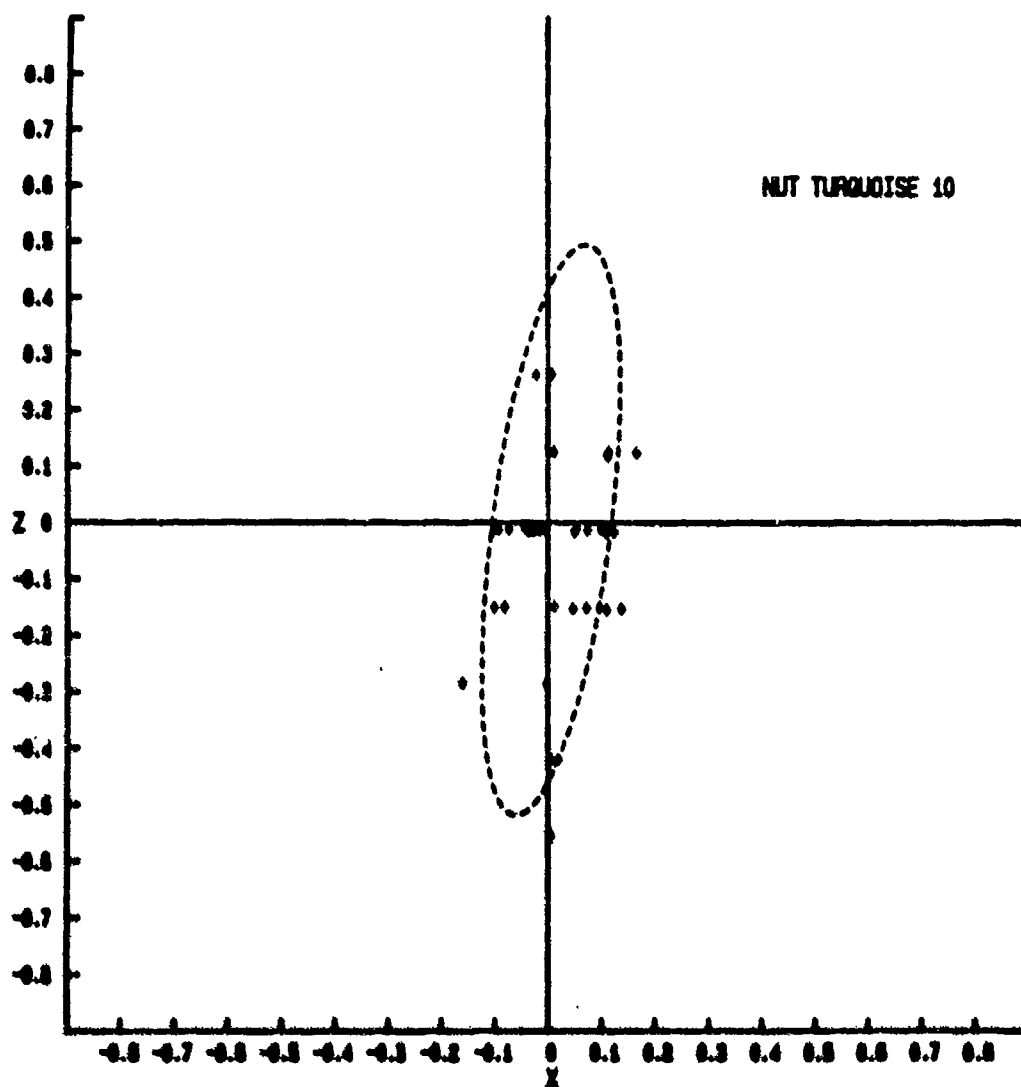
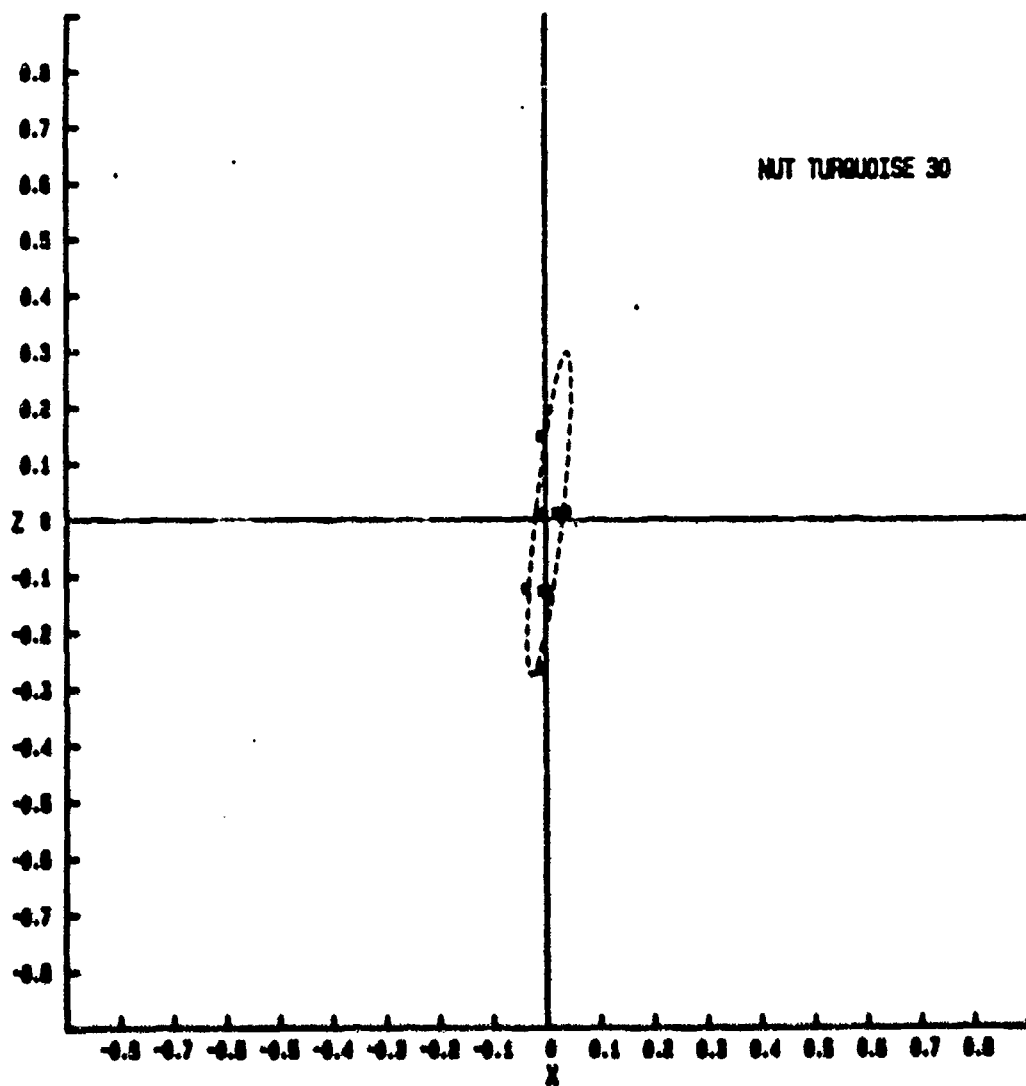


Figure C-13. Individual data points with fit ellipse. Figure legend indicates observer, background condition, and target size.





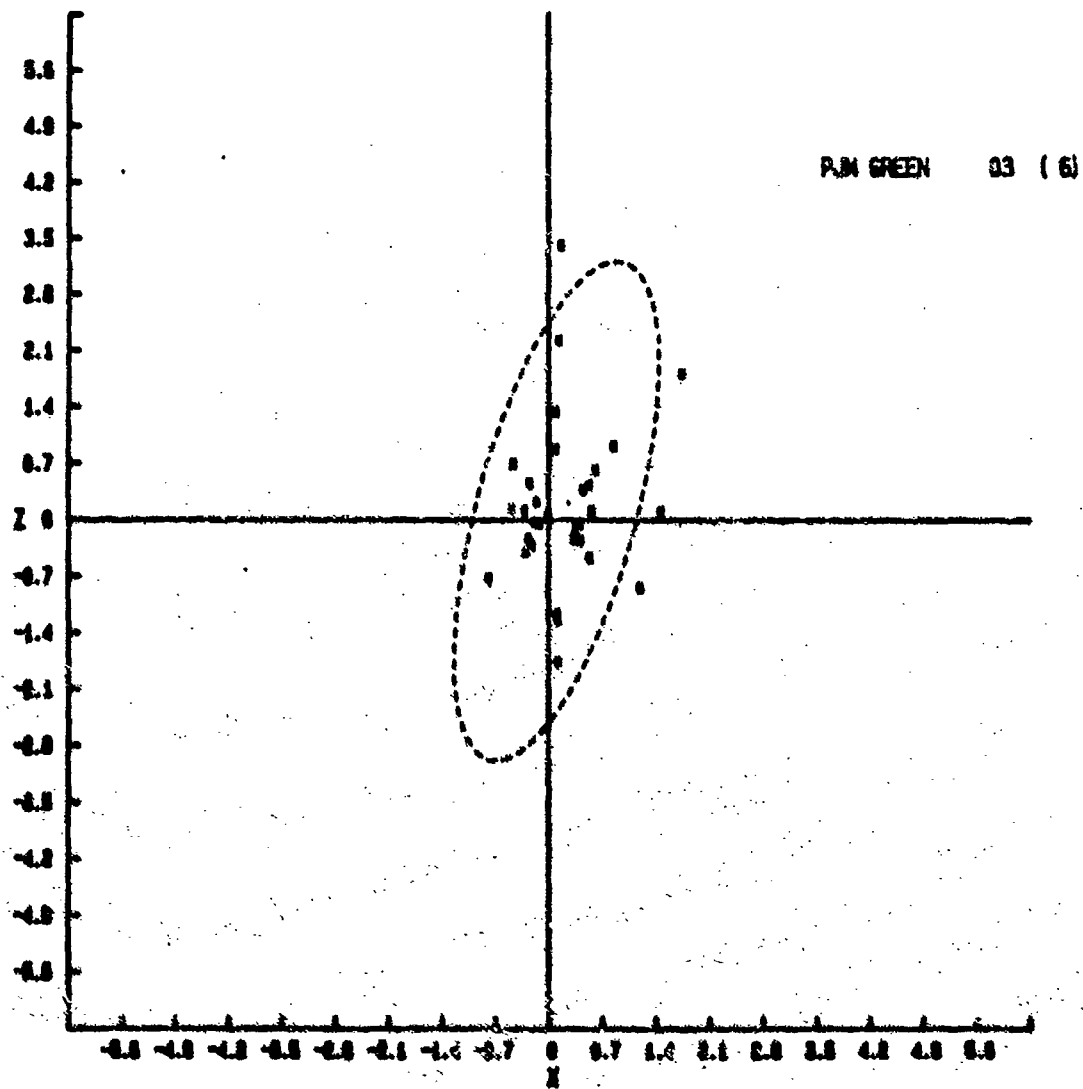


Figure C-15. Individual data points with fit ellipse. Figure legend indicates observer, background condition, and target size.

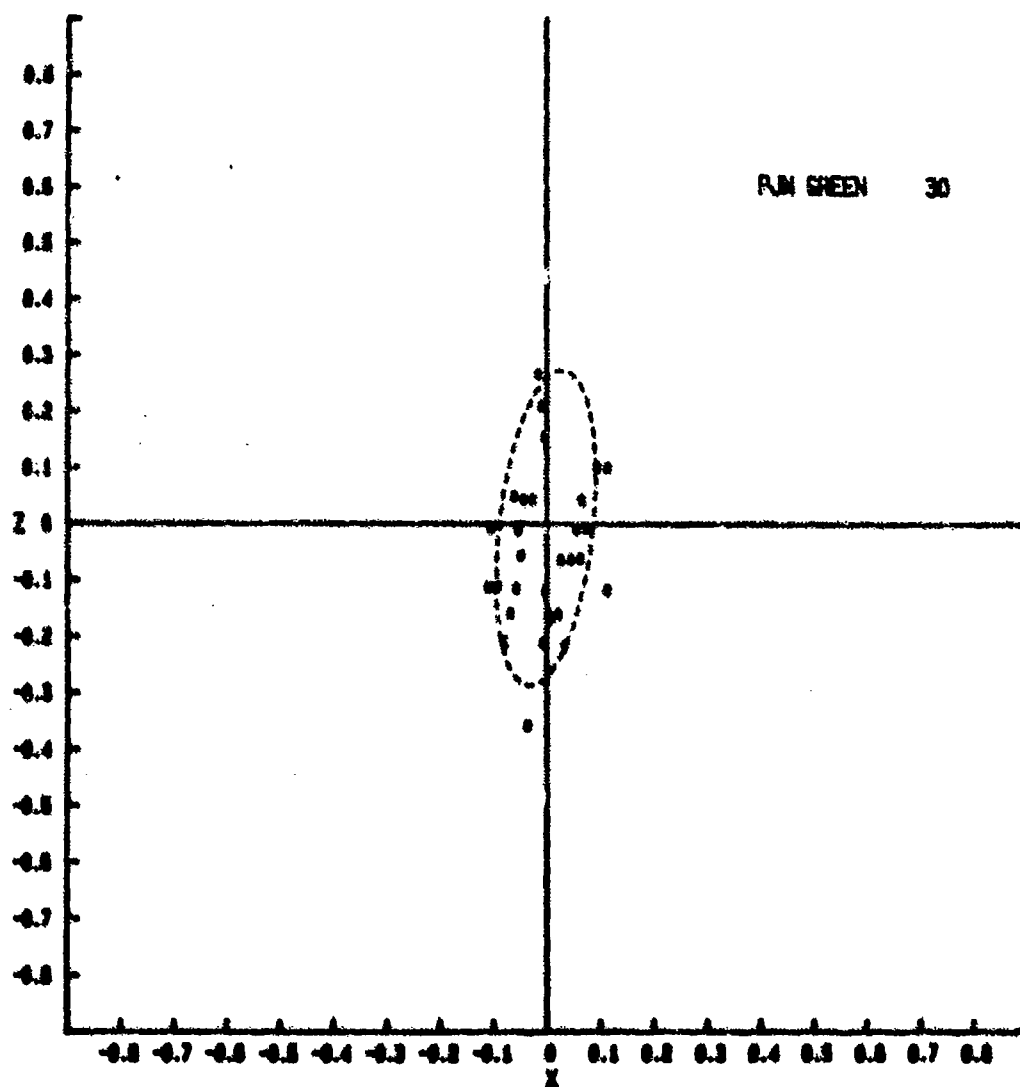


Figure C-16. Individual data points with fit ellipse. Figure legend indicates observer, background condition, and target size.

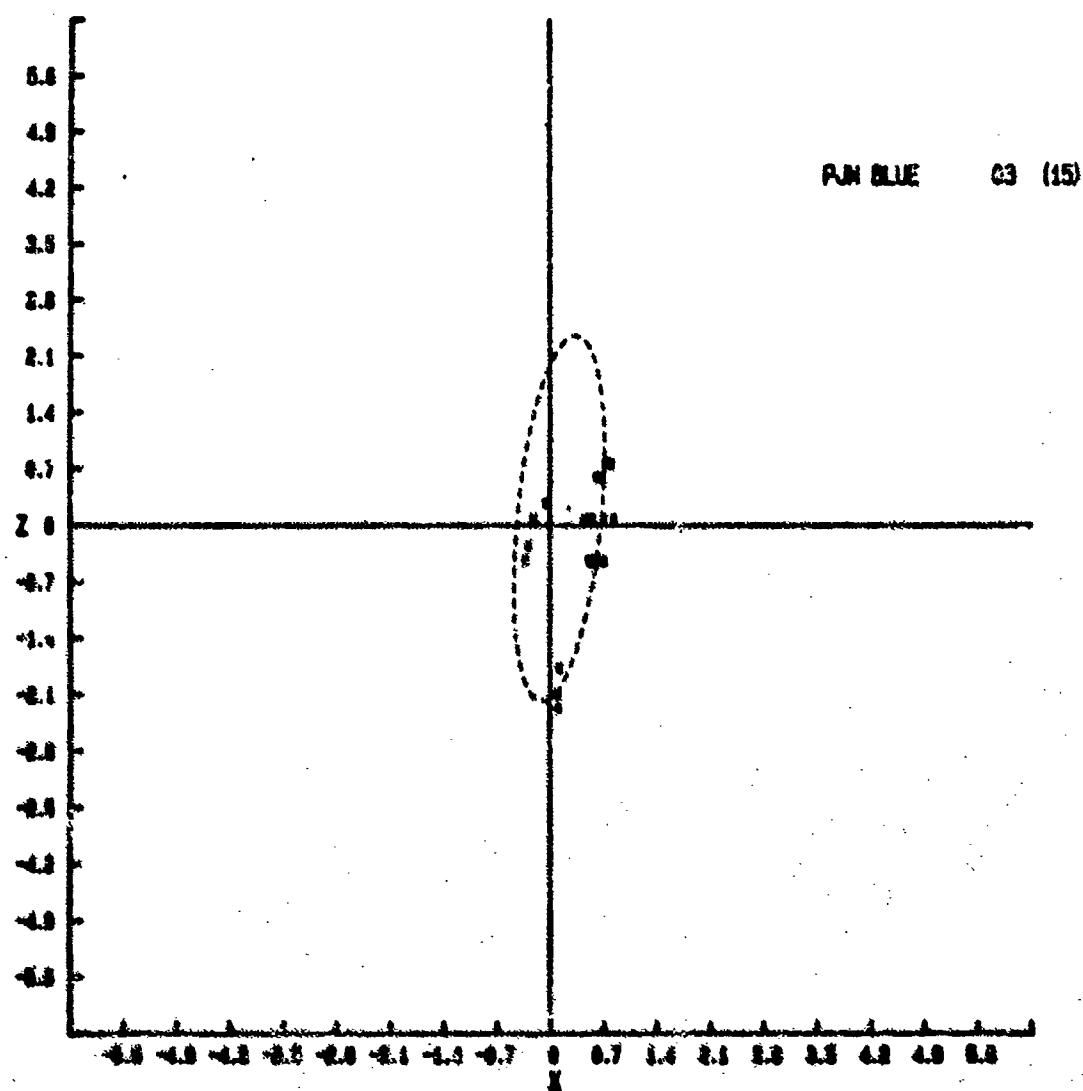


Figure C-17. Individual data points with fit ellipse. Figure legend indicates observer, background condition, and target size.



**C-19**

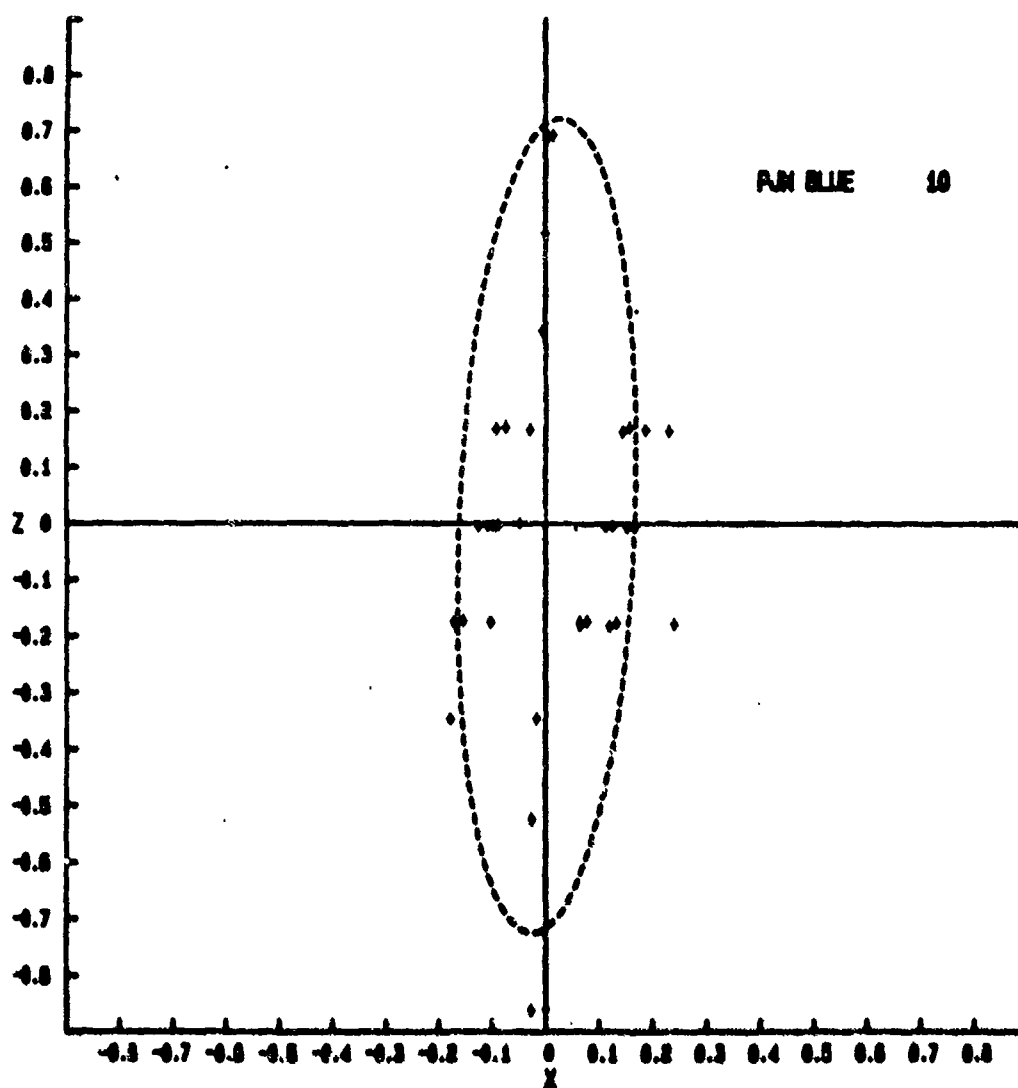


Figure C-19. Individual data points with fit. ellipse. Figure legend indicates observer, background condition, and target size.

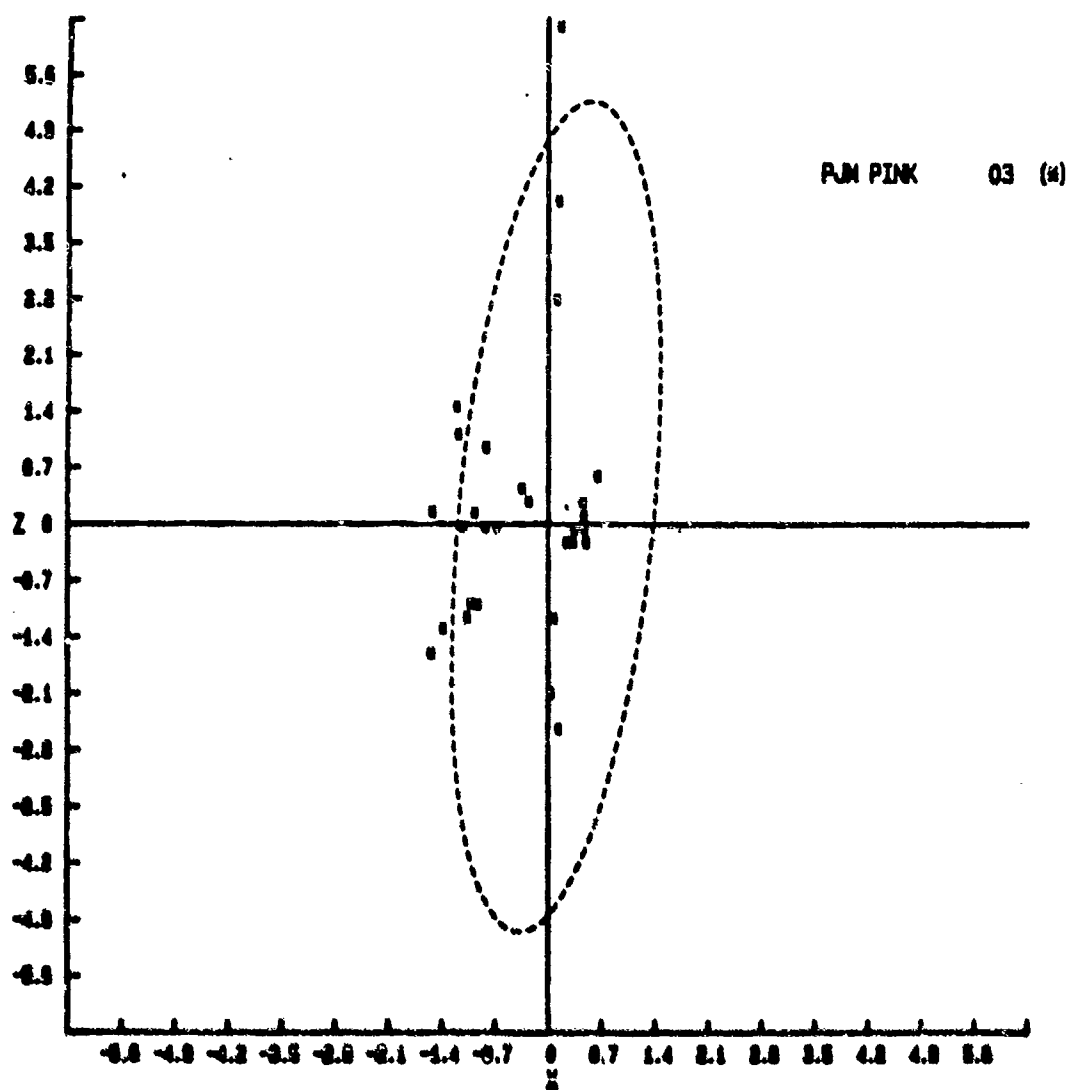


Figure C-20. Individual data points with fit ellipse. Figure legend indicates observer, background condition, and target size.

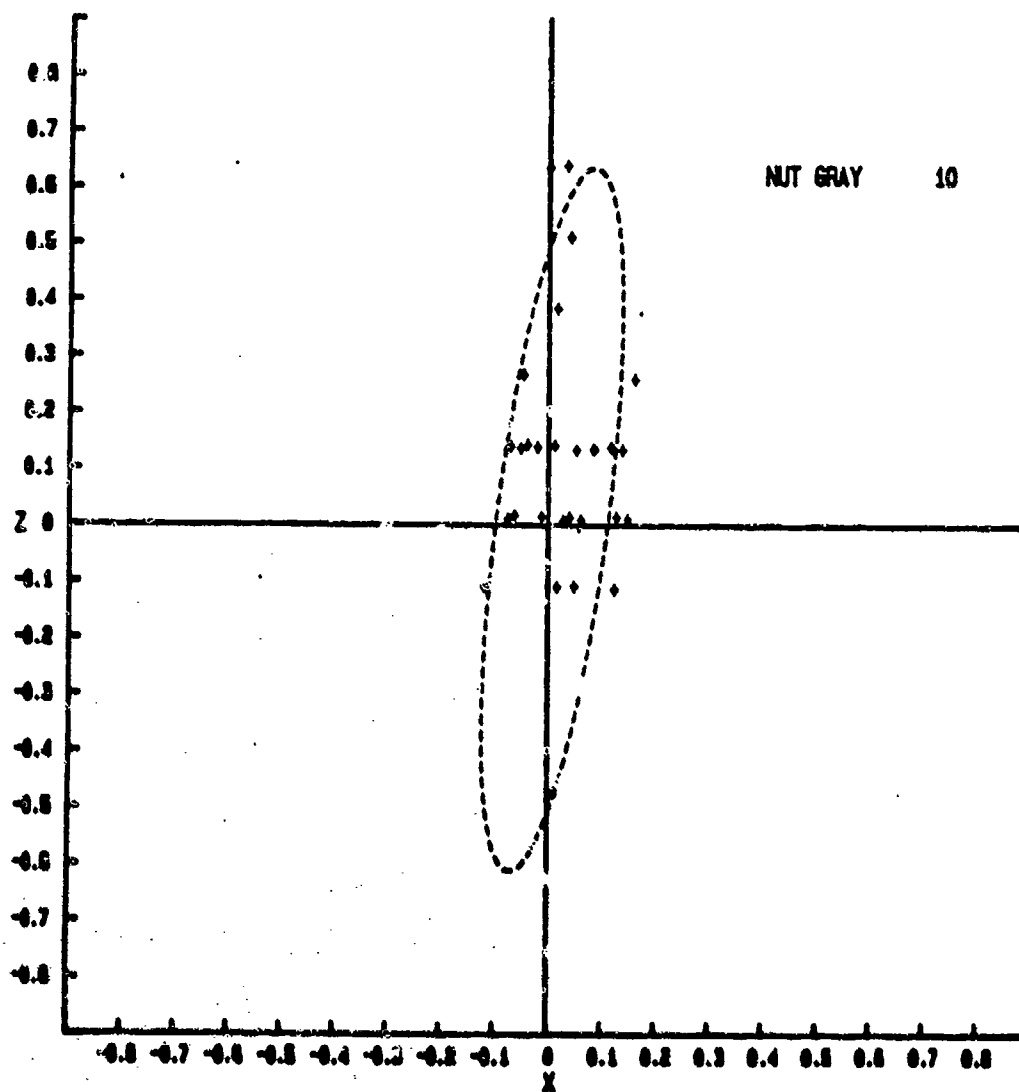


Figure C-21. Individual data points with fit ellipse. Figure legend indicates observer, background condition, and target size.



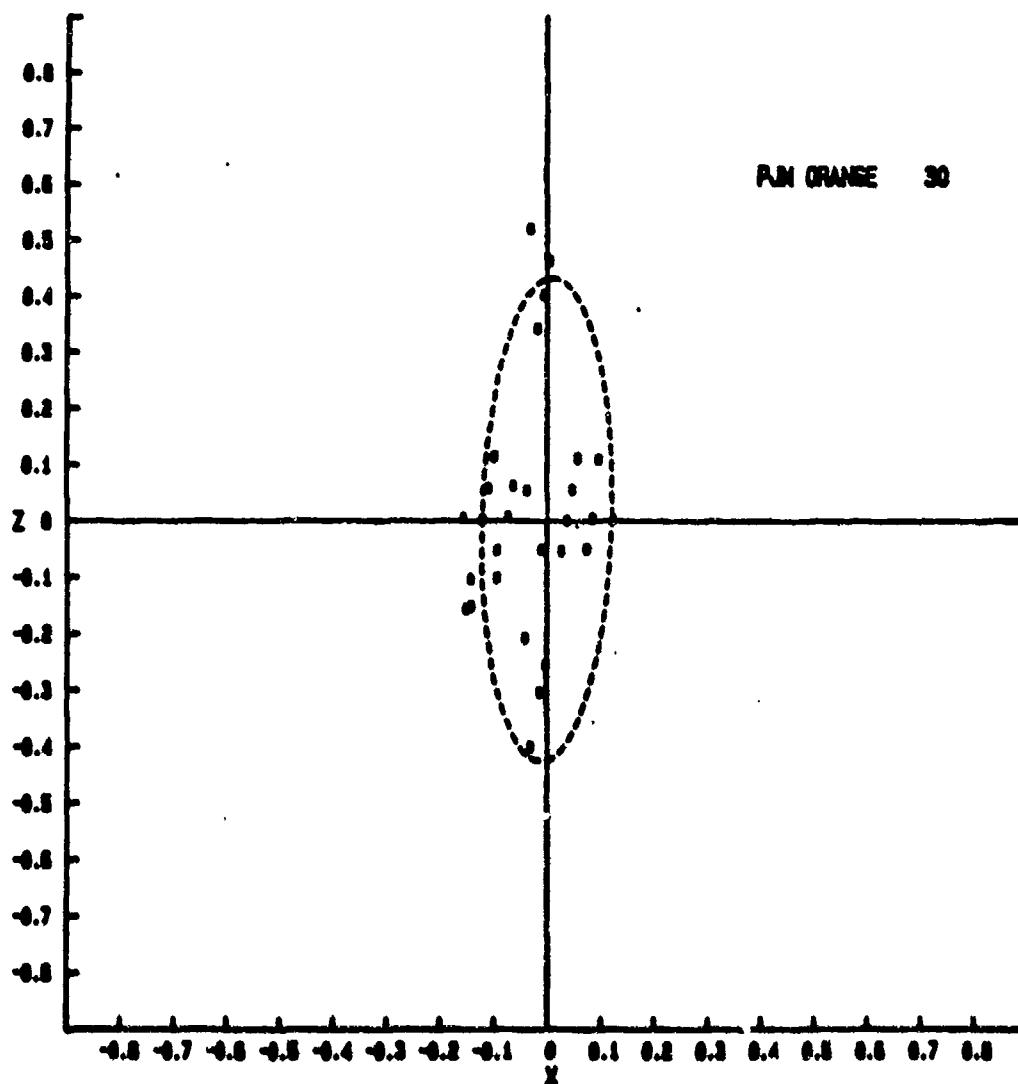


Figure C-22. Individual data points with fit ellipse. Figure legend indicates observer, background condition, and target size.

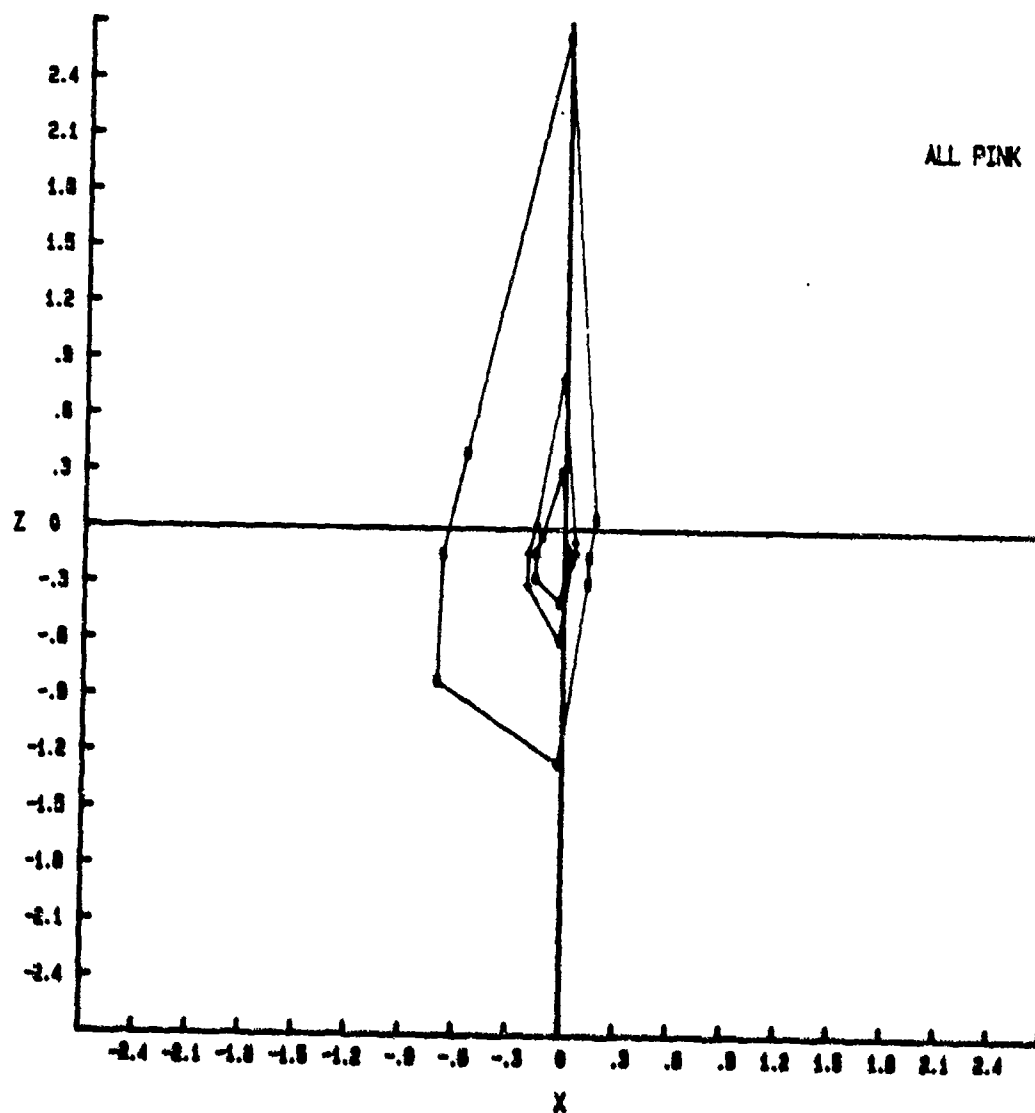


Figure C-23. Average threshold deviation contours, XZ plane.

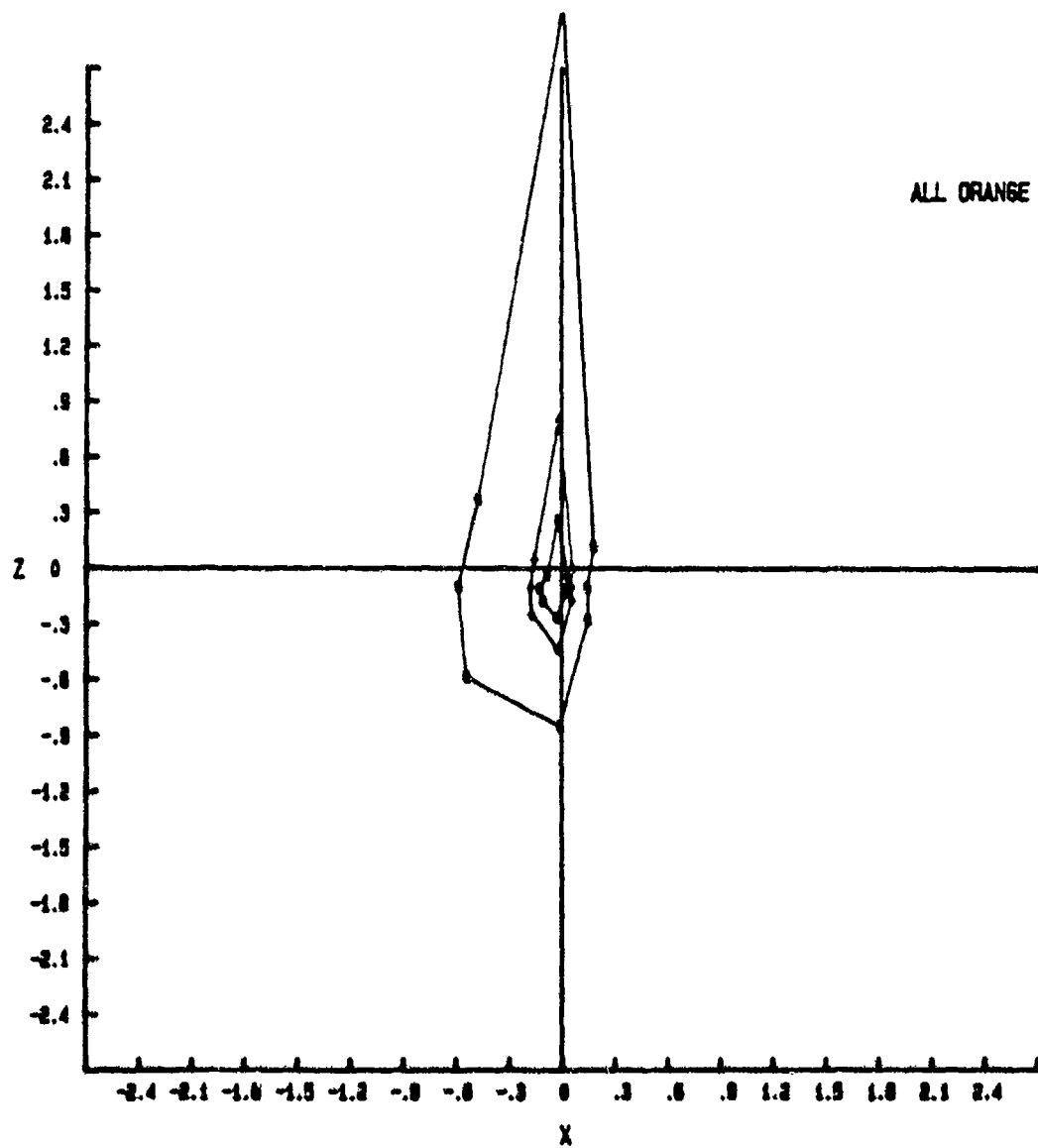


Figure C-24. Average threshold deviation contours, XZ plane.

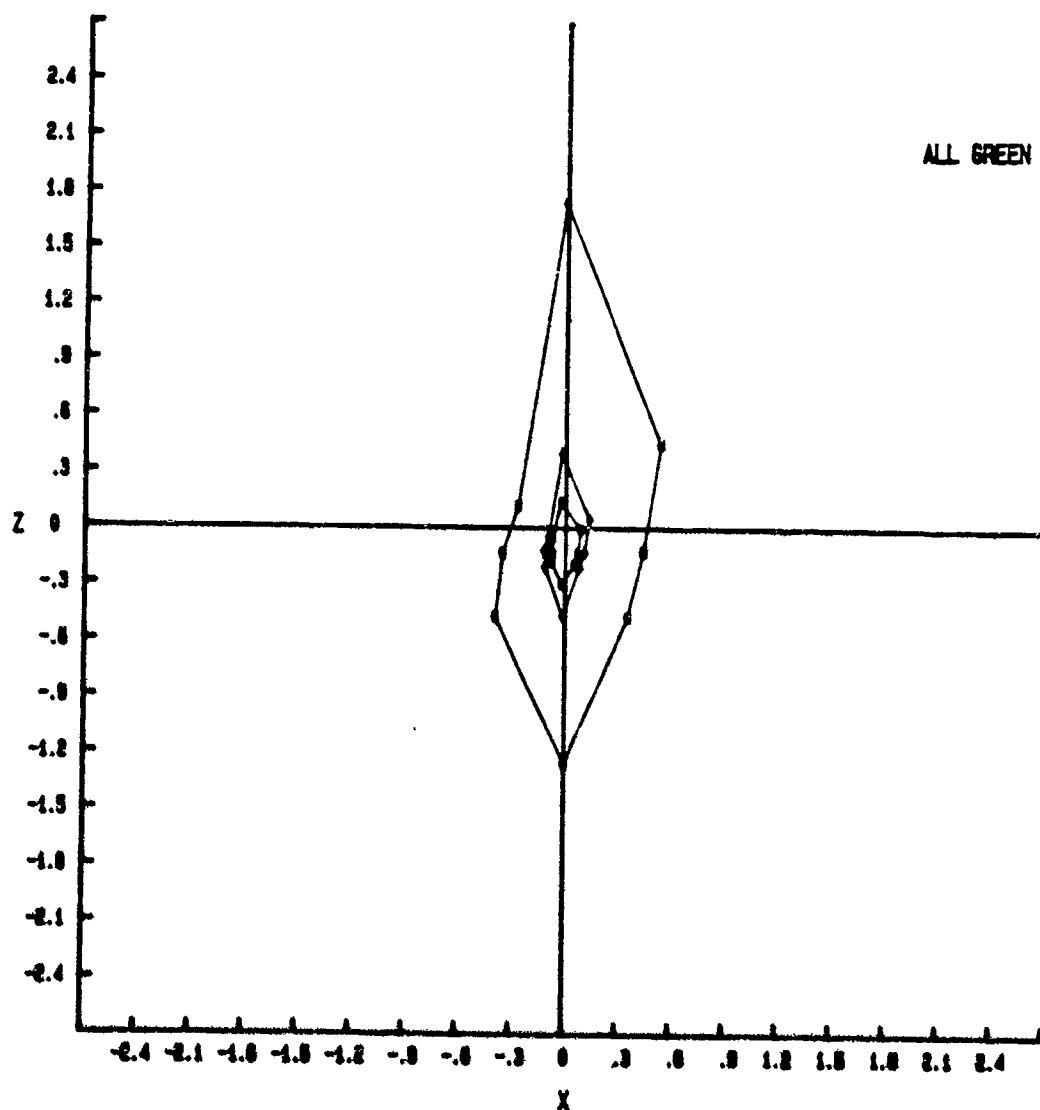


Figure C-25. Average threshold deviation contours, XZ plane.

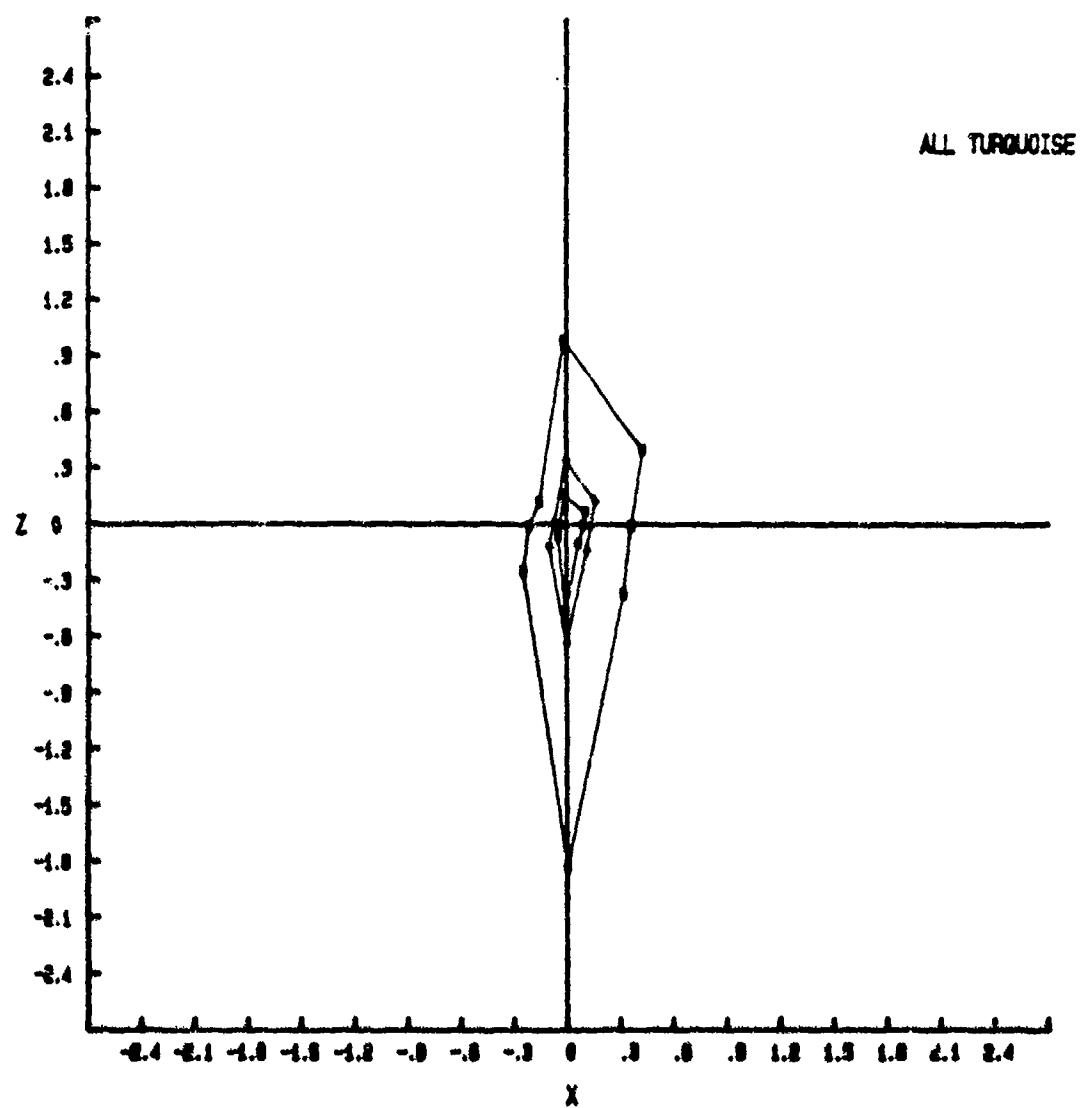


Figure C-26. Average threshold deviation contours, XZ plane.

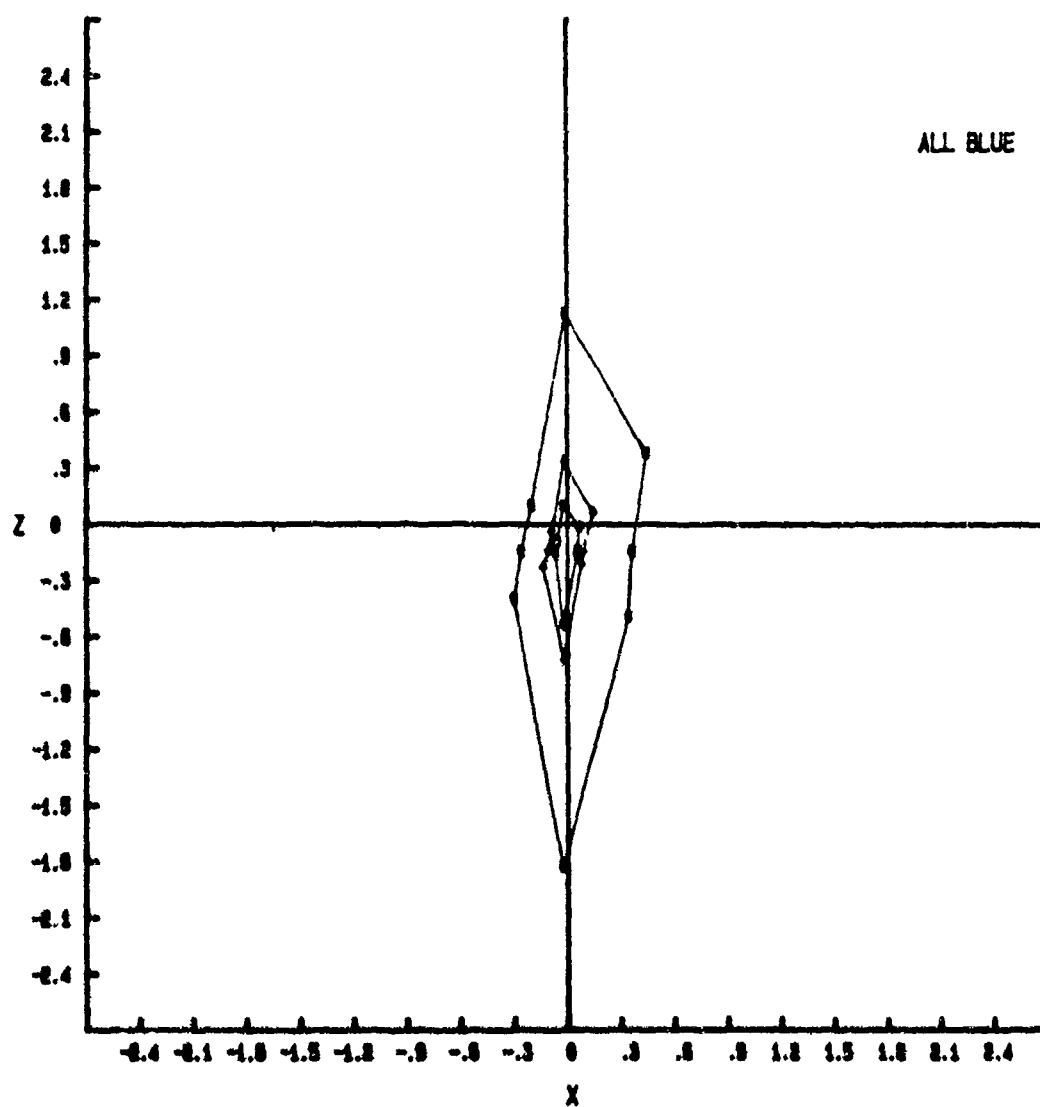


Figure C-27. Average threshold deviation contours, XZ plane.

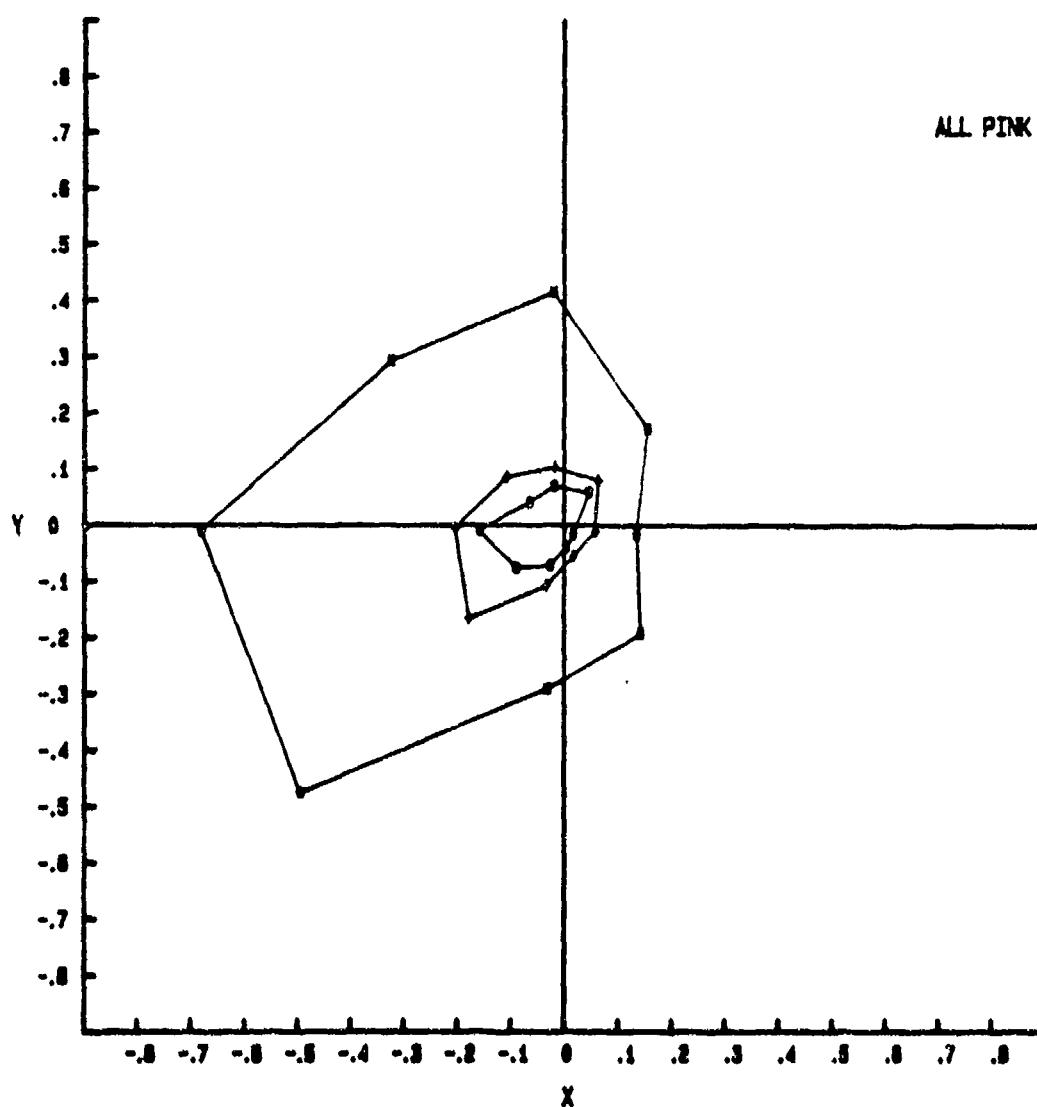


Figure C-28. Average threshold deviation contours, XY plane.

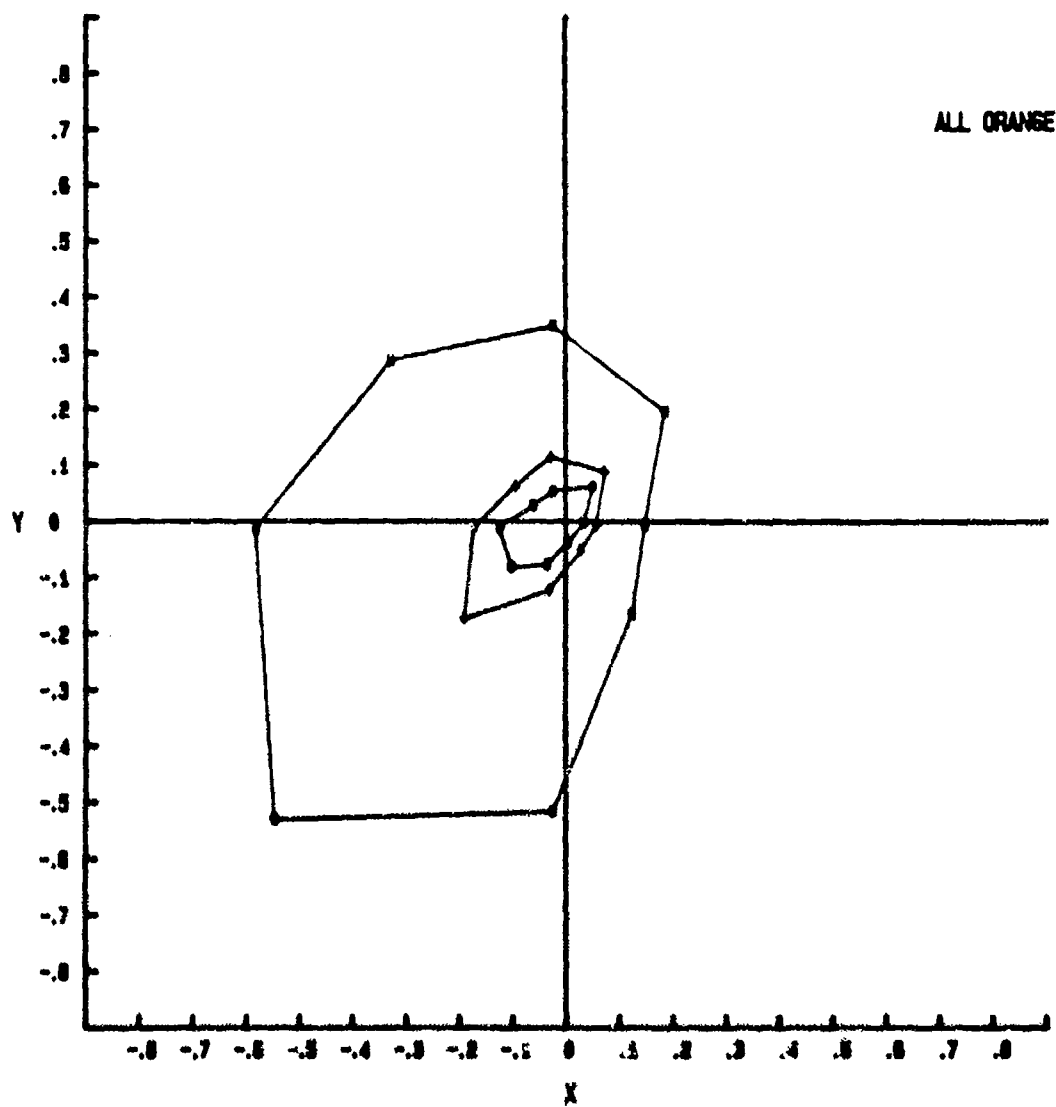


Figure C-29. Average threshold deviation contours, XY plane.



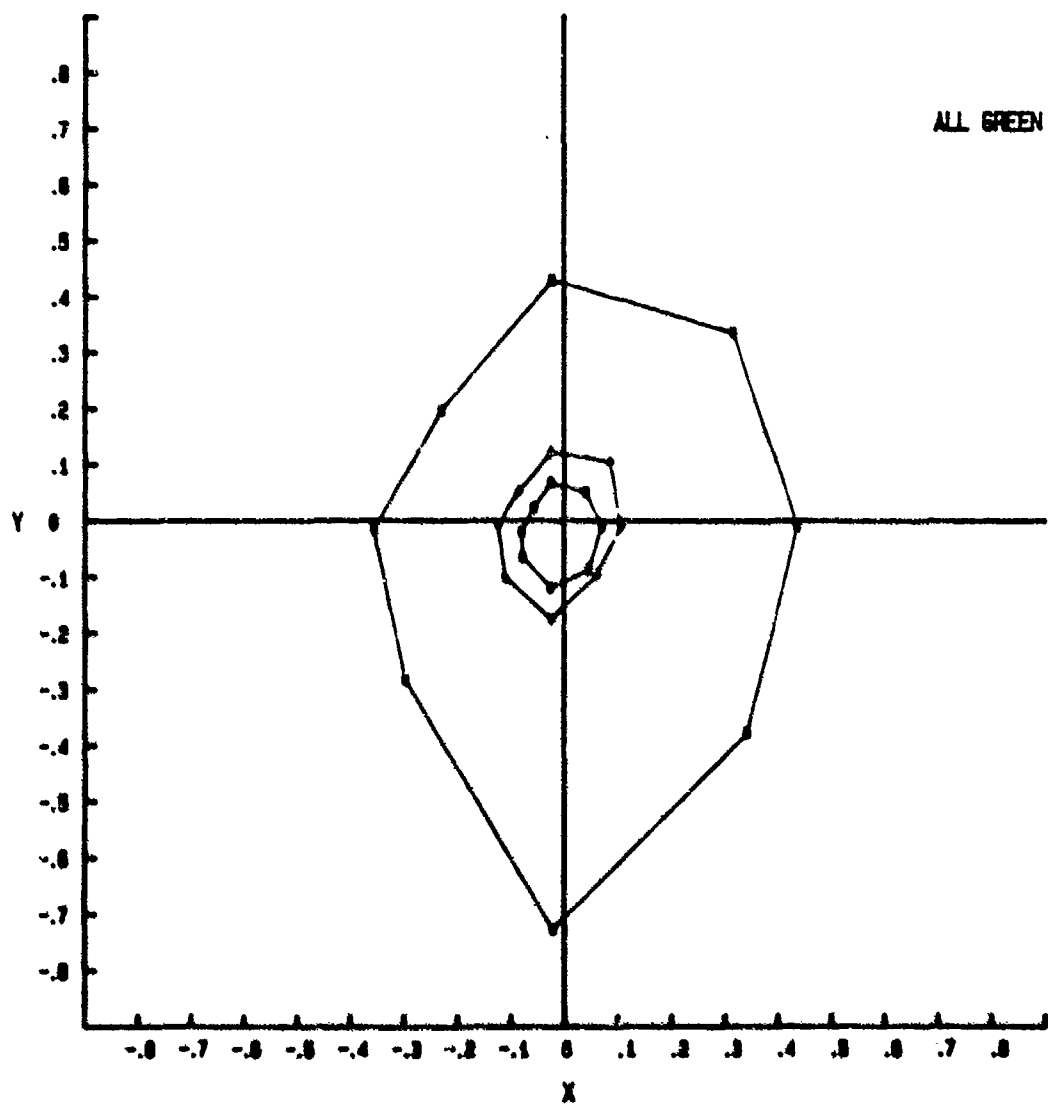


Figure C-30. Average threshold deviation contours, XY plane.

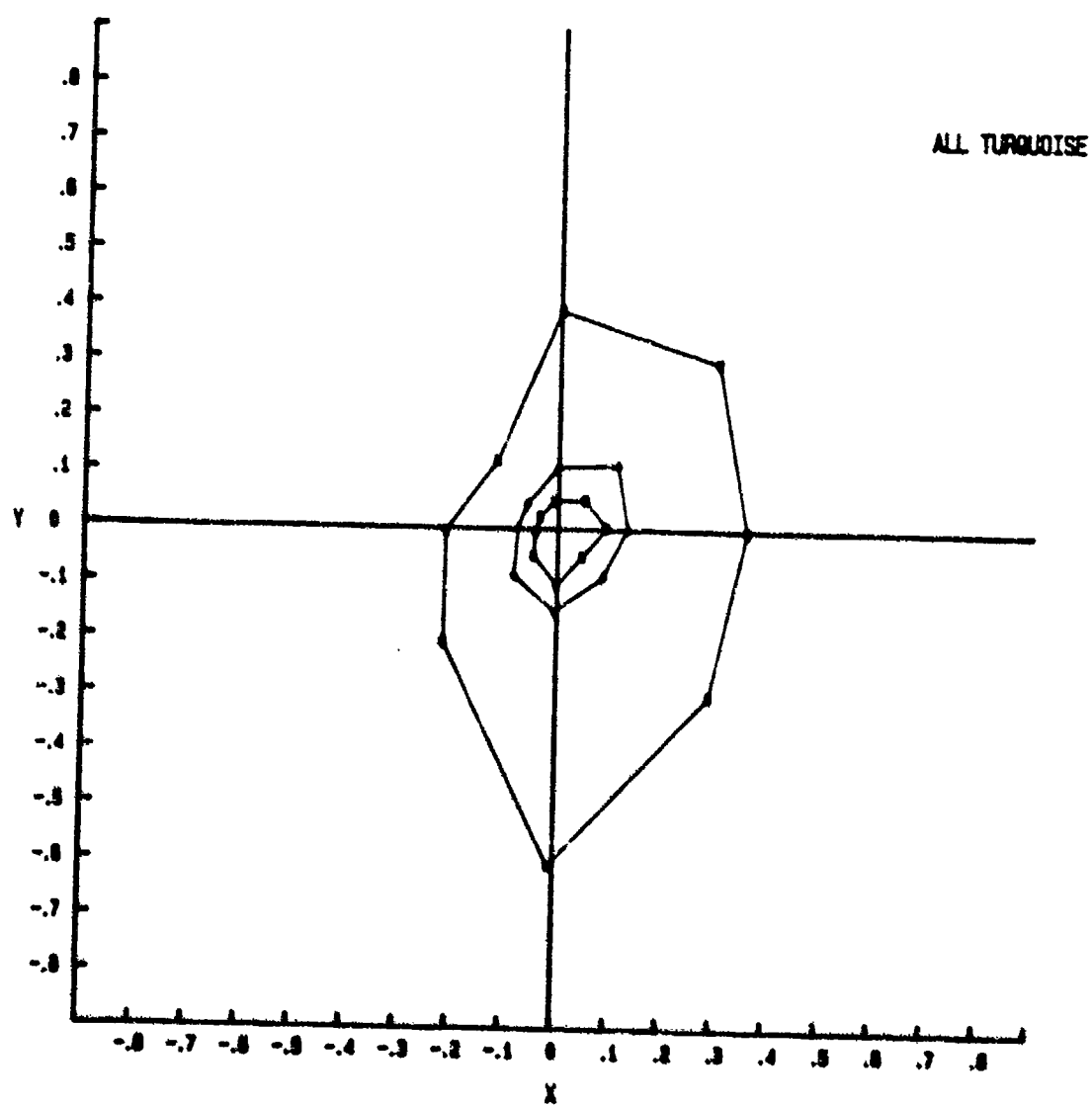


Figure C-31. Average threshold deviation contours, XY plane.

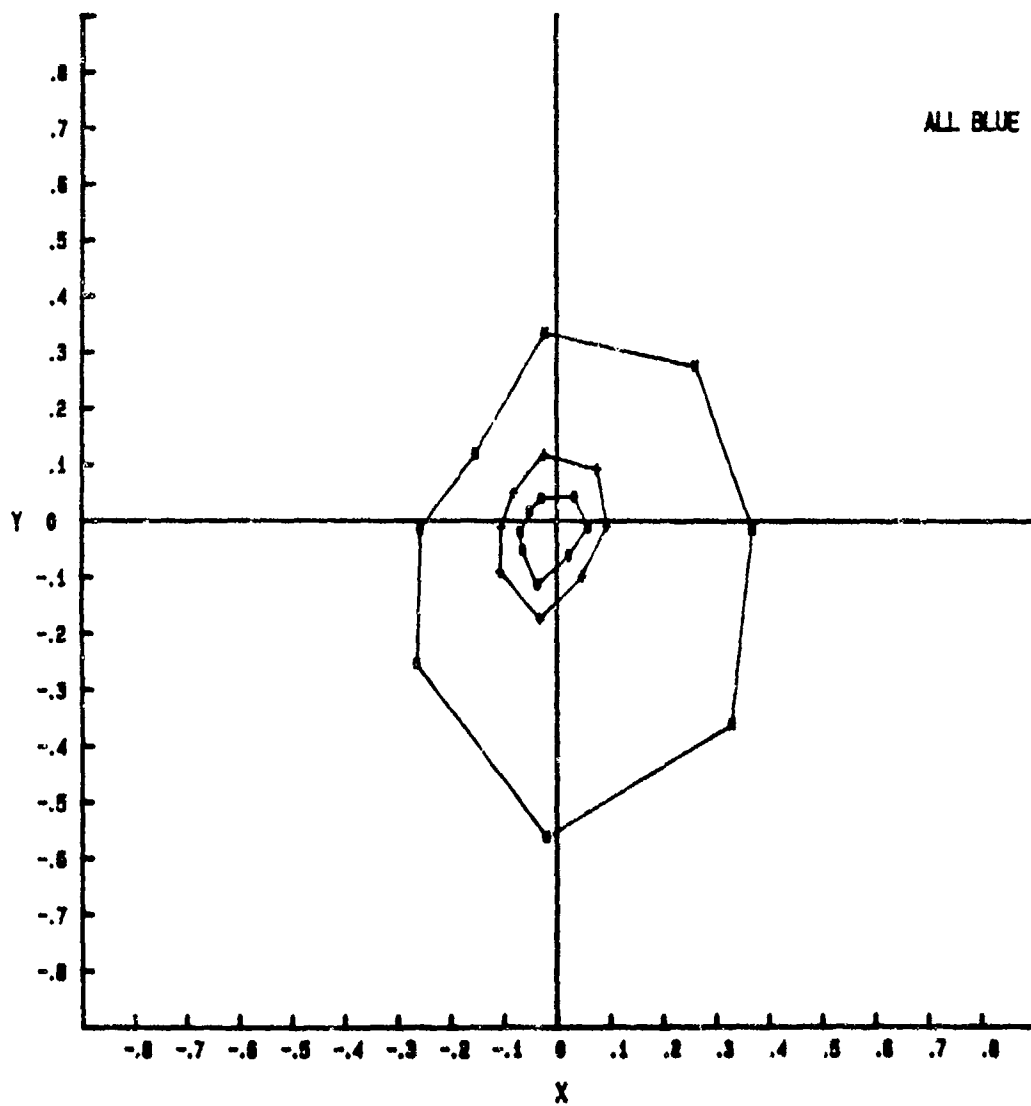


Figure C-32. Average threshold deviation contours, XY plane.

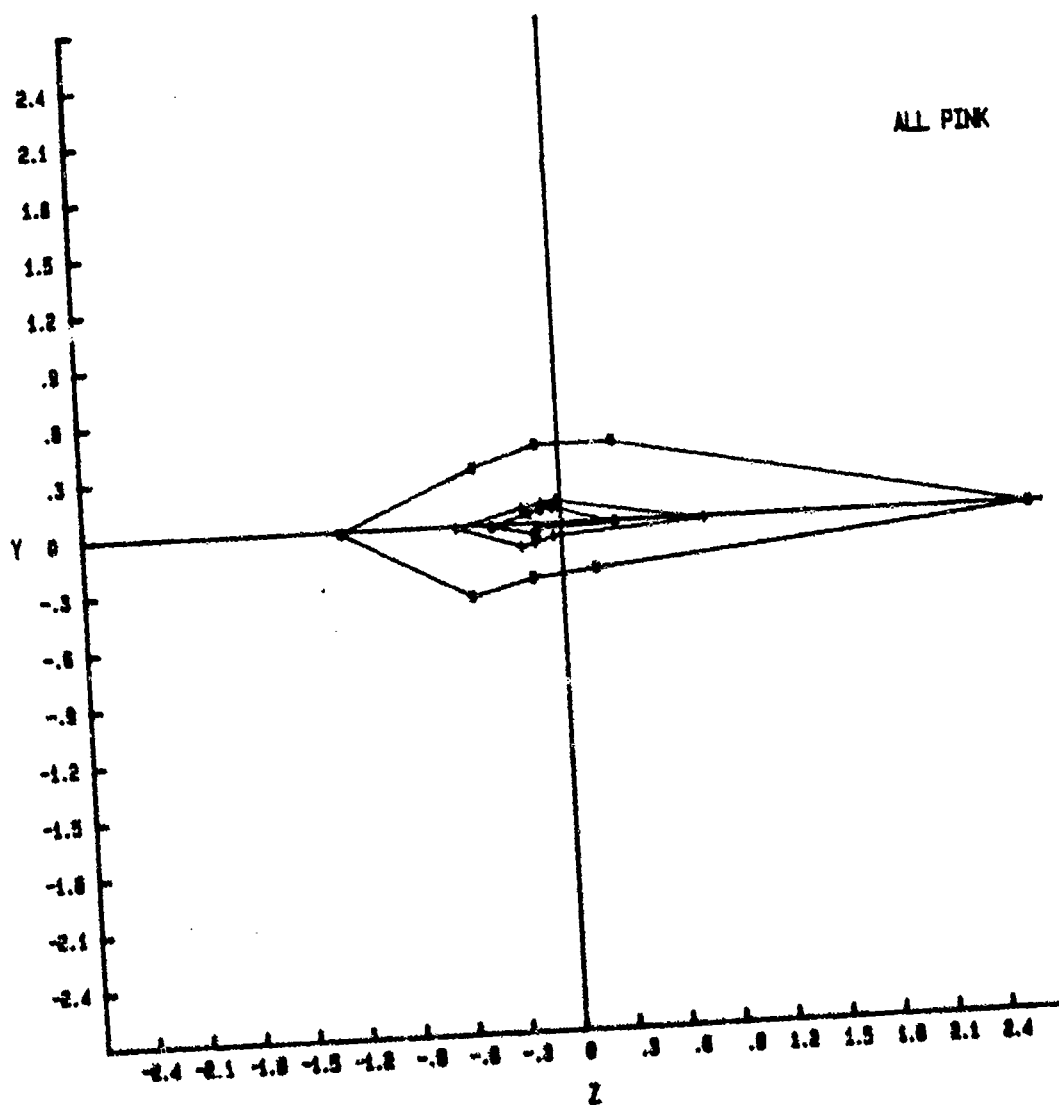


Figure C-33. Average threshold deviation contours, YZ plane.

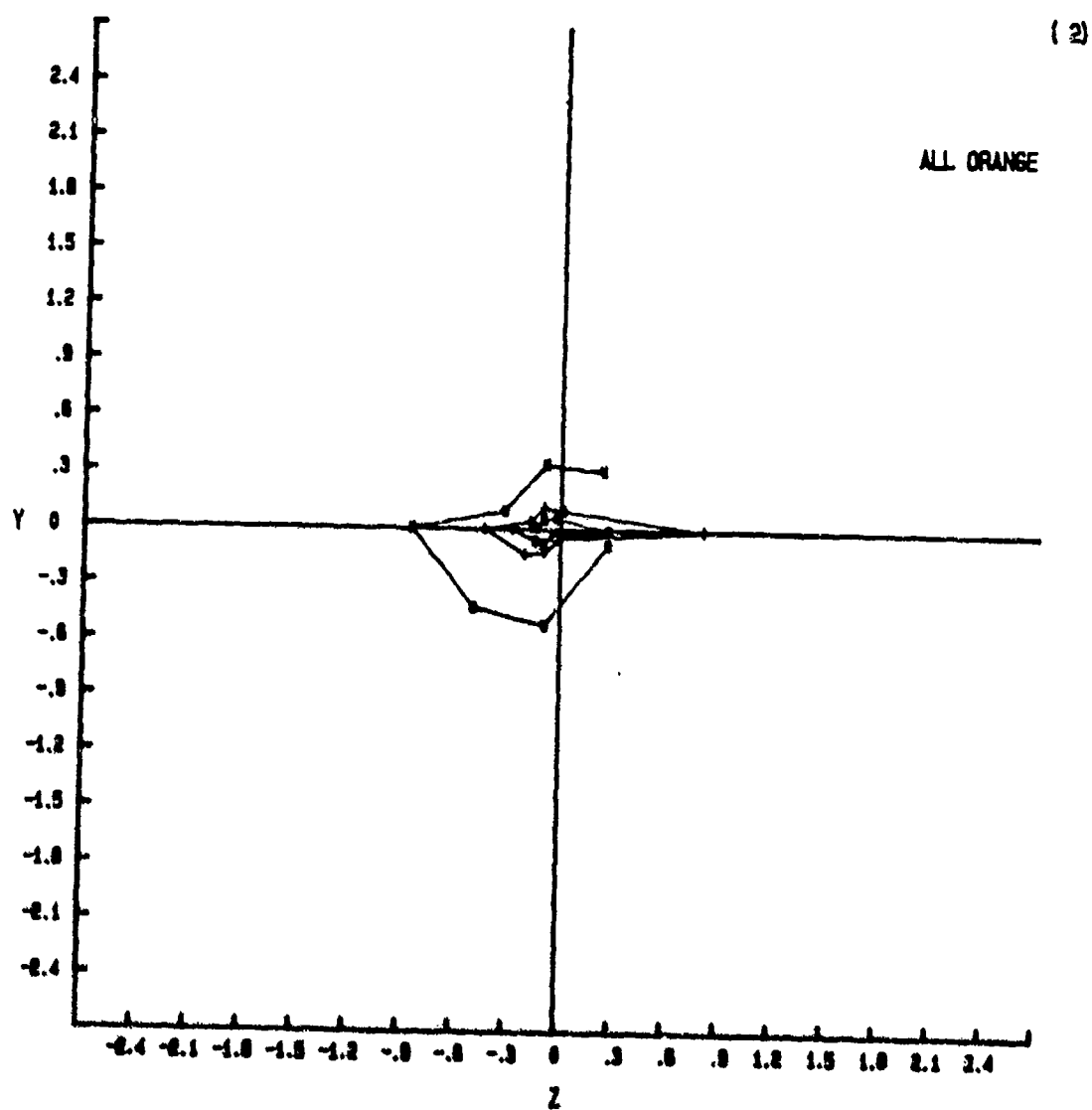


Figure C-34. Average threshold deviation contours, YZ plane.

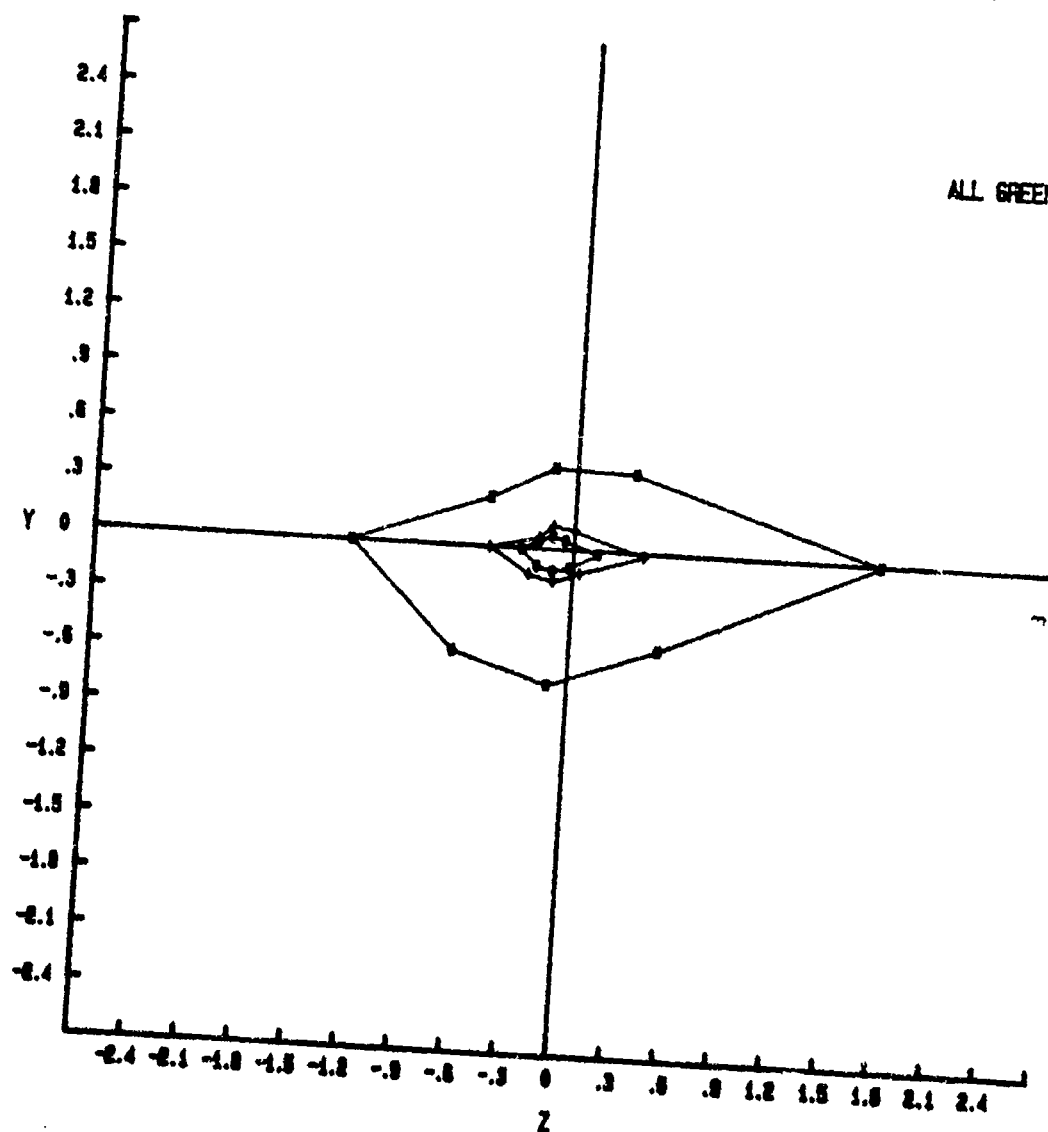


Figure C-35. Average threshold deviation contours, YZ plane.

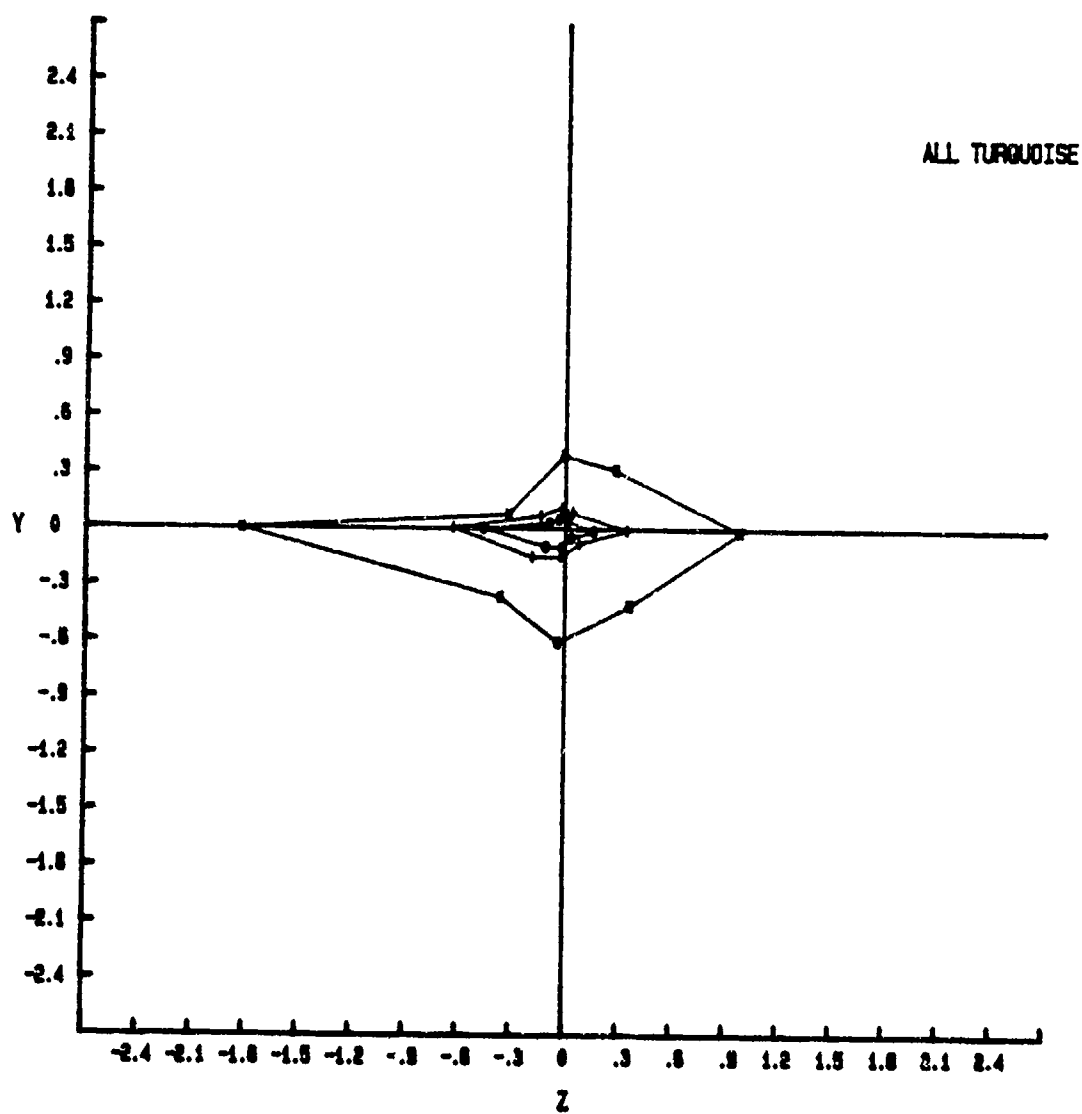


Figure C-36. Average threshold deviation contours, YZ plane.

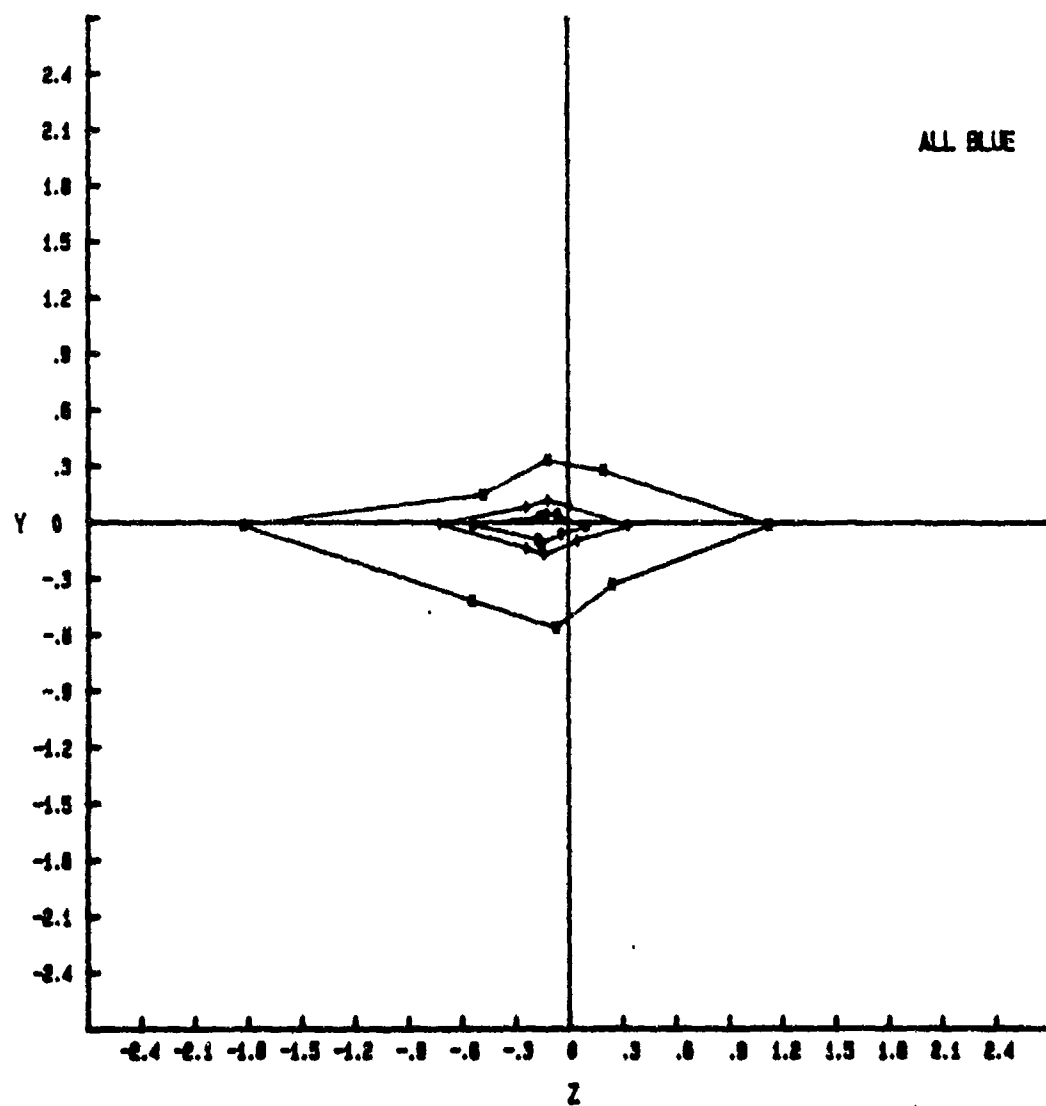


Figure C-37. Average threshold deviation contours, YZ plane.